By Land, Water, and Air: An Evaluation of the Impact of Embankment Setbacks and Two-Stage Channel Design on Flood Characteristics of the Upper River Nith

Breanna Van
Masters by Research Thesis
School of Geographical and Earth Sciences
University of Glasgow

Abstract

River channelisation is a method of hard engineering that laterally constrains and straightens a river, with the twofold aims of increasing a river's hydraulic efficiency and minimising land loss due to flood-related erosion. However, in catchments with low sediment supply, such as Scotland, rivers typically respond to channelisation with channel incision and bed armouring, which further reduce floodplain connectivity and physical habitat diversity. Recently, two-stage channel design and embankment setbacks have been applied as a restoration method to return sediment mobility to channelised rivers with the goal of improving both biodiversity, bank stability and channel-floodplain connectivity. These techniques include carving out small benches to act as a floodplain and pushing back existing embankments to allow for increased river movement. In late-2019, the Scottish Environmental Protection Agency (SEPA) completed restoration works on an upper section of the River Nith near New Cumnock, Scotland by implementing embankment setbacks and two-stage channel design to two sections of the river with the goal of demonstrating natural flood management approaches for this type of channelised, incised river. This thesis investigated the restoration works completed by SEPA and analysed the difference in flood impacts including inundation extent, flow depth, and shear stress, between the pre-restoration and post-restoration topography using a variety of field survey techniques and numerical modelling software. Specifically, data from previous Airborne light detection and ranging (LiDAR) and bathymetry surveys were used in conjunction with unmanned aerial vehicle (UAV) LiDAR, real-time kinematic Global Navigation Satellite System (RTK-GNSS), and echo-sounding via acoustic Doppler current profiler (ADCP) surveys that were conducted as part of this dissertation in 2022. The digital elevation models (DEMs) created from these surveys were then input into Geomorphic Change Detection (GCD) software and the Hydrologic Engineering Center – River Analysis System (HEC-RAS) flood modelling program to quantify topographic change due to channel-floodplain modification and flood impacts by modelling multiple recurrence interval events. Overall, the findings of this thesis suggest that, for particular design flood events, the embankment setbacks and two-stage channel design have increased flood extent and floodplain connectivity while reducing the amount of flow overtopping embankments and decreasing overall water depth and bed shear stress.

Declaration

I, Breanna Van, declare that this thesis is the product of my own work, except where indicated, and has not been submitted by myself or any other person for any previous degree at this or any other university.

Date: 17 January 2023

Signature of Breanna Van

Acknowledgements

I would like to sincerely thank my primary supervisor, Professor Richard Williams, for providing me with this amazing opportunity to complete my thesis in Glasgow, Scotland and for his guidance in this investigation into embankment setbacks and two-stage channel design. I am also extremely grateful to my supervisor, Dr. Laura Quick, for being an amazing mentor as well as for the endless support and proofreads she provided. Thank you to the internal and external examiners of this thesis for comments to improve the clarity of the investigation. A big thanks as well to Craig Macdonell and Kenny Roberts for their endless patience, assistance, and willingness to explain field equipment and software programs to me. A sincere thank you to all of the landowners for providing access to their land for surveys as well as to SEPA for informative conversations and data sharing. I would like to specially thank Dr. Sara Rathburn, my undergraduate geology professor, who has inspired my love for rivers, desire to pursue fluvial geomorphology, and always urged me to push myself. Additionally, thank you to Dr. Jim Finley for being an amazing first supervisor and providing guidance during my first few years of a "real-world" job as well as to Rachael Peavler and Stan Smith who have been my work supervisors during the completion of this degree for the support they provided as I navigated the balance between work and university. I am also thankful to Dr. Sven Egenhoff for encouraging me to pursue a graduate degree and helping me get here. A special thank you to the River Cluster Group who have provided important peer support. Additionally, my sincerest gratitude to my parents and sister for encouraging me to go on this journey and who have been endlessly supportive from across the pond. Lastly, a huge thank you to the new friends I have made in Scotland, without whom I could not have completed the last year.

Table of Contents

Figures

Tables

Preface

An excerpt from the poem *Apostrophe, to the River Nith* by John Mayne (1806):

"Hail, gentle stream! Forever dear

Thy rudest murmurs to mine ear!

Torn from thy banks, tho' far I rove,

The slave of Poverty and Love,

Ne'er shall thy Bard, where'er he be,

Without a sigh remember thee!

For there my infant years began,

And there my happiest minutes ran;

And there, to love and friendship true,

The blossoms of affection grew!

Blythe on thy banks, though sweetest stream

That ever nurs'd a Poet's dream!"

1 Introduction

1.1 Background

Flooding is one of the most detrimental natural disasters, the occurrence of which is predicted to increase in a large number of locations globally due to climate change (Hirabayashi et al., 2021), with some estimates projecting a 187% increase in global flood risk by 2050 (Arnell & Gosling, 2014). According to Wahlstrom (2015), floods accounted for 47% of all weather-related disasters from 1995-2015 and 2.3 billion people were affected during this period. In the UK alone, flood-related maintenance costs £1.1 billion annually (Heritage & Entwistle, 2020). As well as damage from flood waters, floods also cause land loss through erosion which has a potentially detrimental impact on critical infrastructure (e.g., bridge structures) and agricultural, industrial, and urban areas. River-related erosion includes removing sediment from channel beds and banks. These lateral erosion and scour processes may result in morphological change that can, for example, cause damage to farmlands and associated agriculture and productivity (Maniatis et al., 2020; Perfect, 2013).

In an attempt to mitigate the loss of valuable land from flooding-related erosion, a high proportion of UK rivers have been channelised. Channelisation is an anthropogenic activity that involves artificially straightening channels through hard engineering (Heritage & Entwistle, 2020) in order to route water downstream as efficiently as possible and minimise flooding to land adjacent to the channelised reaches. This process reduces the river's ability to migrate laterally across valley bottoms and therefore narrows the active width of the river, hence maximising land that is available for agricultural use, and industrial and urban development. However, in catchments with low sediment supply, the presence of hard engineering structures used to channelise rivers may cause channel incision, and the removal of fine sediment and subsequent bed armouring (Heritage & Entwistle, 2020). These processes decrease hydraulic diversity, and consequently reduce geomorphic and habitat diversity (Williams et al., 2020). Additionally, channelisation can also increase the effects of flood pulses, making flood events more damaging to the rivers and surrounding floodplain as water is forced to spill out of the bankfull channel rather than distributing energy through sediment transport and channel adjustment (Burrel et al., 2007).

Developing ways to return dynamic hydraulic and morphological characteristics, such as floodplain connectivity and lateral mobility, to a river system is important to lessen the associated damage of flood events. Two methods of restoration that encompass these goals are two-stage channel design and embankment setbacks (Krider et al., 2017; Larsen et al., 2006). While there is a general understanding of the effects that channelisation has on river systems, there is a gap in knowledge of the effects that two-stage channel design and embankment setbacks have on restoring river flood- and morpho- dynamics.

Along with many rivers in Scotland and all over the world, the River Nith, located in Dumfries and Galloway, Scotland has been channelised for centuries (Perfect, 2013). Channelisation along the Nith has resulted in a narrow channel susceptible to flooding during high rainfall events and a substantially degraded river in terms of habitat and ecological diversity. In the study area, which is downstream from New Cumnock, embankment overtopping during floods have occurred frequently over the original man-made embankment located directly up against the river channel. As part of the Scottish Environmental Protection Agency (SEPA) pilot catchment project, restoration construction was conducted in two distinct areas along the upper River Nith (Phase 1 and Phase 2) (CBEC, 2015) in 2019.

This restoration work included both embankment setbacks and two-stage channel design which aims to encourage more natural river processes and increase both physical habitat and ecological diversity.

While the study area is a small portion of a single river system, it represents the wide-spread characteristics associated with heavily channelised and engineered rivers such as reduced floodplain-connectivity and habitat diversity. Findings from this investigation will enhance the understanding of the impacts that river restoration techniques have on geomorphic change and flood inundation for this type of river system.

1.2 Research aim, objectives and research questions

The aim of this thesis is to determine the differences in flood impacts as a result of the SEPA restoration works conducted on the River Nith. Specifically, this thesis will assess how the topography, inundation extent, and flood dynamics such as flow depth and shear stress have changed from pre-restoration to post-restoration. Different field techniques used to collect elevation data and construct digital elevation models (DEMs) included unmanned aerial vehicle light detection and ranging (UAV LiDAR), real-time kinematic Global Navigation Satellite System (RTK-GNSS), and acoustic Doppler current profiler (ADCP). These DEMs were subsequently used as input data for Geomorphic Change Detection (GCD) analysis and the Hydrologic Engineering Center – River Analysis System (HEC-RAS) two-dimensional hydraulic modelling program to evaluate areas of erosion and deposition, as well as changes in the patterns of fluvial processes.

The specific objectives of this thesis are to:

1. Create DEMs for both pre-restoration and post-restoration topography of the River Nith (Phase 1 and Phase 2).
2. Compare the topographic and geomorphic change between pre-restoration and post-restoration topography.
3. Predict floods for both pre-restoration and post-restoration at difference return intervals (1-, 2-, 5-, 10-, 20-, 50-, and 100-year).

The following research questions are to be assessed after completion of the objectives:

1. Is there geomorphic or topographic change observed between the pre-restoration and post-restoration DEMs of the River Nith (Phase 1 and Phase 2)?
2. Does flood inundation extent change between pre-restoration and post-restoration?
3. Do cross-sectional hydrographs change between pre-restoration and post-restoration?
4. Does flow depth and shear stress change between pre-restoration and post-restoration?

1.3 Thesis Structure

This thesis firstly consists of a Literature Review, which investigates and examines the relevant literature regarding river morphology, river restoration, monitoring geomorphic change, and modelling flood dynamics. This is followed by a Methodology chapter, which provides justification and reasoning for the selection of various techniques and software packages to contract DEMs, calculate geomorphic change, assess flood inundation patterns, and compare depth and shear stress changes. The findings of the data analysis are reported in the Results section. The findings are then examined and analysed in the Discussion, followed by a summary and review of the research questions in the Conclusion.

2 Literature Review

This literature review focuses on river morphology characteristics, channel engineering effects, and fluvial monitoring techniques as they relate to assessing the impacts that two-stage channel design and embankment setbacks have on geomorphic change. This provides the context to the field surveys and modelling investigations conducted for this project on the River Nith in Scotland.

2.1 River Morphology

On a basic level, river morphology can be broadly characterised into the following categories: braided, meandering, and straight. The morphology of a river system is usually determined by the sediment load, channel gradient, and water discharge (Zachariah, 2019). Due to the consistent year-round rainfall and minimal seasonal variation (NRFA, 2022a), the UK is classified as a temperate climate. Alongside the consistent temperate climate, the UK is also tectonically inactive so rivers in the UK generally have low sediment loads, particularly bedload. The combination of a consistent temperate climate and low sediment loads is conducive to the formation of meandering rivers.

2.1.1 Meandering Rivers

Meandering rivers are dynamic systems defined by a sinuous channel form and features such as point bars and cutbanks that are instrumental in promoting channel and habitat heterogeneity (Larsen et al., 2006). They generally form as a consequence of low gradients which reduce stream velocity and allow for a high volume of suspended sediments and deposition (Gilvear et al., 2002). The bends that are characteristic of meandering channels act as an obstacle to flow, reducing velocity when the flow collides with the banks and is directed around the bends (Blanckaert, 2010). Meandering systems also promote pool and riffle formation which aids in the function and structure of the channel as well as floodplain connectivity which supports biodiversity (Konrad et al., 2008).

Flood plain connectivity is an important aspect of meandering rivers and refers to the connected processes and sediment exchange between the river channel and adjacent floodplains. Key processes that highlight this connectivity and encourage biodiversity are channel migration, bend cut-offs, and point-bar deposition, which result in oxbow lake and riparian habitat formation and assist in creating new floodplains (Larsen et al., 2006; Power, 1995). Additionally, the floodplain connectivity that meanders provide reduces flow velocity within the channel as water is dispersed onto the floodplain (Opperman et al., 2010). While floodplains encourage biodiversity, they are also some of the most modified and vulnerable ecosystems in the world and it is therefore important that processes associated with these features are preserved. Without this connectivity, biodiversity is reduced, and important flood mitigation features are lost.

2.1.2 Channelisation

Channelisation is a method of river engineering designed to laterally contain a river by preventing and limiting meanders. It aims to reduce floodplain erosion to increase the amount of land available for agricultural use (Heritage & Entwistle, 2020) and to remove water from valley bottom floodplains as rapidly as possible. Research focused on readjustments of sinuous rivers in north-western Europe over the past 6,000 years suggests that hydraulic engineering processes, including channelisation, have been ongoing since the 11th century in parts of Europe (Vayssière et al., 2020).

This type of river engineering leads to fragmentation of the river system that has a negative impact on both flood-water absorption and buffering capabilities, causing both to decrease (Mondal & Patel, 2018; Pierce et al., 2012) and enables both sediment aggradation and degradation as well as bank instability. The resulting erosion or deposition is influenced by river morphology (e.g., meandering vs. straight) and sediment supply. For example, in catchments with high rates of sediment supply relative to transport capacity, constricting channel dimensions can cause sediment to accumulate at a faster rate, which causes the riverbed to aggrade. Raising the riverbed reduces the channel's capacity for holding water, making avulsions more likely and increasing flooding in downstream reaches where there might not have previously been flood risk (Sinha, 2008). Constricting channel dimensions can also have the opposite but equally detrimental effect of deepening the riverbed, in catchment settings with low rates of sediment supply relative to transport capacity. This happens when flood velocities and shear stress increase for a given discharge as a result of the confined river that has nowhere to erode or migrate, thus causing incisions. The latter effect is most common in the UK and as a result, flood pulses become more dangerous with larger intensity, magnitude, frequency, and damage (Burrel et al., 2007).

Additional adverse effects these anthropogenic forces have on river systems include disrupting flow regimes, segmenting channel-floodplain connectivity, decreasing the replenishment capacity and channel transport capacity, facilitating homogenous flow, and reducing the floodwater outlets and seepage zones (Mondal & Patel, 2018). These effects on the hydrologic regime forces flows to become more spatially concentrated, thus allowing for more powerful flood events that damage the river channel and negatively impact habitats (Cluer & Thorne, 2014). These modifications to river hydraulics also results in a loss of important habitat structures including pool and riffles which promote aquatic life and the decline of which decreases the ecological diversity within the river.

2.1.2.1 Scottish Rivers

Rivers in Scotland have an extensive engineering history that originally stemmed from plans to divert water to populations centres, mainly Edinburgh and Glasgow (Soulsby et al., 2002), to support domestic, industrial, and agricultural water supply needs as well as hydropower production (Gilvear et al., 2002). This background includes implementation of flood banks, land drainage, channelisation, and dredging in the late 18th and early 19th centuries which affected middle and lower courses of Scottish rivers. Embankments here were further extended and raised in the later 19th centuries as the demand for land increased following the wars and railway development (Perfect, 2013). As a result of the channel modification that has been ongoing over the last few centuries and the more recent implementation of flow regulation, there is a substantial lack of fluvial landforms that are not anthropologically impacted, as well as "natural" middle and lower order channels in Scotland (Gilvear et al., 2002).

Studies have found that while rivers in Scotland have naturally high water-quality, they do not necessarily have good ecological quality (Gilvear et al., 2002), which is based on a combination of water-quality, hydrology, and geomorphology. A SEPA survey conducted in 2010 found that a total of 46% of rivers in Scotland were categorized as being in moderate to poor ecological condition, with the rest in at least good condition. The River Nith has been characterised as moderate since surveys began in 2007. This classification is largely a result of channelisation that reduced in-channel and floodplain habitat diversity.

Information comparing the characteristics of minimally altered meandering systems to those associated with channelised rivers is important to understand the impact that each has on the

surrounding environment. This understanding helps outline underlying processes and can contribute to clarifying restoration goals.

2.2 River Restoration

Solutions to bank erosion and aggradation have historically included bank protection measures and dredging of the channel bed, both of which are damaging to river habitat and ecological quality (Gilvear et al., 2002). As a result of the negative impacts of river engineering, there has been a shift in recent years from river engineering to river restoration. Examples of river restoration methods that aim to improve the hydrologic regime include riparian buffers (Kundzewicz, 2002), embankment setbacks, in-channel structures such as woody debris, and floodplain storage ponds (SEPA, 2015).

Geomorphic attributes of the hydrologic regime include channel dimensions and shape, channel and floodplain features, and substrate (Cluer & Thorne, 2014). These different characteristics provide a variety of benefits, depending on the structural characteristics of the river. For example, in restored channels confluences provide ecological hotspots (Benda et al., 2004) as a result of the convergence of different ecological communities and floodplain connectivity which allows for carbon and sediment storage and nutrient processing. River restoration is also likely to enable sediment sorting, which helps habitat formation when the material has different rates of mobility and is able to self-organize. Another ecological and habitat-enabling feature is vegetation, the presence and abundance of which affects various aspects of river morphology such as fluvial processes and channel geometry. Vegetation is typically sparse when rivers are channelised (Cluer & Thorne, 2014), however, in restored reaches vegetation is more likely to grow and in turn provides stability and habitat. For example, exposed tree roots provide cover and shade to river fauna as well as habitat by reducing flow velocity. Grasses and other shrubs stabilize bank slopes through root-growth. In order for vegetation to provide these benefits, these flora and fauna need time to become fully established, and to do so must be resilient.

Restorative flood management is a method of mitigating flooding events by using river and catchment restoration, rather than river engineering. While river restoration requires more space than river engineering, the increases in habitat and eco-diversity outlined above and potential reduction of risks to both property and human safety make it a preferred option (Cluer & Thorne, 2014). According to Montgomery (2008), a straight, single-thread channel is not the self-sustaining channel form that should be aimed for during restoration. Rather, depending on the site, multi-threaded or sinuous channels may be the most self-sustaining river geometry and the stages of this type of river should be considered in restoration, where this planform is appropriate for the contemporary local controls on channel pattern (Brierley & Fryirs, 2009). Important methods of river restoration in rivers impacted by channelisation include two-stage channel design and embankment setbacks, both of which are implemented to help promote healthy river environments.

Multiple model-based investigations have been conducted to assess the impacts that lowering and removing embankments have on channel-floodplain connectivity. In an assessment by Clilverd et al. (2012), a section of the River Glaven was modelled and the hydro-geomorphic effect that embankment removal had on the river system was quantified by comparing the amount of wet grassland meadow both before and after the restoration occurred. Similarly, another study conducted by Acreman et al. (2003) modelled hypothetical river changes on the River Cherwell associated with embankment removal. Findings indicate that channel cross-sectional area and bankfull capacity were both reduced with the removal of the embankments (Clilverd et al., 2012). Additionally, both

investigations found an increase in peak flow of approximately 150% when embankments were implemented compared to when they were removed and indicate that the removal of embankments increases channel-floodplain connectivity (Acreman et al., 2003; Clilverd et al., 2012). While two-stage channel design and embankment setbacks do not fully eliminate embankments, the impacts to flood characteristics and hydrological connectivity are similar and therefore relevant to these studies.

2.2.1.1 Two-Stage Channel Design

Two-stage channel design (Figure 1) is a restoration method implemented by carving out two "small benches on both sides of the low-flow channel to serve as a floodplain" (Krider et al., 2017). This creates a bankfull channel, allowing the river to spread out laterally and disperse fluvial energy during flood events (Ward et al., 2004). When constructing two-stage channels, it is recommended that the bankfull width to low-flow channel width ratio is between 3:1 and 5:1. Increased fluvial stability, which is a common result of two-stage channel design, provides benefits by reducing erosion at the toe of banks which decreases mass-wasting, therefore decreasing sediment accumulation (Krider et al., 2017). Pool and riffle formation is another potential benefit of two-stage channel design that results from variable velocities and heterogeneous deposition that two-stage channel design provides compared to channelised stretches. The variety of velocities and depths that result from pool and riffle formations (slower velocities and larger depths in pools than riffles) provide a larger variety of habitat and thus increase the biodiversity in a river reach.

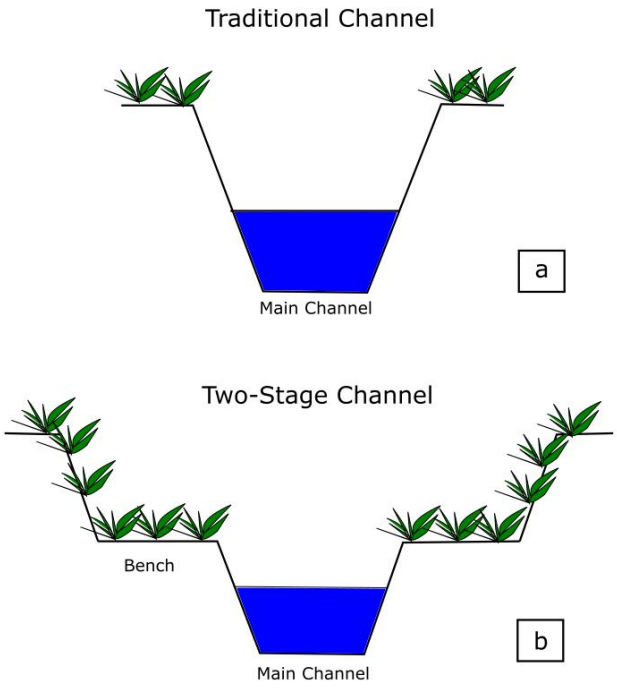

Figure 1. Schematic cross-sections of a traditional and two-stage channel. Channelised channel (Figure 1a) and a two-stage channel (Figure 1b).

Two-stage channel design restoration was completed on a conventional agricultural drainage ditch in Mower County, Minnesota in 2009 to improve water quality and stream habitat (Krider et al., 2017). This project found that following construction of the two-stage channel, the bank vegetation had stabilized the sediment supply, which in turn effectively stabilized the channel bed elevation. The conversion to two-stage channel design also increased pool-riffle formation by 12 times, with a depth increase at the pools and depth decrease at the riffles. These pool and riffles were likely able to form

due to increased bank stability which decreased the amount of erosion occurring and effectively decreasing the sediment supply. Unexpectedly, the post-construction channel widths were observed to have increased over time, suggesting an increase in high-flow events or an increase in flow-velocity. There was also a notable increase in sediment aggradation from pre-construction to post-construction, which is the opposite of what would be expected with an increase in stability provided from the two-stage ditch construction. However, this increase is likely a short-term effect that resulted from pre-construction instability and construction efforts before revegetation. It is expected that as the system becomes more stable following construction, the sediment levels will stabilize as well.

2.2.1.2 Embankment Setback

Embankment setbacks are another restoration method aimed at mitigating flood effects while still enabling river processes and maintaining riparian habitats (Figure 2). Pushing back the bank constraints alleviates the pressures exerted on the river from channel stabilization structures and allows for more river processes to occur. These channel processes include migration and cut-off events which enable heterogeneous environments that encourage habitat formation (Larsen et al., 2006).

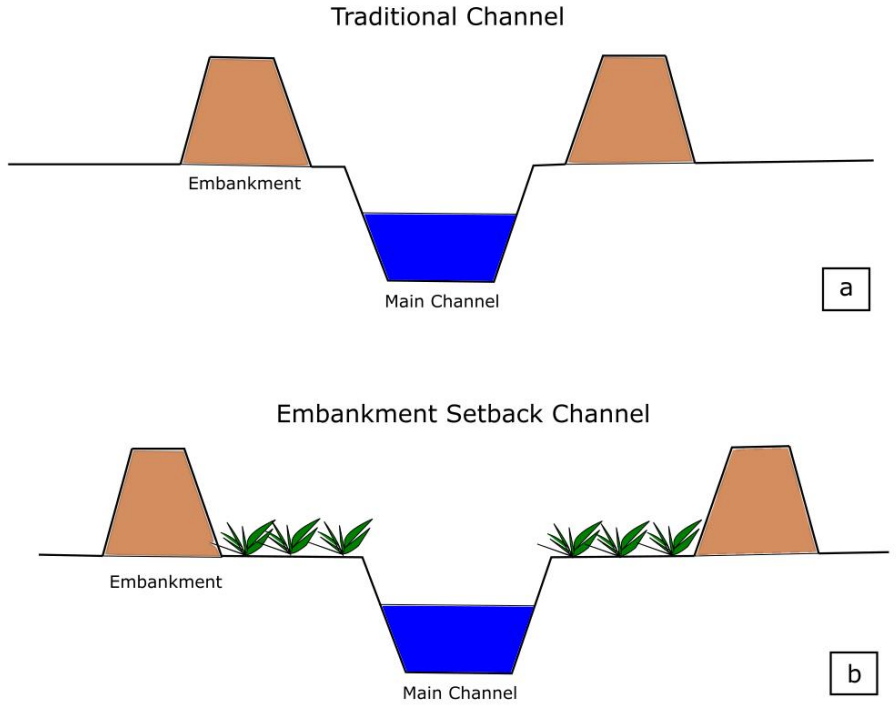

Figure 2. Schematic cross-section of a traditional and embankment setback channel. Channelised channel (Figure 2a) and an embankment setback channel (Figure 2b).

For embankment setbacks to be beneficial, they must enable hydrological connectivity and a variable flow regime by providing a large enough area for these processes to occur. Embankment setbacks allow for reconnection between the floodplain and river channel which allows for increases in overbank and shallow subsurface flow, erosion of floodplains and delivery of sediments to the river channel, and deposition and sediment sorting (Konrad et al., 2008). These processes also allow for an increased area for new vegetation growth.

These benefits of embankment setbacks have been shown in several studies that compare confined river channel sections with those that have been set back. One such example is an investigation conducted on a 28 km stretch of the Sacramento River in California, USA that modelled the

relationship between constraint setback distance and formation of riparian and off-channel aquatic habitat (Larsen et al., 2006). The simulation modelled 100 years of channel migration with embankment setback distances varying from 0.5 to 4 times bankfull width and the results indicated that all setback scenarios result in an increased reworked area compared to the current situation of forced channelisation via riprap. Three river channel migration patterns were observed and included complete cut-off restriction, partial cut-off restriction, and no cut-off restriction, with cut-off restriction referring to the ability of river bend cut-offs to occur via channel migration. Specifically, embankment setbacks of slightly more than one channel-width resulted in a transition from compete cut-off restriction to partial cut-off restriction, while approximately three channel-widths resulted in a transition from partial cut-off restriction to no cut-off restriction. The relationship between increased setback width to increased channel mobility indicates that embankment setbacks are an effective way of enabling river processes.

Another investigation into the effects that embankment setbacks have on river health was conducted along the Puyallup River in Washington, USA, and compared the habitat differences between river reaches with confining embankments and setback embankments (Konrad et al., 2008). Results from this investigation indicated that the reach with setback embankments had a river corridor that was 66% covered by vegetation and 22% by exposed sediment while the reach with confining embankments showed corridor areas were covered by 35-48% exposed sediment. While land cover type is one effect of embankment setbacks, flood velocity distributions are also influenced. The mean velocities between the two reaches were similar, however, the flood velocity cross sections differed with 41% of the setback embankment cross section having velocities less than 1 m/s while only 4% of the confined embankment cross sections had velocities less than 1 m/s. Additionally, there was higher shear stress in the confined embankment river corridor than in the setback embankment reach despite there being a coarser bed in the confined reach. These observed differences in velocity and shear stress were a result of water-surface gradients and mean water depths. The reach with embankment setbacks had a lower water-surface gradient during high flows than normal flows, which reduced the shear stress applied to the riverbed. However, the confined reach had the same water-surface gradient for both high and low flows.

The positive effects that embankment setbacks have on flood impacts, as indicated by the Puyallup River, was further supported by another project on the Sacramento River that evaluated the effects removing an old embankment and constructing 11 km of embankment setback from the river channel 1.6 km would have on flood risk (Opperman et al., 2010). The plan indicated that the setback embankment protected the area from a 75-year recurrence interval flood while the original confining embankment only provided protection from a 10-year recurrence interval flood.

Understanding the potential effects of different restoration techniques is important to assess whether these structured have influenced the environment. This information can then be used during topographic surveys and models to target specific areas where geomorphic change is likely to have occurred. As these are dynamic systems with a variety of distinct features, it is important that an assortment of reliable methods are used to capture these data.

2.3 Monitoring Geomorphic Change and modelling Flood dynamics

River monitoring is fundamental in the determination of whether restoration implementations have been impactful and can be achieved through a variety of different methods. A more recent approach for monitoring fluvial geomorphic change and the associated changes in flood inundation and risks is through the creation of DEMs which are spatial representations of the topography of a given area and

provide a template for analysing potential site-specific events (Passalacqua et al., 2015). DEMs can be created using different high-resolution topographic (HRT) survey methods such as UAV LiDAR, Structure from Motion with Multi-View Stereo (SfM-MVS) photogrammetry, and echo-sounding using an ADCP (Tomsett & Leyland, 2019). These resulting DEMs can then be used as a template in a variety of programmes such as GCD and HEC-RAS.

2.3.1 Topographic Surveys

HRT surveys are important to provide boundary data to characterise or simulate mass and energy transfers such as water, sediment, and nutrients (Passalacqua et al., 2015). Repeat HRT surveys can be used to identify changes in slope, curvature, and roughness, which are all surficial characteristics which affect fluvial processes such as flood events. Transfer of mass and energy can be understood through DEMs by evaluating the changes of results (sediment deposition, bank erosion, vegetation growth) and heterogeneity characterisation (type of vegetation, sediment size and distribution). DEMs are important as they help identify and quantify individual features over a large area (e.g., 1-10 km). Some of these features, such as changes in grain size, are on the scale of millimetres and have only recently become identifiable at DEM scales as a result of HRT survey methods, such as terrestrial laser scanning (Passalacqua et al., 2015).

There is a lot of information provided from DEMs, however, there are also factors that make it important to choose the most appropriate data collection survey type to reflect the project specifics such as channel planform, gradient, and vegetation type and coverage (Bangen et al., 2014; Passalacqua et al., 2015). Accuracy and precision should also be taken into account and the uncertainty permitted should be reliant on the project goals and assessed to determine if the signal of the DEM data is larger than the associated noise (i.e., error) (Passalacqua et al., 2015). There are three types of uncertainties associated with data collection surveys: positional, classification, and surface representation. Positional depends on the sensor precision and scan geometry, classification refers to bare earth extractions such as vegetation and slope, and surface representation includes the resolution and interpolation method. Common sources of error include poor alignment between coordinate systems and elevation models, improper methods of data resampling, erroneous co-registration and flawed classification methods.

It is important to distinguish between two different topographic models that are both categorized as a DEM: a Digital Surface Model (DSM) and a Digital Terrain Model (DTM). While both display a multitude of elevation values for a given area, DSM values include the ground surface as well as any objects on the surface such as treetops and rooftops while DTM values include only the ground surface, using interpolation to remove any objects. When being applied to flood modelling, the preferred topographic model is a DTM as this provides a more realistic measure of the topographic influences on a fluvial event. The topography of the ground surface determines the flood route and therefore it is important that the elevation model be representative of the bare earth surface in situations where vegetation is not significant in controlling flow routing.

2.3.1.1 UAV Lidar

One method of collecting high resolution topography data for DEM creation is UAV LiDAR surveys. These platform/sensor configurations commonly use a pulsed laser to illuminate the Earth's surface, reflect pulses back, and measure the distance with a sensor (Li et al., 2021) although some contemporary UAV LiDAR systems use solid state LiDAR (Štroner et al., 2021). As described by (Gallay & Jozef, 2013), "airborne laser scanning is an active remote sensing technique that uses its own source

of electromagnetic energy to ascertain the characteristics of the land surface". The UAV LiDAR system consists of airborne components such as the laser scanner, airborne platform, and position/orientation system and ground elements such as a global navigation satellite system (GNSS) base station (Wehr, 2009). The base station communicates with the UAV to collect static coordinate data so that the LiDAR location can be correctly identified, and the ground control points increase the accuracy of real-time data (Gallay, 2013; Wang, et al., 2021). A large benefit of these operating system components is that there is no reliance on sunlight for accurate measurements, rather, the accuracy is dependent on variables such as slope angle, flight altitude, GPS signal quality, inertial system, and scanner parameters (Gallay, 2013). Elevation data collected with LiDAR is precise, rapid, and high-resolution (Brede et al., 2017). An example of a UAV LiDAR device is the DJI Matrice 300 RTK drone (Figure 3).

Figure 3: DJI Matrice 300 RTK Drone

Steps for collection of LiDAR data include UAV operation, both preparation and flight, as well as pre-treatment, data accuracy verification, and classification of laser point cloud data (Li et al., 2021). To guarantee that the entirety of the area of interest is captured, field of vision and height of the UAV must be considered as these determine how wide the scanned surface will be (Gallay, 2013). During the flight, an inertial measuring unit (IMU) records the orientation of the scanner and the GNSS receiver records the GPS location. To ensure the survey is as accurate as possible, the IMU frequency should be at least 100 Hz and the location measurement frequency should be at least 2 Hz. A limitation of LiDAR data collection is the inability to acquire bathymetry data below bodies of water. This is due to water adsorbing the infrared pulse from the LiDAR scanner that then prevents reflection of the signal to be recorded from the water surface. Therefore, to encompass topography that is below water into the final analysis, additional bathymetry models need to be undertaken. These are described below in the *Bathymetry Survey* section.

The output of a UAV LiDAR flight is a 3-D representation of the surface that is generated from analysing the difference in wavelengths and laser return times (Li et al., 2021). The LiDAR point clouds consist of both surface and non-surface points; therefore, a filtering algorithm is used to delineate points based on slope parameters which helps accept or reject points based on height differences and classify vegetation. During data processing, the 3D point cloud model is transformed into a DEM, DTM, or DSM.

2.3.1.2 *UAV Photogrammetry*

Another method of gathering high-resolution topographic data to generate DEMs is SfM-MVS photogrammetry, which is a low-cost substitute to LiDAR scanning (Smith et al., 2015) that collects high quality topographic data from aerial imagery via a UAV (Marteau et al., 2017). Similar to the UAV LiDAR system, the UAV photogrammetry system has airborne elements including the laser scanner, airborne platform, and position/orientation system and ground components including a global navigation satellite system (GNSS) base station (Wehr, 2009). The MVS are the algorithms applied to the photogrammetry survey to increase the point density of the point cloud (Smith et al., 2015). While cheaper in cost, the quality of data produced from image-based UAV surveys are similar to those from LiDAR UAV surveys, as indicated by a study by Leitão (2016). With reduced costs, no special expertise necessary, and adequate data quality the collection and processing of topographic survey data is more accessible than it has been in the past (Smith et al., 2015) Additionally, using SfM-MVS allows for the ability to collect topographic data at a variety of spatial scales while maintaining a sufficient resolution (Marteau et al., 2017).

Steps for collection of UAV photogrammetry data collection include pre-flight camera tests, camera calibrations, setting up of ground control points (GCPs), and the actual survey flight (Marteau et al., 2017). The goal of data acquisition is to capture the surveyed area from a variety of viewpoints, ideally with 360-degree coverage (Smith et al., 2015) as good coverage and image quality is important to produce a high-quality model. It is important to be aware during the survey that smooth and reflective surfaces, such as bodies of water, are difficult for SfM-MVS to pick up and usually result in data holes (Smith et al., 2015) and will therefore require additional surveying using bathymetric techniques, similar to what was described in the *UAV LiDAR* section. The main reason for this gap is that turbulence, turbidity, and depth of light penetration all present limits to the SfM-MVS penetration (Marteau et al., 2017). The accuracy of the survey is dependent on the coordinates of the base station and the survey range, as well as the GCPs which need to be easily identifiable to ensure accurate scaling and georeferencing (Smith et al., 2015), usually resulting in cm scale errors. Following the survey, the data is filtered to distinguish between ground surface and other points such as vegetation and buildings and a DEM can then be generated. One shortcoming of the SfM-MVS technique is that the data quality can only be determined after the field visit, rather than during, when any potential issues could be fixed.

2.3.1.3 *Bathymetry Survey*

LiDAR and SfM-MVS are unable to capture the topography of anything covered by water, therefore, in addition to topographic surveys it is necessary to capture the channel bathymetry using different methods that can penetrate the water surface in order to create a comprehensive DEM. A widely used method for this is echo-sounding using an ADCP which is usually attached to a moving boat and RTK-GNSS (Williams et al., 2013). A benefit of acoustic instruments is the versatility of operation, high spatial and temporal sampling resolution, and minimal calibrations required which allows for data collection in areas that are generally expensive and challenging to access with conventional instruments (Muste, 2012). Because of this, ADCPs and other acoustic instruments have influenced the way that morphological and bathymetric data are collected.

Key components of an ADCP include a depth sounder that is connected to a GPS unit which consists of an antenna that receives differential GPS corrections to track the location of each depth measurement (Muste, 2012) (Figure 4). A sound pulse is emitted by the transducer or echosounder which is then reflected back after reaching the channel bottom and the time interval over which this

occurs is used to calculate the water depth. The output of a single beam operation is one coordinate pair with corresponding elevation per signal emanated. The accumulated single beam points from a survey are used to create a two- or three-dimensional representation of the river channel bed which can then be fused with topographic data to create a complete map for use in river models.

Figure 4: ADCP Setup

There are some drawbacks to using ADCPs as they are challenging to deploy in shallow and high-velocity waters and the sampling frequency is somewhat small, with approximately 6% of the area near boundaries going unmeasured (Muste, 2012). However, these obstacles are generally outweighed by the advantages of ADCPs which include speedy deployment and data collection, minimal intrusiveness to the surrounding system, and the ability to obtain micro-scale measurements.

2.3.2 Geomorphic change detection

Determining topographic changes of an area over time is important for understanding past geomorphic processes to both predict site-specific changes (James et al., 2012) and assess whether restoration works have influenced the landscape. As stated by Brasington et al. (2003), "The relationship between river channel form and process is one of sensitive mutual adjustment in which river morphology is both a control and consequence of fluvial processes." This describes a methodological shift that has occurred in recent decades to acknowledge that channel morphology patterns can be used to predict fluvial process rates, and not just vice versa (Brasington et al., 2003). This shift of using form to understand process rather than the other way around is a fundamental change in geomorphology. An example of this is sediment budget analysis which is a main indicator of geomorphic change in fluvial settings since channel morphology is mainly influenced by bedload (Church, 2006). A method of volumetrically calculating the sediment change is by using the DEMs of Difference (DoD) method, which are "spatially distributed maps of elevation changes" (Wheaton, 2008) and involve comparing topographic surveys in order to quantitatively measure changes in geomorphology processes (Williams, 2012). DoDs offer a morphological method of measuring erosion, deposition, and volumetric change as an alternative to using traditional sediment transport

measurement methods (James et al., 2012; Wheaton et al., 2010). Some other useful applications of DoDs include estimating bedload transport rates and bed level fluctuations, assessing fluvial processes such as channel fill and avulsion, determining ecological habitat reduction of disturbance, and validating hydraulic models (Williams, 2012).

An assumption in calculating DoDs is that both maps correctly represent the true morphological qualities of the surveyed areas (Williams, 2012). Therefore, DEM accuracy and co-registration are key factors in ensuring that the DoD results are accurate and consequently, high-resolution survey techniques such as LiDAR and photogrammetry are ideal. There are inherent uncertainties affecting DEMs including sampling, survey precision, topography, resolution, and interpolation; all of which can be amplified through DoDs. Assessments of these uncertainties need to estimate the uncertainty of each DEM, consider the potential expansion of DEM uncertainties into DoD, and evaluate the importance of the identified errors (James et al., 2012).

2.3.3 Flood Modelling

Flood modelling is an integral part of flood hazard and inundation predictions that uses observational data gathered in the field to simulate potential fluvial events. As flooding becomes a growing concern for many populations all over the world, it is increasingly necessary to have reliable methods of generating flood hazard maps based on everchanging and evolving information (Huţanu et al., 2020). Models can be curated for both large- and small-scale areas. It is essential to assess impacts in these types of areas as flooding results in material and economic losses which influences the wellbeing of the population (Huţanu et al., 2020). Correctly representative flood models allow for accurate predictions and effective preventative measures, which subsequently lessens these economic damages (Grimaldi et al., 2019). Some applications of hydraulic models include predictions of flow depth, velocity (Jowett & Duncan, 2011) and shear stress patterns (Reid et al., 2018).

Multiple studies recommend using two-dimensional hydraulic models as part of large-scale flood assessments (Falter et al., 2015; Huang & Hatterman, 2018; Merz et al., 2016;). While one-dimensional models are useful for predicting flood inundation surrounding main channels, two-dimensional models are beneficial when there is varying flow direction, embankment overtopping, and spatially large flow areas (Huţanu et al., 2020). Results from these models include flood extent, which encompasses inundation boundary shapefiles, and flood depth based on depth patterns; both of which vary for different recurrence intervals. From these and other different components, a flood vulnerability assessment can be created to classify hazards associated with different areas. In order to accurately assess two-dimensional hydraulic model predictions, it is first necessary to collect precise and high-resolution field data (Williams et al., 2013) as these are the key controls on the quality of the model outputs (Bates, 2000). As mentioned previously, both LiDAR, photogrammetry, and ADCPs are reliable ways to collect topography and bathymetry data, which are then combined to generate a complete map (Williams et al., 2013). Models are created using mesoscale information (such as grain size) to predict macroscale events (such as flooding inundations).

There are uncertainties associated with all models such as parameters and inputs, therefore it is important to understand the parts of the model effected by these uncertainties so that further assessment can occur and data collection is deployed appropriately (Grimaldi et al., 2019). Uncertainty analyses quantify uncertainties related to model calibration and boundary conditions by comparing how changing these components affects flood inundation projections (Hall et al., 2005). While sensitivity analyses quantify the differences between changing specific parameters, calibration involves fitting the model parameters to improve how the predicted outputs relate to observations.

These model-influencing parameters include channel and floodplain roughness coefficients. An example of a model calibration would be adjusting the bed roughness and comparing predicted model results such as a flood inundation to actual flooding extent based on satellite images. These assessments help improve accuracy of model parameters, however, there are multiple possible models that give similar results, and this must be noted as a limitation of calibrating hydraulic models. The overall goal of calibration and validation is to identify areas where there is uncertainty and determine if those have a large contribution to the model.

2.4 Summary

While it appears that two-stage channel design and embankment setbacks have potential for river restoration of incised channels, there is a lack of widespread knowledge on how different types of river environments will respond to this restoration method. Of the above-mentioned studies, all are on rivers located in the United States, mostly on the West Coast, and two are on the same river (the Sacramento River), representing a very small sample pool. The River Nith in Scotland represents a river in a different environment with a much longer history of channelisation. Investigating the impact that embankment setbacks have on a Scottish river will increase the understanding of the effects that these river restoration techniques have on flood hazards while allowing for applications of these techniques to potentially be expanded to new locations.

The data collection methods used in this thesis include LiDAR and echo-sounding via an ADCP and, while the topographic surface representations produced have a variety of potential uses, they are fundamental for providing topographic boundary data for flood models. These topographic surveys were used to help determine important factors in flood prediction on the River Nith such as shear stress and flow direction, both of which influence the flood intensity and inundated area (Li et al., 2021). With climate models forecasting an increase in local flooding in the coming years (Hirabayashi et al., 2021), the following investigation on the River Nith represents a meaningful evaluation on the effectiveness of two-stage channel design and embankment setbacks to restore incised rivers and potentially contribute to mitigating climate change impacts.

3 Study Area

3.1 Scotland

The hydrology of Scotland is characterised by high elevation areas in the west and lowlands in the east, each with an average annual precipitation of 3,000 mm and 800 mm, respectively (Scotlandinfo.eu, 2022; Soulsby et al., 2002). Evapotranspiration rates are much lower, ranging from 350 to 400 mm/year (Soulsby et al., 2002). As a result of this high net-amount of water, there is an abundance of rivers in Scotland, over 6,000 in total, and a total stream length of more than 100,000 km (Mackay et al., 1998; SEPA, 2007; Smith & Lyle, 1994). The flow regimes of these rivers are characterised by high runoff per unit area, which results in "flashy regimes" from the combination of steep slopes and thin podzolic soils (Gilvear et al., 2002).

Climate change is predicted to affect the hydrology of Scotland through wetter winters, with winter precipitation potentially increasing by 5% in the UK (Gilvear et al., 2002). The increased precipitation will increase flood magnitude, frequency, and seasonality in Scottish rivers (Black & Werrity, 1997; Sargent & Ledger, 1995; Steel et al., 1999) which will subsequently increase channel instability, bank erosion rates, channel incision, channel shifting, and bedload transport rates (Gilvear et al., 2002). Additionally, rivers in Scotland are highly engineered which limits the mobility of a river and inhibits channel-floodplain connectivity (Mondal & Patel, 2018). Channelisation prevents rivers from geomorphically adjusting to increased flow (as predicted by climate change) and this lack of lateral mobility negatively impacts bank stability and enables incision. These combined effects highlight the need for sustainable flood management, such as two-stage channel design and embankment setback, to mitigate climate change impacts.

3.2 Upper Nith Catchment

The River Nith is a 70 km long river (Duck, 2011) with a total catchment size of approximately 1,200 km^2 (NDFSB, 2008) located in south-western Scotland, traveling from its headwaters located in the Carsphairn Hills of East Ayrshire, south through Dumfries, and into Solway Firth (Figure 5). It has been calculated by Geikie (1868) that approximately 112,000 to 120,000 cubic yards of sediment are deposited annually into the Solway Firth solely via the River Nith (Duck, 2011; Geikie, 1868) While the lower section of the Nith has a history of severe flooding (McDonald & Ledger, 1981), flood embankments and engineered channel structures in the upper portion contribute to channel constriction and flood hazards further downstream. As with most rivers in the UK, the flow patterns of the Nith are largely influenced by seasonal temperature variations rather than seasonal precipitation variations, although there is a modest tendency towards an autumn/winter precipitation maxima. This is due to the increased temperature and associated evaporation rates in the summer coupled with generally consistent rainfall (NRFA, 2022a).

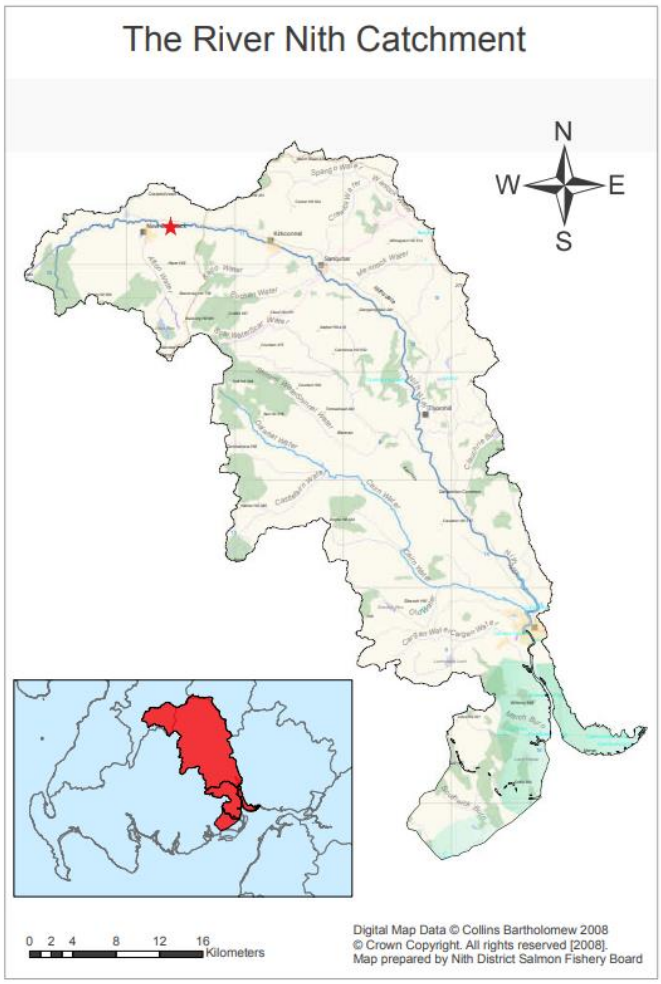

Figure 5: Map of Nith catchment area (NDSFB, 2008) with red star in northwest corner indicating the study site. The inset map shows the south-west part of Scotland.

While exact records of historical channelisation on the River Nith are difficult to retrieve, farmlands have lined either side of the Nith for centuries, and embankments have therefore been in place for a similarly long time to protect the lucrative land from damage by erosion and flooding. There are several engineering documents that suggest channelisation has been ongoing since at least the mid-1800s (Newall, 1847; Stevenson & Stevenson, 1861). These civil engineering plans detail proposed construction for sections of the river located outside of the study area but can be used to generalize when channelisation was occurring. Additionally, river relocation for the purpose of coal mining occurred as recently as 2000 (Flatley, 2018). This construction was near the study site, just outside of New Cumnock.

In the mid-1990s the World Wildlife Fund (WWF) started a "Wild Rivers" initiative which aimed to restore rivers through catchment-based methods (Griffin et al., 2015). This initiative was recognized by the Scottish Natural Heritage (SNH) during a review of catchment management (Griffin et al., 2015). In 2012, the River Nith was identified by SEPA as a pilot catchment, meaning it would be prioritised for restoration work (CBEC, 2015) with the goal of progressing the area to fit the Water Framework Directive definition of "good ecological status" and to improving natural flood management (CBEC, 2013). Less than 15% of UK rivers are considered to have a natural flow regime and the section of the River Nith near New Cumnock was categorized as having a "poor" morphological status as a result of "extensive embankments upstream of Hall Bridge, preventing lateral interaction with floodplain and

promoting over-deepening" (CBEC, 2013; NRFA, 2022a). These embankments are also associated with hard bank protection, another prevalent pressure on river morphodynamics for this part of the river (CBEC, 2013). Therefore, restoration on this segment was deemed a preferred option to less impacted segments, and it was determined embankment removal and setback would provide multiple benefits such as increasing the ecological status and reducing flood risk (CBEC, 2013). For the purpose of this study, both embankment setbacks and two-stage channel design restoration works were looked at collectively, rather than individually, as both designs are methods for increasing floodplain size that were co-implemented as part of the restoration scheme. The construction of restoration works was completed for Phases 1 and 2 in late 2019 and mid-2020, respectively. A map of the sections restored during Phases 1 and 2 indicates where embankments were setback (Figure 6). An example of this change can be seen at the upper portion of Phase 1 where the setback embankment has allowed for a point bar to form (Figure 7). For Phase 1, the embankments on river-right were setback while the river-left embankments were unchanged and for Phase 2, embankments on both side of the channel were setback. The intention of this work was to help alleviate flood impacts by allowing for more floodplain connectivity and lateral mobility. Therefore, this study area provided an ideal setting to conduct topography and bathymetry surveys, assess topography changes using software such as GCD, run flood models through HEC-RAS using the newly created DEMs and ultimately evaluate the flood model outputs to establish if the restoration work was effective and if change has occurred from pre-restoration in 2019 to post-restoration in 2022.

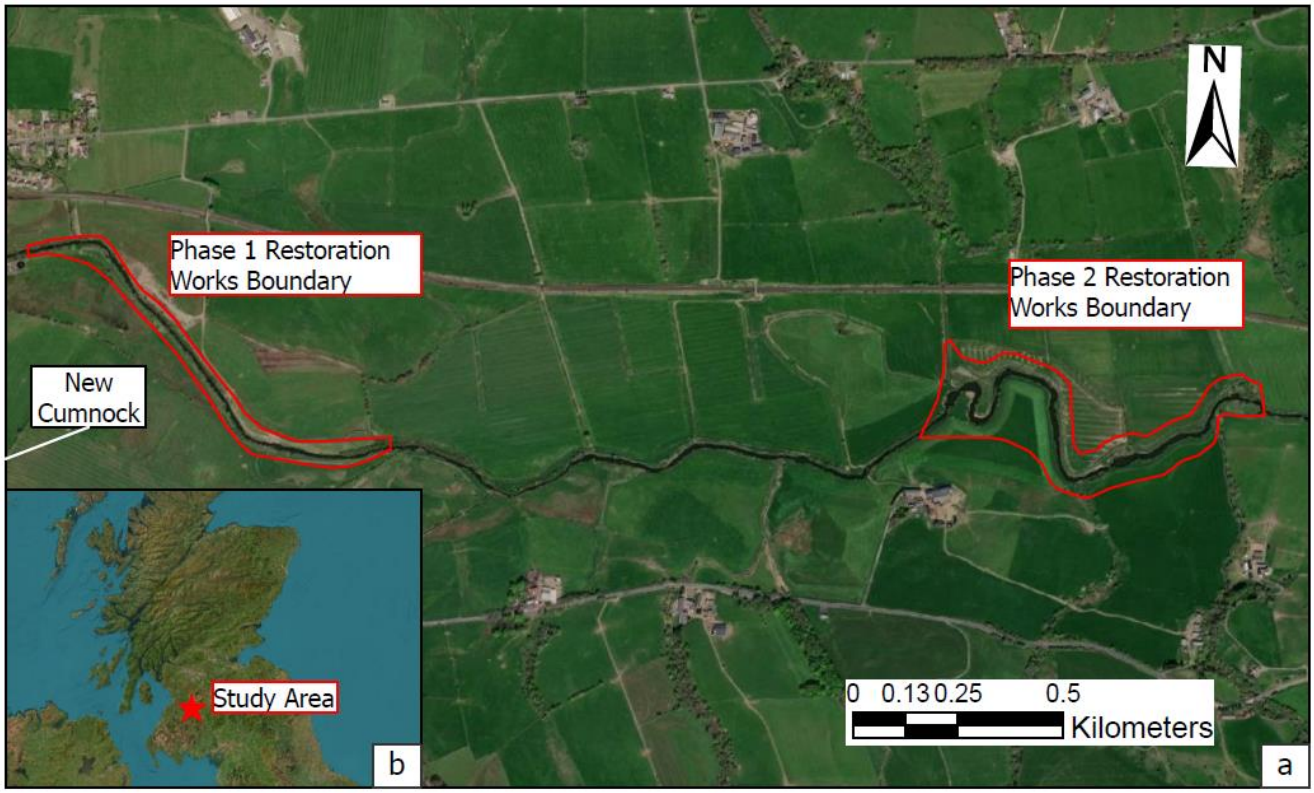

Figure 6. Study site and restored area boundaries. Red boundaries indicate areas restored for both Phase 1 and 2 (Figure 6a). Red star indicates where the study area is in Scotland (Figure 6b).

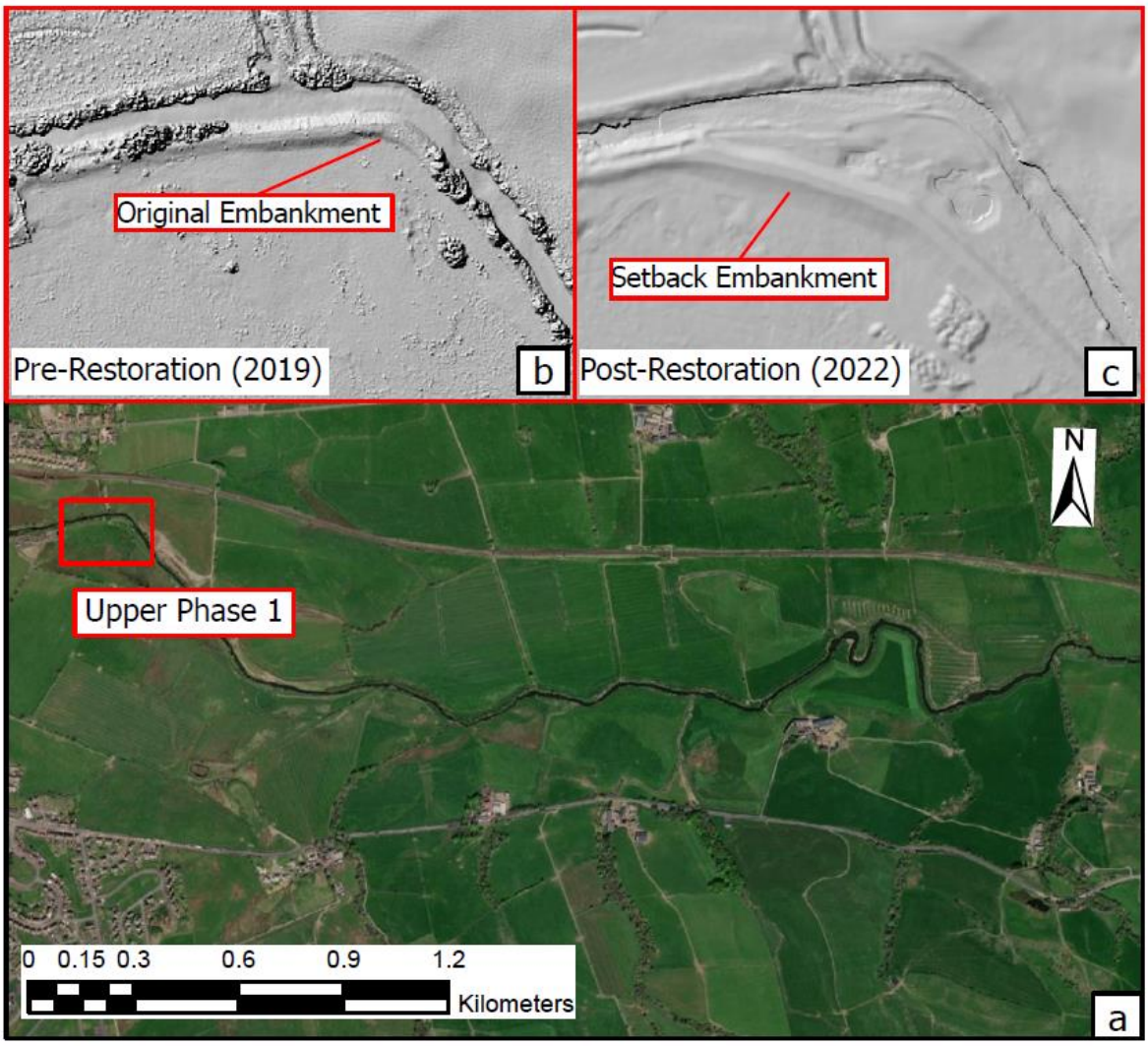

Figure 7. Study site and upper Phase 1 embankment setback. Red boundaries indicate upper Phase 1 embankment setback and the associated, newly formed point bar (Figure 7a). Pre-restoration location of the embankment (Figure 7b). Post-restoration location of the embankment (Figure 7c). The DEMs in Figure 7b and Figure 7c were generated as part of this thesis, the processes of which are described in the Methodology section.

4 Methodology

4.1 DEM Construction

Two DEMs were created to represent the topography of Phases 1 and 2 both pre-restoration and post-restoration using a combination of topographic and bathymetric surveys conducted over various time periods, which are shown in Table 1. A description of these surveys and collection methods are provided below.

Table 1. Surveys used in this investigation. Type of survey (bathymetry or topography), year the survey was conducted, organisation that conducted the survey, method (LiDAR, RTK-GNSS, or ADCP) and whether the survey covered Phases 1 or 2.

Survey	Year	Organisation	Method	Phase
Bathymetry	2019	CBEC	RTK-GNSS	1
Topography	2019	Digimap	Airborne LiDAR	1 & 2
Bathymetry	2020	University of Glasgow	RTK-GNSS	1
Topography	2020	University of Glasgow	RTK-GNSS	1
Bathymetry	2022	University of Glasgow	RTK-GNSS	1 & 2
Bathymetry	2022	University of Glasgow	Echo-sounding with ADCP	2
Topography	2022	University of Glasgow	UAV LiDAR	1 & 2

4.1.1 Previous Surveys

Archived data from previous topography and bathymetry surveys were incorporated into the construction of both pre- and post-restoration DEMs. The first was a bathymetry survey of Phase 1 conducted by CBEC in March 2019 using RTK-GNSS equipment. Another survey of the Phase 1 bathymetry was completed in September 2020 by the University of Glasgow and used Leica GS10 RTK-GNSS equipment to survey both the channel bathymetry as well as that of the adjacent topography.

The topographic data used for the pre-restoration DEM were sourced from Digimap, an online UK-based map and data delivery service. The chosen data were a LiDAR point cloud of a composite DTM at 50 cm resolution for the Phase 4 Scotland Survey that was conducted between 2017 and 2019 (Digimap, 2020a & Digimap, 2020b).

4.1.2 Topography

UAV LiDAR surveys were conducted over the River Nith floodplains where the Phase 1 and 2 SEPA restoration works were completed (Figure 8) with the goal of collecting topographic information to represent the post-restoration landscape. Specifically, these surveys used conventional infrared LiDAR, a key limitation of which is the inability to penetrate water surfaces (Gallay, 2013). The process of collecting LiDAR data included flight preparation tasks, operation of the UAV by a trained professional, verification of the data accuracy, and organization of laser point cloud data (Li et al., 2021). These surveys used the DJI Matrice 300 RTK drone (Figure 3) which weighs up to 9 kg on take-off with the DJI Zenmuse L1 solid state LiDAR sensor attached. The aircraft flew at 70 m above the take-off location and at approximately 10 m/s when collecting LiDAR data at a rate of up to 160 kHz, with up to three returns from a single outgoing measurement. The LiDAR sensor unit was mounted on a three-axis gimbal, and the position of each LiDAR point measured is calculated during the flight using data from the onboard GNSS receiver and high-accuracy inertial measuring unit (IMU) (Gallay, 2013).

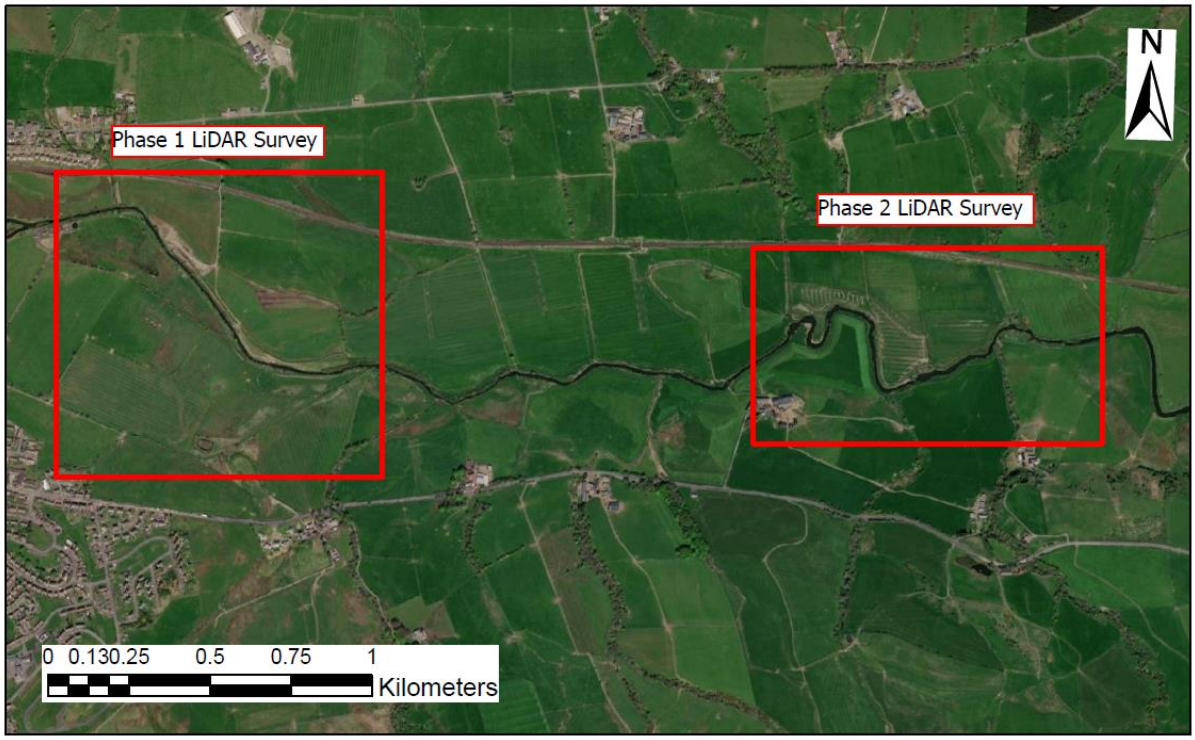

Figure 8. UAV LiDAR survey boundaries. Red boundaries indicate UAV LiDAR surveys that were conducted in 2022 over Phases 1 and 2.

A total of 36 ground control targets were positioned with RTK-GNSS over a total survey area of 1.6 km^2. For Phase 1, a total of 19 GCPs were used over 0.95 km^2 and for Phase 2 a total of 17 GCPs were used over 0.65 km^2. Resulting data from the UAV LiDAR surveys were in the form of a point cloud, which was then filtered to distinguish ground points from non-ground points. This was done using the Multiscale Curvature Classification (Evans & Hudak, 2007) algorithm through the lidR library within R software (Roussel & Auty, 2022; Roussel et al., 2020). The resulting ground classified points were interpolated using the Topo to Raster tool (with no hydrological corrections) in ArcGIS Pro (Hutchinson & Gallant, 2000) creating a DEM of 0.5 m resolution.

In addition to the UAV LiDAR surveys, SfM-MVS surveys were conducted over the topography of Phases 1 and 2, with a total of 10 GCPs each, for a much smaller area than the LiDAR surveys. These additional surveys used the DJI Phantom 4 RTK drone and were carried out to provide an assortment of data to choose from for flood modelling inputs. Imagery data collected from these surveys were processed using Pix4D software to produce a Digital Surface Model (DSM) and Orthomosaic. There were a total of 2293 and 1863 images produced from the Phase 1 and 2 surveys, respectively and, using Pix4D, these were geolocated by identifying and processing the ground control points and corresponding coordinates.

4.1.3 Bathymetry

While LiDAR is an ideal method capturing dry topographic data, these surveys are unable to obtain bathymetry data for water-covered areas because the infrared pulse from the LiDAR scanner is adsorbed by water (Gallay, 2013; Smith et al., 2015). Therefore, a separate bathymetry survey was necessary and involved using ADCP and RTK-GNSS techniques.

The upper portion of Phase 1, just downstream of the wastewater treatment plant to where the point bar currently is (Figure 7), was surveyed during the 2022 field event using RTK-GNSS. The equipment

used included a Leica GS10 base station, which featured an AS10 antenna, radio link with GS16 antenna and CS20 controller (Figure 4). The handheld RTK-GNSS equipment used to measure topography points in the channel and surrounding areas was the Leica System 1200, which included a GS08 antenna and CS10 controller. Collecting bathymetry data this way allowed for a higher density of points than would be feasible with just the ADCP alone. As this area was considered to be the most geomorphically variable, extra precision was necessary.

The section of channel, downstream from Phase 1 through the end of Phase 2, is considered less geomorphically-active and had never been surveyed prior to 2022. As this length of river is approximately 3 km long, the most efficient survey method was determined to be the ADCP, supplemented by manual RTK-GNSS measurements in shallow areas. The instrument used was the Sontek M9, a single-beam ADCP instrument that is remote controlled, attached to a moving boat, and connected to RTK-GNSS. While this instrument has the capability to measure water column velocity, for the purpose of this investigation just the echo-sounding features were used for topographic measurements. This hands-off method allowed for efficient profiling of the channel bathymetry and was an improvement from past techniques involving pulling the boat across the river channel via a rope.

Once the bathymetry points were collected, the ADCP and RTK-GNSS data points from 2022 and previous years needed to be merged together to form one cohesive bathymetry surface. With the combination of multiple surveys and methods used to collect bathymetry data, determining which interpolation technique best represents the actual topography was important. Triangular Irregular Networks (TINs) join measured data points together using triangles and, while there are different ways of doing this, the most common technique is Delaunay Triangulation which searches for Thiessen neighbours to create the most realistic triangles. Each triangle surface defines the value of all nodes within (Fuller & Hutchinson, 2007). An advantage of using the TIN method is that it can manage fluctuations in data density and incorporate break lines. Additionally, it only uses actual measured values to create the triangles, which is beneficial for accuracy purposes but can have uneven spacing that results in unrealistic bathymetry depictions. Another interpolation method is Kriging, which uses weighted least squares (Fuller & Hutchinson, 2007) geostatistical interpolation to assign values to the area between measured points. Kriging develops a variogram specifically for the data set which then determines the weights used and subsequently characterises the spatial variability (Chappell et al., 2003; Fuller & Hutchinson, 2007). Data points closer to the node are assigned a larger weight since there is a higher probability the values are similar (Curran & Atkinson, 1998; Fuller and Hutchinson, 2007). For this project, the high point density of the 2019, 2020, and 2022 surveys of Phase 1 allowed for the TIN method to be uniformly applied. For the ADCP survey downstream of Phase 1 through Phase 2, it was decided that both interpolation methods would be used, with TIN applied to the whole of the bathymetry and Kriging then inserted in areas where the TIN created unrealistic bathymetry. The determination of which bathymetry was feasible was based on knowledge of both the field site as well as fluvial geomorphological processes. An example of this process is shown in Figure 9.

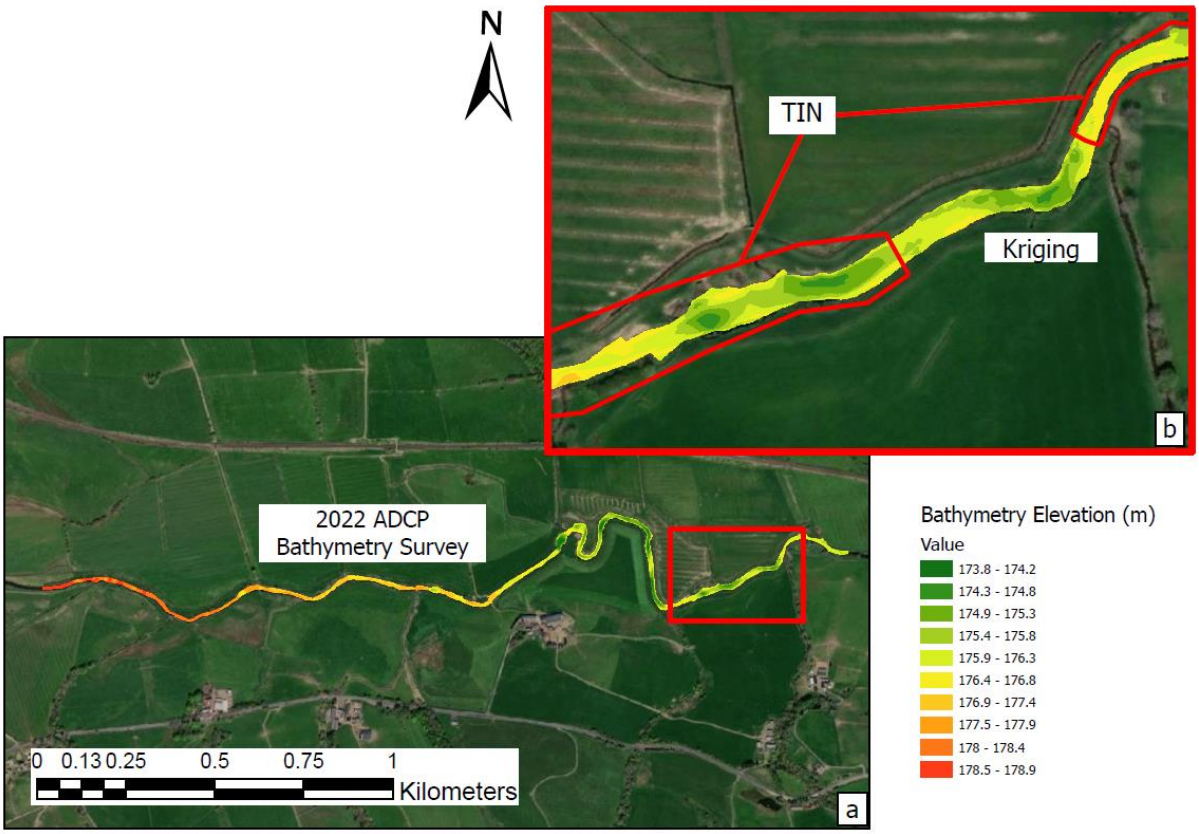

Figure 9. Bathymetry method combination example. Extent of 2022 ADCP bathymetry survey and associated elevations used in raster compilation (Figure 9a). Example of how both TIN and Kriging methods were used in the final bathymetry product (Figure 9b).

4.1.4 DEM Compilation

The pre-restoration DEM merges Digimap Airborne LiDAR and bathymetry survey data from both 2019 and 2022, as shown in Figure 10. While the Digimap survey was collected from 2017-2019 and the restoration works were conducted from June through August 2019, the Digimap Airborne LiDAR data shows the old embankment, indicating the topography data was collected prior to the restoration work and is therefore applicable for use in the pre-restoration DEM. A discrepancy between this survey and the surveys conducted in 2022 was the lack of filtering completed to remove non-bare-earth surfaces such as rooftops and trees. While it would be preferred for these items to be removed, it is clear between DEMs where these objects are located and easy for them to be excluded from most analyses. For example, in the DEM comparison, areas presenting large elevation differences (on the scale of meters) were ignored as these could be attributed to trees and houses. The bathymetry data for Phase 1 was created using data from a March 2019 bathymetry survey conducted by CBEC prior to the restoration construction. This survey extended to the downstream portion of Phase 1; however, it did not cover Phase 2 or the gap between Phases 1 and 2. Consequently, the ADCP survey conducted in 2022 was used for the pre-restoration channel bathymetry of these areas. While this data was collected significantly after the restoration works were completed, these areas are considered to be less active than the upstream area that encompasses Phase 1 and it is unlikely that significant morphological change has occurred within the channel here. Because of this and the lack of previous data, the decision was made to incorporate the 2022 ADCP channel data downstream of Phase 1 into both pre-restoration and post-restoration DEMs.

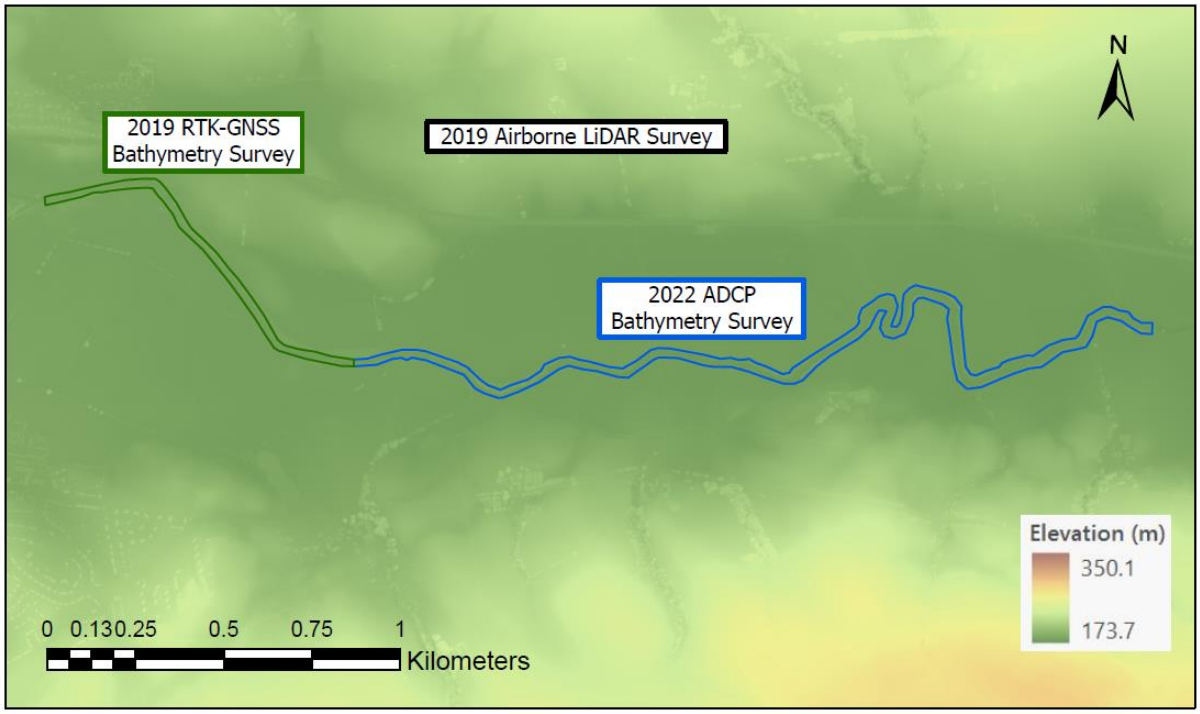

Figure 10. Different input layers of the pre-restoration DEM. Background obtained from the 2019 Digimap Airborne LiDAR survey. Green and blue boundaries represent areas that used data from the 2019 RTK-GNSS and 2022 ADCP surveys, respectively.

The post-restoration DEM merges 2019, 2020, and 2022 LiDAR and bathymetry data (Figure 11). For the topography of Phases 1 and 2, UAV LiDAR data collected from the 2022 field events was used. This data was chosen over the SfM-MVS data collected because it encompasses more area and has a higher accuracy, both of which are important for generating reliable flood models. Additionally, UAV LiDAR was the preferred method as it would provide continuity with the 2019 Digimap Airborne LiDAR survey.

The original UAV LiDAR survey area of Phase 1 was reduced to account for the drone losing connection with the RTK-GNSS in the northeast corner of the survey. This area was removed from the 2022 DEM, as it was not in the proximity of the active channel area the results were not affected by this. The total areas used from the 2022 UAV LiDAR surveys were 0.63 km^2 and 0.54 km^2 for Phases 1 and 2, respectively. Since there were no construction activities completed in the area between Phases 1 and 2, it was expected that the topography here had changed minimally over the last few years and, therefore, the 2019 Digimap Airborne LiDAR data that was used in the pre-restoration DEM was used again in the post-restoration DEM. Bathymetry for Phase 1 was a combination of both 2020 and 2022 RTK-GNSS data. The upper portion of Phase 1 is considered highly variable due to the substantial embankment set back, which allows for more movement from the river as is evidenced by the present point bar. Therefore, manual RTK-GNSS measurements from 2022 were used for this part of the DEM to obtain a higher density of measured points than is achievable with the ADCP. Downstream from this area, the river is more channelised, and it is therefore unlikely that substantial geomorphic changes have occurred here. Considering this, as well as the time it would take to conduct an RTK-GNSS survey over this length of river, it was determined that the lower portion of Phase 1 would not be re-surveyed in 2022. Instead, RTK-GNSS survey data from a 2020 field event was deemed appropriate to use for the post-restoration DEM and, while not as recent as a 2022 survey, this data was still collected post-construction.

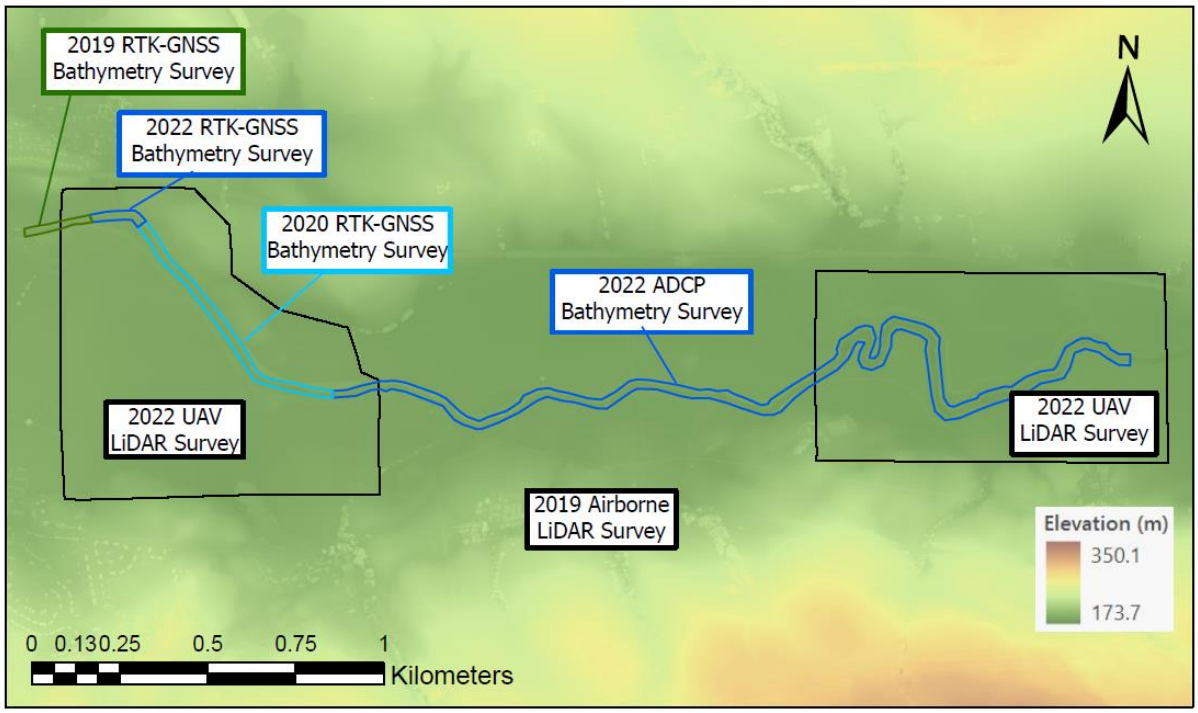

Figure 11. Different input layers of the post-restoration DEM. Background obtained from the 2019 Digimap Airborne LiDAR survey. Black boundaries indicate the areas used from the 2022 UAV LiDAR surveys of both Phase 1 and 2. Green, light blue, and blue boundaries indicate the bathymetry surveys (RTK-GNSS and ADCP) from 2019, 2020, and 2022.

4.2 Geomorphic Change Detection

Calculating geomorphic change is important for establishing the topographic changes that have occurred in a specific area to understand past and present geomorphic processes (James et al., 2012). Specifically, DoDs help identify geomorphic processes such as erosion and deposition, that can then be used to determine shifts in fluvial processes that are revealed from hydraulic models that use different topographic boundary conditions (Williams, 2012).

To calculate the geomorphic change that occurred in Phases 1 and 2 between 2019 and 2022, it was necessary to create a DoD map, which is a product of subtracting the old DEM from the newer, most recent DEM (Williams, 2012) and indicates areas of surface lowering and surface rising. To distinguish between changes associated with geomorphic and anthropogenic processes, erosion and deposition will refer to geomorphic changes while cut and fill will refer to anthropogenic changes. The standard way of determining the error associated with DODs is by determining the signal to noise ratio, which is a method of analysing error that involves relating the variability due to geomorphic change to that caused by error (Williams, 2012). GCD Software was used to create the DoD map. This software is available as an ArcMap add-in or standalone version. For this investigation the standalone version of GCD was used in conjunction with ArcGIS Pro for post processing.

The GCD was run to create DoDs for two separate areas: Phase 1 and Phase 2. The inputs for running the Phase 1 and Phase 2 DoD included the two DEMS (2019 and 2022) and an error mask polygon for each. The area in between Phase 1 and Phase 2 was excluded from the GCD analysis as the data used to construct this region is the same in both DEMs (e.g., 2019 LiDAR (dry area) and 2022 bathymetry (wet area)).

Each of measurement techniques (LiDAR and ADCP derived bathymetry) have their own unique error, and in many cases the magnitude of geomorphic change is similar to the magnitude of uncertainties associated with each instrumental measurement. Therefore, error masks had to be used to account for these measurement errors to confirm that the change we observe in the DoD is real geomorphic change. The errors for the different LiDAR surveys, are shown in Table 2. Every individual LiDAR survey has a unique associated error, therefore there are three different errors associated with the 2019 Digimap Airborne LiDAR survey, 2022 Phase 1 UAV LiDAR survey, and 2022 Phase 2 UAV LiDAR survey. A previous investigation into the accuracy of different topographic survey methods by Bangen et al. (2014) found that the standard deviation of error for RTK-GNSS is 0.1 m when used to survey wetted channel areas and streambanks. Therefore, because some of the previous surveys had unknown error values, a uniform error of 0.1 m was used for all bathymetry surveys (RTK-GNSS and ADCP) for consistency. These error values were applied to an error mask for each phase and year, giving a total of four different masks.

An active river area polygon was created to define the processing extent for both Phase 1 and 2 (Figure 12). This area, which included the topography within the channel area as well as outside of the restored embankments on either side of the channel, represents the portion of river channel and surrounding floodplain where both geomorphic change (e.g., river processes) and topographic change (e.g., anthropogenic cut and fill processes) were likely to have occurred between 2019 and 2022.

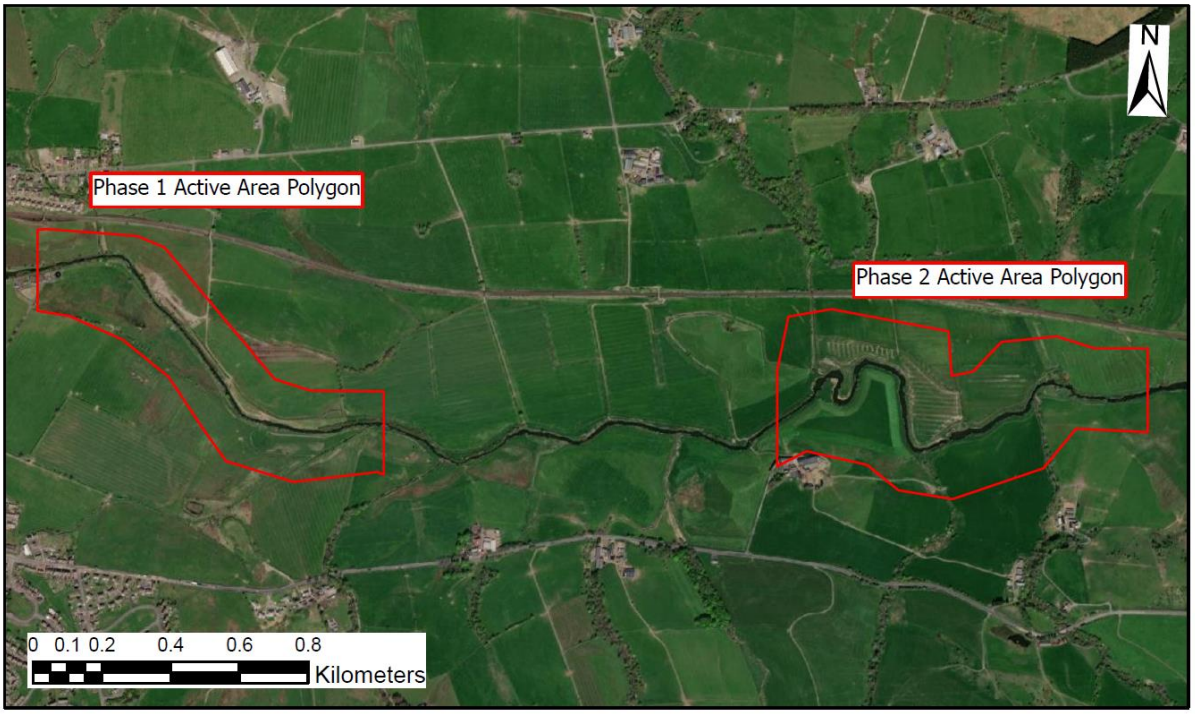

Figure 12. Active area polygons. Red boundaries indicate active area polygons that were applied to Phases 1 and 2 in the GCD software.

Table 2. Error values applied to the GCD error masks for each survey.

Type	Survey	Error (m)
Airborne LiDAR	2019 Digimap	0.060
UAV LiDAR	2022 Phase 1	0.060
UAV LiDAR	2022 Phase 2	0.093
RTK-GNSS	2019 CBEC	0.1
RTK-GNSS	2020 University of Glasgow	0.1
RTK-GNSS	2022 University of Glasgow	0.1
ADCP	2022 University of Glasgow	0.1

The method of GCD analysis used was probabilistic thresholding at confidence intervals from 65% to 95% with 5% differences between analyses. This method was chosen over a variety of other processing variations including basic DEM differencing, minimum level of detection, and error propagation which involve simply subtracting the elevation values of one DEM from another, applying a uniform minimum detection level to the DEMs as a whole, and applying minimum detection levels on a cell-by cell basis (Wheaton et al., 2010). Probabilistic thresholding takes this one step further and determines the probability of the change being real (Wheaton et al., 2010).

4.3 Hydraulic Flood Modelling

Two-dimensional models are instrumental for predicting flood inundation in situations where there is the potential for embankment overtopping, significant flow areas, and differing flow directions over floodplains (Huţanu et al., 2020). One of the most widely used flood modelling programs is HEC-RAS, which has been developed by the U. S. Army Corps of Engineers (Huţanu et al., 2020). HEC-RAS is commonly used to evaluate small-scale and medium-scale catchment areas susceptible to flooding (Huţanu et al., 2020). The HEC-RAS flood modelling program was used to evaluate the varying flood potential of the upper River Nith both prior to and following the SEPA restoration works; using the DEMs created for 2019 and 2022.

The 2D model setup includes importing topography and bathymetry data (2019 and 2022 DEMs), setting boundary conditions for both the inlet and outlet, adjusting parameters (resolution, breaklines and Manning's roughness coefficients), and defining the input flow conditions. The projection was set to British National Grid to align with the projections used during the field surveys. Geometry features applied were perimeters and breaklines for the 2D flow area and boundary condition lines (Figure 13). The perimeter area included the channel of Phase 1, Phase 2, the area in between, and a substantial amount of surrounding flood plains, totalling 3.59 km^2 (Figure 14). The resolution of the flow area was set to 2 m x 2 m to allow for a reasonable model runtime while retaining significant detail. A higher resolution of 1 m x 1 m was applied to the channel via breakline, repeating outwards for 6 m on either side of the breakline to encompass the average channel width.

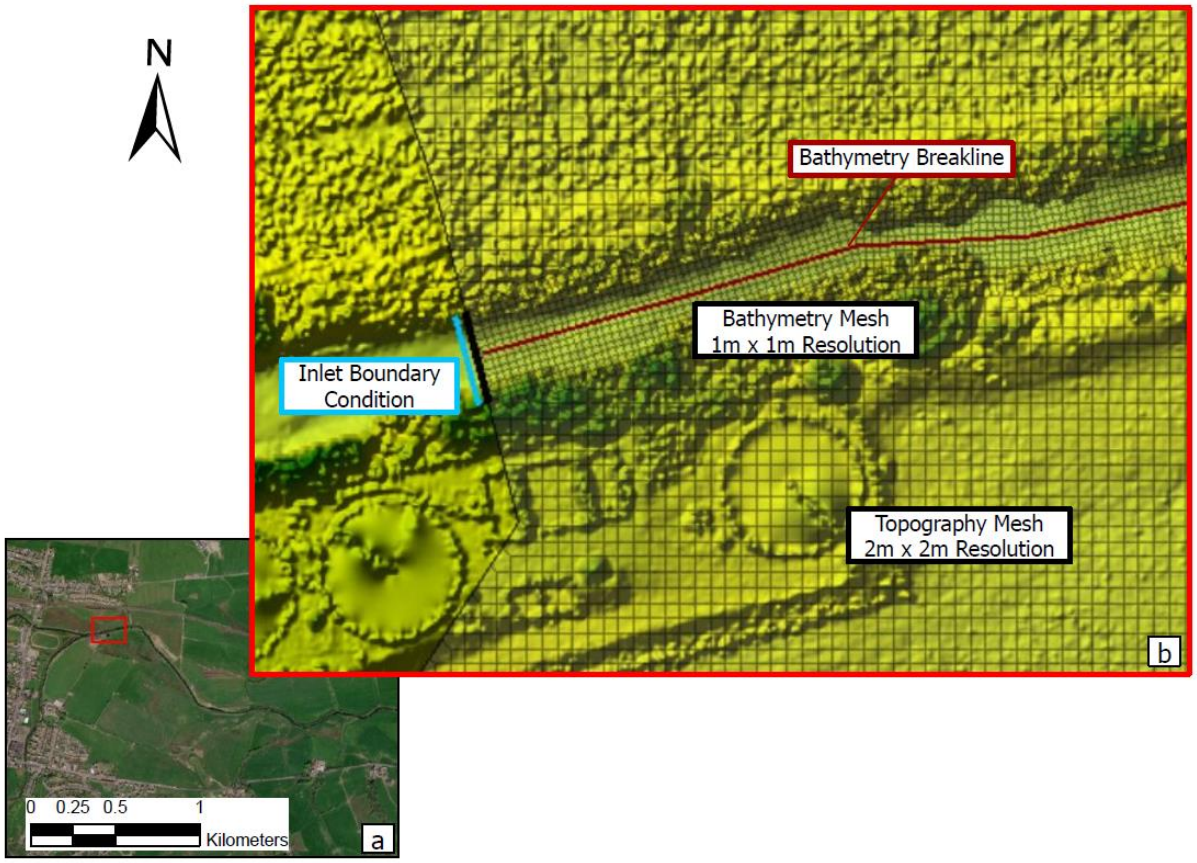

Figure 13. Example of HEC-RAS input parameters at the model inlet. Red boundary indicates the HEC-RAS model inlet within the study site (Figure 13a). Different components of HEC-RAS, such as the inlet boundary condition, bathymetry breakline, and bathymetry and topography mesh layers with associated resolutions (Figure 13b).

A uniform Manning's roughness coefficient of 0.03 was applied across the DEM, and this was determined based on both grain size measurements from the Nith and knowledge of land use type. The cumulative grain-size distribution, which ranges from 52 to 8 mm, falls within the size range for gravel of 2 to 64 mm which has a corresponding Manning's roughness coefficient of 0.028 to 0.035 (Arcement Jr. & Schneider, 1989). The surrounding floodplain was categorized as National Land Cover Database (NLCD) type 82 which corresponds to cultivated crops and has a Manning's roughness value range of 0.020 to 0.05 (USACE, 2022a). Due to the similar range in potential Manning's roughness values, a coefficient of 0.03 was applied to the entire model.

Boundary lines just outside of the perimeter were added across the channel width on both the upstream and downstream ends of the model area. These lines are drawn from left bank to right bank and indicate the inlet and outlet of the hydraulic boundary. This final component of the geometry allows the flow files to run through the model.

Flow files were created to define the conditions of the hydrograph that would be applied to the model. The boundary condition of the outlet was set to "Normal Depth" and a channel friction slope value of 0.00074 was applied after being measured in RAS Mapper. Setting a slope at the outlet is necessary for the flow to realistically exit the model rather than building up and impacting results. The boundary condition of the inlet was set to "Flow Hydrograph". Flow values for the inlet conditions were calculated by applying the annual maximum discharge data collected at the Hall Bridge SEPA gauging station (NRFA, 2022a) on the River Nith from 1960 through June 2022 to a Gumbel distribution curve (Figure 15). The project catchment size is approximately 116 km^2 while the total catchment area of the

Hall Bridge station is 155 km^2, as calculated from the UK Center for Ecology and Hydrology's National River Flow Archive (NRFA, 2022b), and therefore the calculated discharges were reduced by 25% to reflect this ratio and provide discharge values associated with the Hall Bridge catchment. Discharges corresponding with 1-, 2-, 5-, 10-, 20-, 50-, and 100-year flood recurrence intervals (RIs) were applied and are shown in Table 3. To reduce model instability, a gradual increase in discharge was applied until the discharge reached the desired return interval discharge, this combination will be referred to as "quasi-semi-state". These were then applied separately to the pre-restoration and post-restoration DEMs, resulting in a total of 14 model scenarios. The hydrograph duration was set to 24 hours to allow time for the flow to stabilize.

Table 3. Recurrence intervals of floods modelled in HEC-RAS and associated discharge rates, calculated from the Gumbel Distribution Curve.

Recurrence Interval (years)	**Discharge (m^3/s)**
1	11
2	41
5	54
10	63
20	72
50	82
100	91

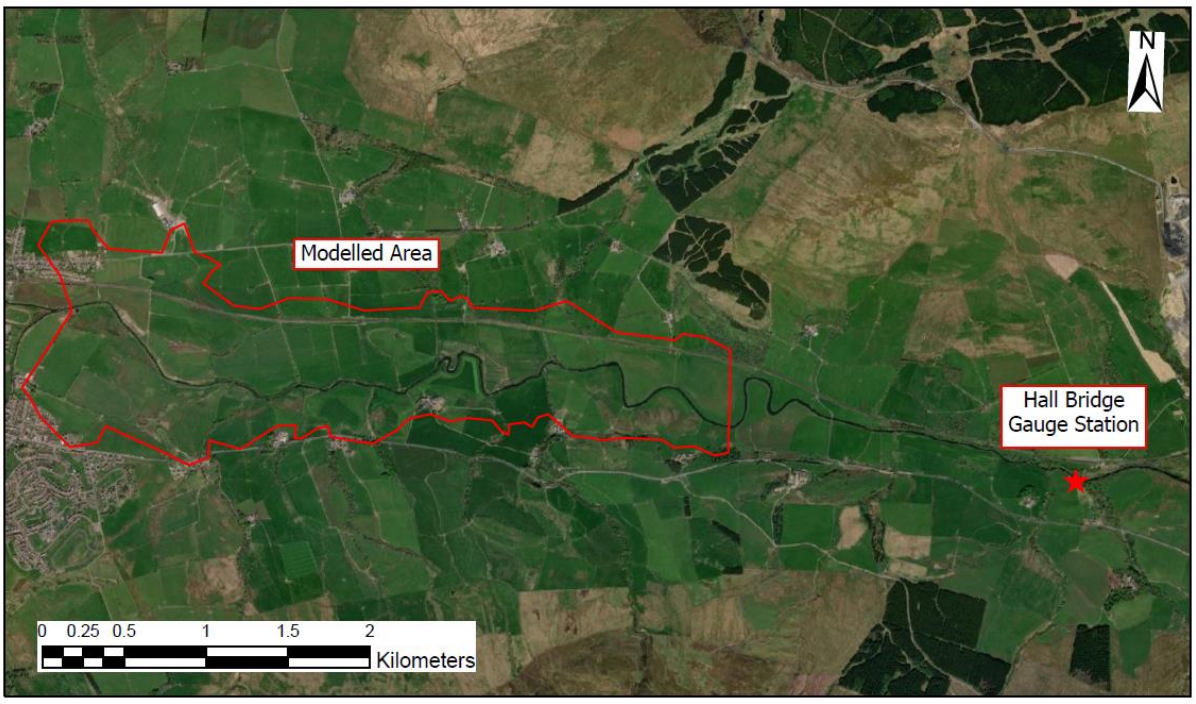

Figure 14. Modelled Area Boundary. Red boundary indicates perimeter area used in the HEC-RAS models. Red star indicates SEPA gauge station at Hall Bridge used to calculate catchment area and discharge rates.

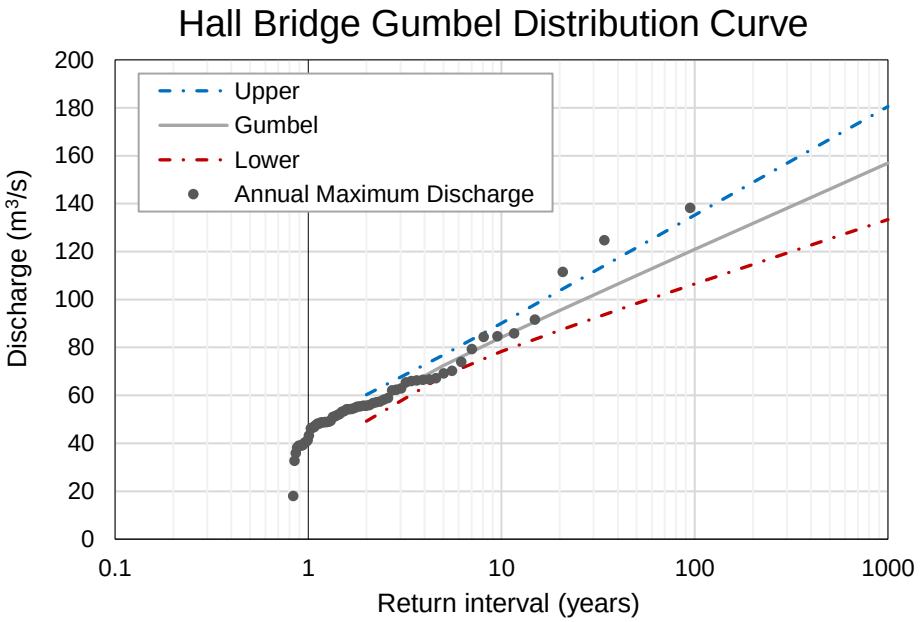

Figure 15. Gumbel distribution curve. Upper, Gumbel, and Lower discharge by return interval trends based on the annual maximum discharge readings from the Hall Bridge SEPA gauging station.

The unsteady flow analysis was run with a computation interval of 10 seconds to create mapping and hydrograph outputs at intervals of 1 hour. The equation used to model the flow through the mesh was the Shallow Water Equations, Eulerian-Lagrangian Method (SWE/ELM) rather than the default Diffusion Wave. The required input computational interval for SWE/ELM is smaller and thus produces more accurate results (USACE, 2022b). Additionally, it is always suggested that SWE be used when modelling dynamic flood waves due to the rapid rise and fall of the flood wave, the sudden velocity changes and that both local acceleration and convective acceleration are included in the calculations (USACE, 2022b). The time-step was based on the Courant (C) number, which uses an adjustive time-step, rather than fixed, and each run had a maximum C of 0.1 and a minimum of 0.015. These values were chosen based on trial runs as larger C values caused by the time-step being too long or the spatial scale being too short can result in the model becoming numerically unstable and crashing.

It is important to note that model calibration, sensitivity analyses, and validation, were not performed. While these processes help to quantify uncertainties associated with model parameters, the scope of this thesis did not allow these steps to be undertaken.

A total of 14 models were run to account for the seven recurrence intervals applied over the DEMs from two different time-periods (2019 and 2022). The HEC-RAS outputs include depth and shear stress maps which were exported to ArcPro. Shear stress is calculated as: YRSf where Y is the unit weight of water, Sf is friction slope, and R is hydraulic radius (USACE, 2010). The mean shear stress for each cell is then interpolated between cells. The depth rasters were cleaned to remove any depth values under 10 cm. Areas in the depth raster which display these low water levels (less than 10 cm) do not represent actual flood inundation, and likely represent simulated flow which got stuck in the middle of the grid and presents falsely as ponded water or “sticky cells”.

The shear stress maps showed improbably high maximum values of up to 3,000 Nm^{-2}, indicating that some of the shear stress calculations were unreliable, potentially due to localised model instability. Therefore, a manual comparison of the flow velocity and depth was conducted in the areas with abnormally high shear stresses. It was found that these high anomalies occurred in areas of low depth

(some values below the 10 cm limit) and improbably high velocity. The velocity in these areas is substantially higher than the channel velocity, which is unlikely to be representative of the actual flood scenario. Additionally, the underlying DEMs were used to compare topography with areas of high shear stress and determine the likelihood that these anomalies were representative of actual fluvial processes. These combined findings were used to determine a maximum probable shear stress value of 200 Nm^{-2} and any values above this were filtered out in ArcPro. Following this, there were still some anomalous values in the 2-year post-restoration shear stress map, and it was subsequently determined that this map needed to be further filtered using a maximum probable value of 85 Nm^{-2}.

5 Results

5.1 Geomorphic Change Detection

Geomorphic change detection DoD results are presented for Phases 1 and 2 between 2019 and 2022 (Figure 16 and Figure 17). While the GCD analysis was performed via probabilistic thresholding at a range of confidence intervals from 65-95% with 5% increments, the DoDs presented were all analysed using probabilistic thresholding at 80% confidence interval. This value allows for a substantial amount of confidence in the accuracy of the results (Bradford et al., 2005; Mapstone, 1995) while also allowing for trends to be displayed that are harder to see in the results from higher confidence intervals, such as some of the depositional zones both within the channel and on channel banks. Additionally, as this analysis is largely looking at overall trends, the lower confidence interval is acceptable.

The results for changes at Phases 1 and 2 (Figure 16 and Figure 17) between 2019 and 2022 clearly show the location of the old embankment, represented as substantial cut, and the new embankment, represented by substantial fill, which is expected as the DoD shows the change in elevation from 2019 to 2022 and during this time the embankment was relocated. Additionally, the trees are shown as areas of erosion as they were filtered out of the 2022 UAV LiDAR data, but not the Digimap LiDAR data from 2019.

The area representative of the new point bar, behind the old embankment and in front of the newly restored embankment, shows that erosion ranging from approximately 0.2 to 1 m has occurred (Figure 16a). The two ponded areas on the point bar have a larger cut range of up to approximately 2 m, which is expected as these areas were excavated during the restoration to promote additional habitat and overall heterogeneity. Therefore, these ponds should not be considered part of natural geomorphic change. The majority of the channel area does not show change. However, a section of the channel in upper Phase 1 shows depositional change, with elevation increases ranging from approximately 0.2 to 0.6 m (Figure 16b). A portion of lower Phase 1 also shows channel deposition, generally around 0.2 m in height (Figure 16c). Additionally, throughout Phase 1 there are thin areas along the channel bank that show deposition, an example is shown in Figure 16d. These areas are right up against the channel edge and range from approximately 0.1 to 0.4 m.

In Phase 2, the point bars between meanders show erosion, with elevation differences ranging from approximately 0.5 to 2.5 m, as shown in Figure 17. While this area largely displays erosion, some deposition has occurred on the outer edges of the meander point bars ranging from 0.3 to 0.5 m (Figure 17a). Farther downstream, a channel bank shows a mix of elevation changes, ranging from 0.6 m of deposition to 1 m of erosion (Figure 17b). There is no geomorphic change observed in the channel of Phase 2.

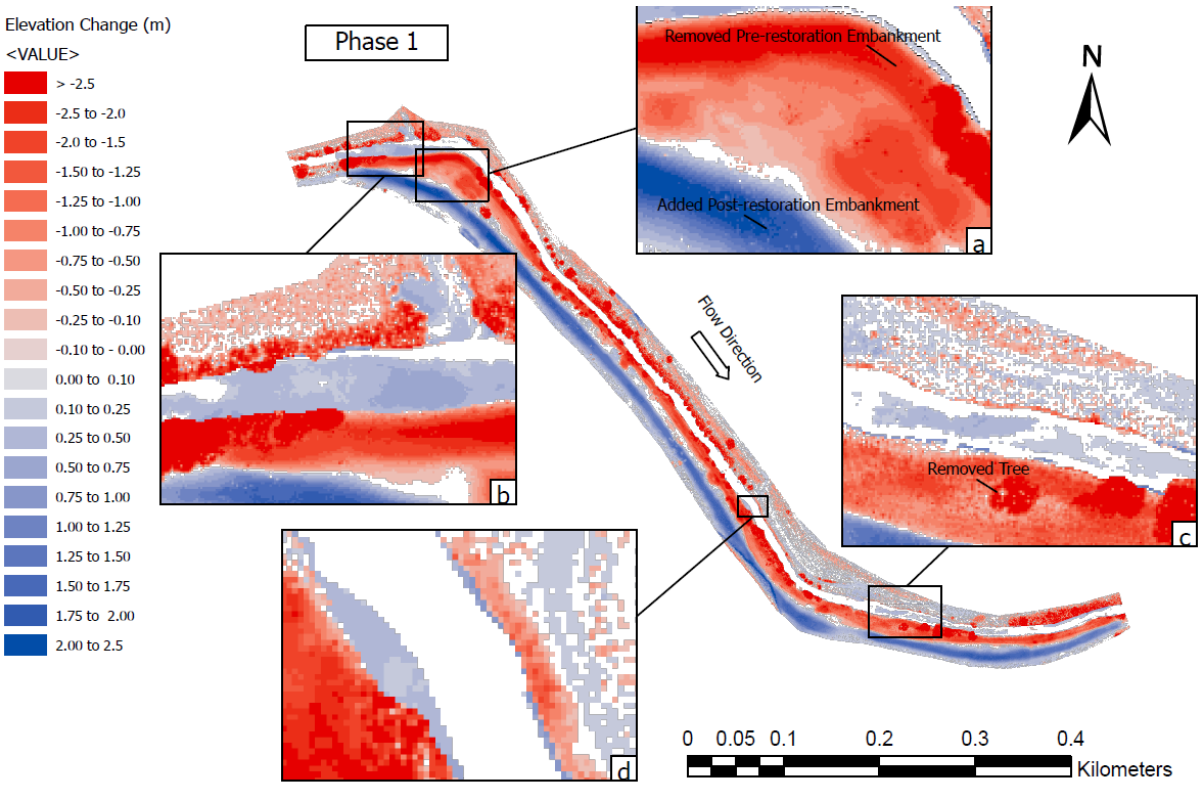

Figure 16. The DoD from 2019 to 2022 for Phase 1. Erosion and cut on the point bar (Figure 16a). Deposition in the upper and lower channel shown (Figure 16b and Figure 16c), respectively. Deposition along channel sides (Figure 16d).

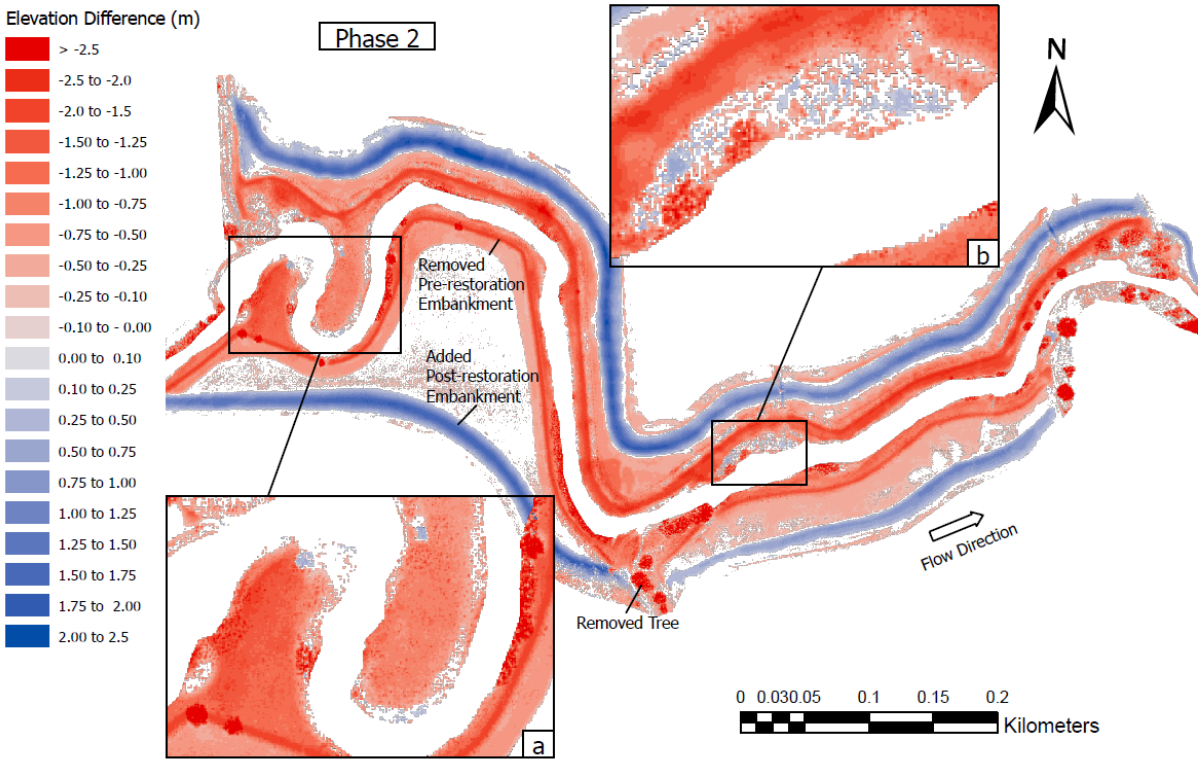

Figure 17. The DoD from 2019-2022 for Phase 2. Erosion on the point bars between meanders (Figure 17a). Mixture of erosion and deposition on the downstream channel bar (Figure 17b).

5.2 Flood Modelling

5.2.1 Inundation Extent

A total of 14 models were run to encompass discharge rates from the seven different recurrence intervals (Table 3) over both the pre- and post-restoration topographies. From these, hydrographs were plotted, and depth and shear stress rasters were exported for comparison in GIS.

The inundation extents are consistently larger for post-restoration flooding compared to pre-restoration (Table 4, Figure 18) for 1-year to 50-year recurrence interval (RI) events. However, for the 100-year RI flood the pre-restoration inundation is larger. The largest difference between inundation extents occurs during the 2-year RI flood with the flooded area being 179,141.25 m^2 larger, more than twice the size, during the post-restoration model run than the pre-restoration model run.

Table 4. Modelled flood inundation area (m^2) associated with each recurrence interval for both the pre-restoration and post-restoration model runs

Return Interval	2019 Inundation Area (Pre-Restoration)	2022 Inundation Area (Post-Restoration	% Change (2019 to 2022)
1	54,628	76,006	139%
2	141,451	320,592	227%
5	399,952	505,217	126%
10	531,581	657,437	124%
20	847,397	948,705	112%
50	1,077,762	1,126,549	105%
100	1,227,035	1,191,982	97%

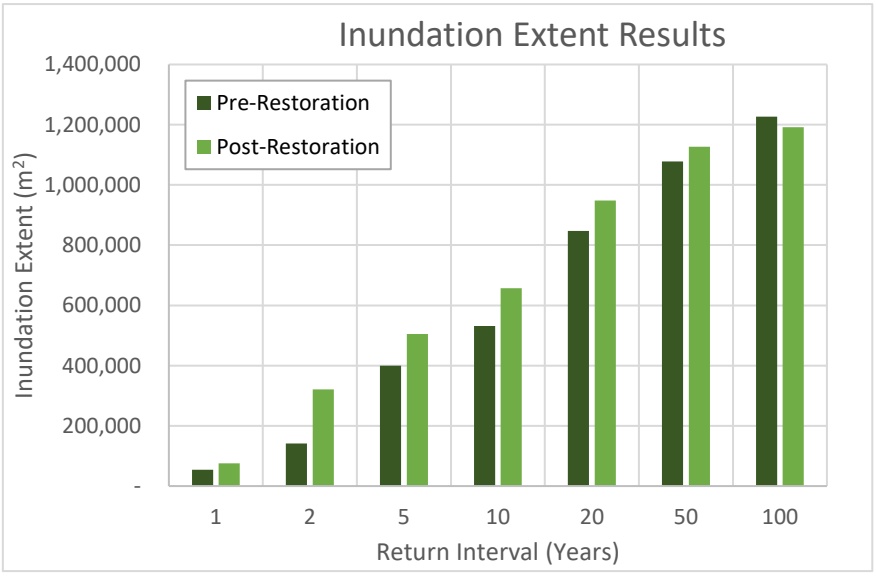

Figure 18. Inundation extent results. Total area of inundation resulting from each recurrence interval flood scenario over both the pre-restoration and post-restoration topographies.

5.2.2 Flood Hydrographs

Hydrographs of discharge events (1-, 2-, 5-, 10-, 20-, 50-, and 100-year RI) were generated for four locations: upstream and downstream of both Phases 1 and 2 (Figure 19). The profile lines that these hydrographs were extracted from extend across the widened post-restoration channel, from the top of one embankment to another, to capture all flow within the channel area. All 14 quasi-steady-state model runs were plotted and the pre-restoration and post-restoration results for each flow were compared against each other. The quasi-steady-state method was chosen to reduce model instability by applying a gradual increase in discharge until the desired return interval was reached so that changes in inundation, depth, and shear stress could clearly be correlated to the topography changes rather than fluctuations in discharge rates. To allow for clear visualisation of trends, results for the seven flow values are split between two graphs per location, with one group showing 1-, 2-, 5- and 10-year RIs and the other displaying 20-, 50- and 100-year RIs, as shown in Figure 20. For the 5-yr to 100-yr RI, the post-restoration floods have larger discharge values than the pre-restoration equivalent at all profile line locations (Figure 20). For example, for the 20-yr RI events, the difference in discharge from pre-restoration to post-restoration ranges from 2 to 35 m^3/s over the four different profile lines. The hydrographs for the 1-year RI flood are approximately the same for pre- and post-restoration over all locations. For the 2-year RI flood, the pre-restoration and post-restoration runs are approximately the same at all locations except for lower Phase 2.

At the upper Phase 1 location, the post-restoration flows are significantly higher than the pre-restoration flows for the same recurrence interval. However, at this location the pre-restoration flows are fluctuating while the post-restoration flow is smooth (Figure 20a and Figure 20b). The difference between flow rates increases with increasing RI, with some post-restoration flows being over 30 m^3/s larger than the equivalent pre-restoration at the upper Phase 1 location. The trends at the lower Phase 1 location are similar to that upstream, with the pre-restoration flows having smoothed out (Figure 20c and Figure 20d). The differences in discharge rates range from approximately 0 to 30 m^3/s between the pre-restoration and post-restoration at the lower Phase 1 location. In general, the flows are relatively similar between pre-restoration and post-restoration runs at the upper Phase 2 location, except for the 50-yr RIs which show a 3 m^3/s difference and the 100-yr RIs which show a 6 m^3/s difference (Figure 20e and Figure 20f). Additionally, for the 100-yr pre-restoration run, the discharge captured by the profile line drops significantly, over 10 m^3/s, after approximately 20 hours (Figure 20f). The largest difference between pre- and post-restoration flood discharges can be seen at the downstream Phase 2 location where the post-restoration flow is generally more than double that of the equivalent pre-restoration flood and differences of up to 40 m^3/s can be seen (Figure 20g and Figure 20h).

Additionally, between profile lines, there is a general trend in changing discharge for pre-restoration and post-restoration events. The changes between events increases as the RI increases. From upstream Phase 1 to downstream Phase 1, a slight increase in discharge occurs. For example, during the 50-yr pre-restoration RI there is a 5 m^3/s increase while for the 50-yr post-restoration RI event there is a 2 m^3/s increase (Figure 20b and Figure 20d). From downstream Phase 1 to upstream Phase 2, flows increase for the pre-restoration events but drop for the post-restoration events. An increase of about 8 m^3/s happens for the 50-yr RI pre-restoration event while a drop of approximately 5 m^3/s occurs for the post-restoration event (Figure 20d and Figure 20f). The largest shift in flow values is seen between upper and lower Phase 2, with an approximately 50 m^3/s drop for the 50-yr RI pre-restoration event and a drop of 15 m^3/s for the post-restoration event (Figure 20f and Figure 20h).

Even for the 2-yr RI, while the post-restoration flood shows no change there is a difference of approximately 23 m^3/s for the pre-restoration flood (Figure 20e and Figure 20g).

Figure 21a to Figure 21d compare the 2-year and 100-year RI pre- and post-restoration floods using unsteady flow (i.e., a hydrograph with a rising and falling limb) to see whether there is a distinct lag time between the floods associated with the two topographies. With an unsteady flow, differences between the flood timing could potentially become more distinct as the discharge rises and falls. These recurrence intervals were chosen so that a range of discharge values could be compared. However, the results from these plots are similar to the previous results shown in Figure 20a to Figure 20g, with no distinct difference in flood timing and trends for pre-restoration and post-restoration being similar for each location. For the upper and lower Phase 1 locations, the 2-yr RI has the same discharge for both pre-restoration and post-restoration while the 100-yr RI post-restoration rate is substantially larger than the pre-restoration (30 m^3/s). The hydrographs at these locations (upper and lower Phase 1) are similar shape, having a distinct peak. Flows in Figure 21c are similar to the other upper Phase 2 hydrographs, with the pre- and post-restoration flows being very similar in the lower RI run, as shown by the 2-yr RI, and post-restoration having slightly higher flows than pre-restoration (5 m^3/s) in the larger RI run, as shown by the 100-yr RI flows. Figure 21d aligns with the other lower Phase 2 hydrographs and shows the post-restoration flows being substantially higher than the pre-restoration flows (over 40 m^3/s difference for the 100-yr RI). The hydrographs through lower Phase 2 are much more rounded in shape than those observed in the Phase 1 locations.

Figure 22 shows the water levels through each profile line for the 2-, 10-, and 100-year RI events as well as both the pre-restoration and post-restoration topography cross section. The pre-restoration topography lines were smoothed to remove obvious impacts from vegetation in order to more clearly represent the actual topography. Results shown in Figure 22a to Figure 22c show the water level difference between pre-restoration and post-restoration at upper Phase 1. The pre-restoration levels are substantially larger, with over 1 m difference shown for the 100-yr RI. The downstream Phase 1 water levels shown in Figure 22d to Figure 22f are generally the same between pre-restoration and post-restoration events, however the 10-yr RI shows the post-restoration levels being slightly larger (approximately 10 cm) than the pre-restoration. Water levels in Figure 22g to Figure 22i show that at the upstream Phase 2 profile location, pre-restoration levels are consistently about 30-50 cm higher than post-restoration levels for all three RIs. At the downstream Phase 2 profile location, the pre-restoration water levels for the 2-yr and 10-yr RIs are approximately 15 cm larger than the post-restoration water levels (Figure 22j and Figure 22k) but for the 100-yr RI events the levels are generally the same (Figure 22l).

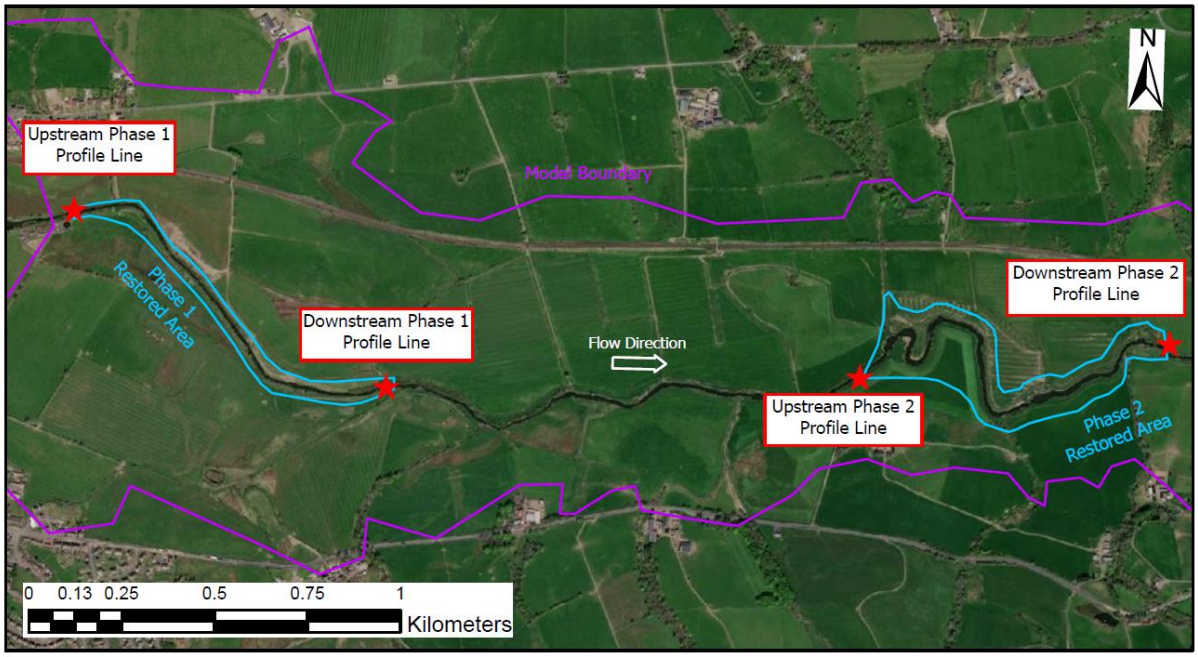

Figure 19. Location of the profile lines for the hydrographs shown in ***Error! Reference source not found.****. Red stars indicate t he location of the upstream and downstream profile lines for Phases 1 and 2. Purple boundary indicates model perimeter. Blue boundary indicates restored area of Phases 1 and 2.*

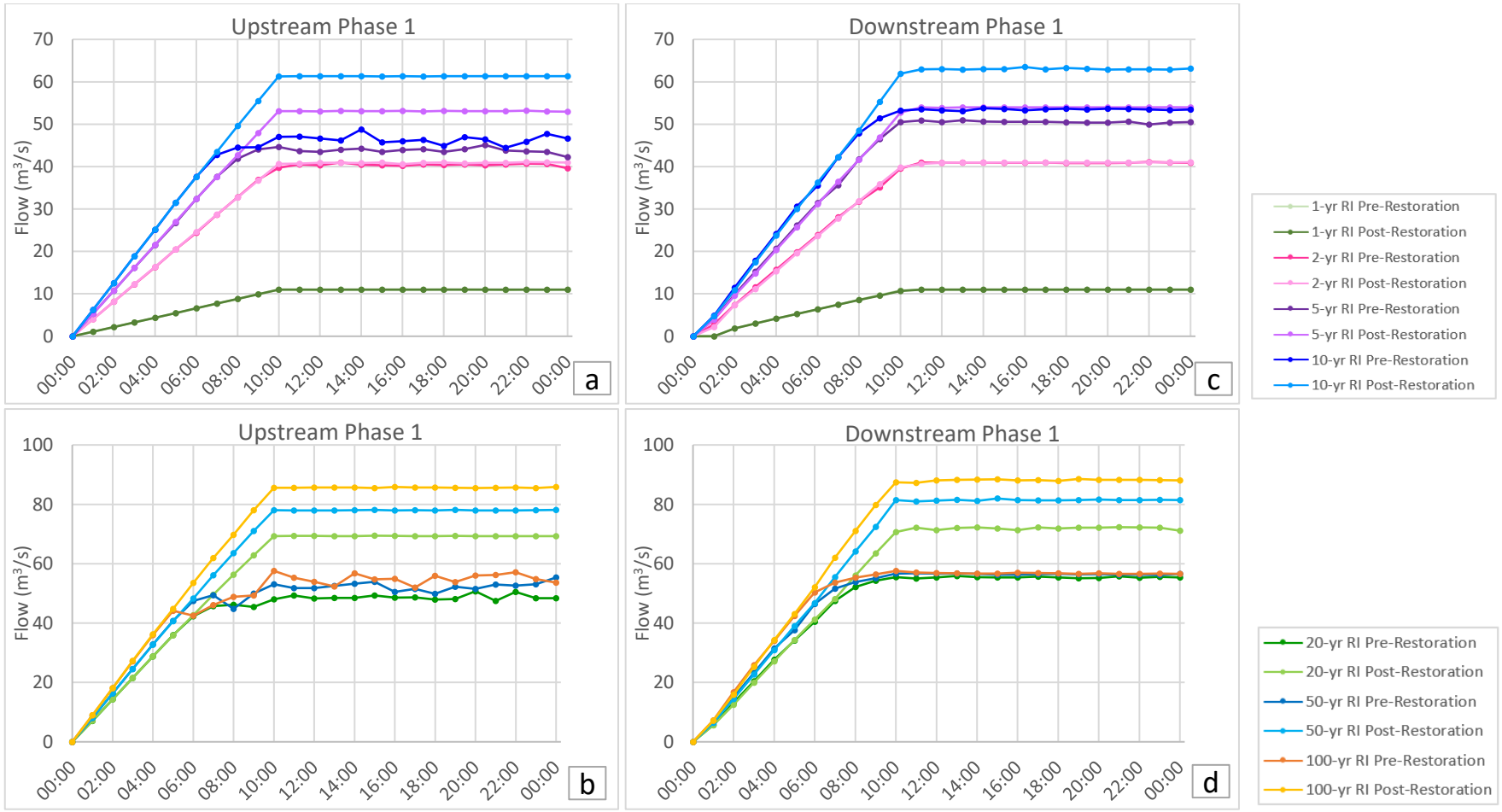

Figure 20. Quasi-steady-state hydrographs through the profile lines. Results for profile lines at Upstream Phase 1 (Figure 20a and Figure 20b), downstream Phase 1 (Figure 20c and ***Error! Reference source not found.****d), upstream Phase 2 (Figure 20e and Figure 20f), and downstream Phase 2 (Figure 20g and Figure 20h).*

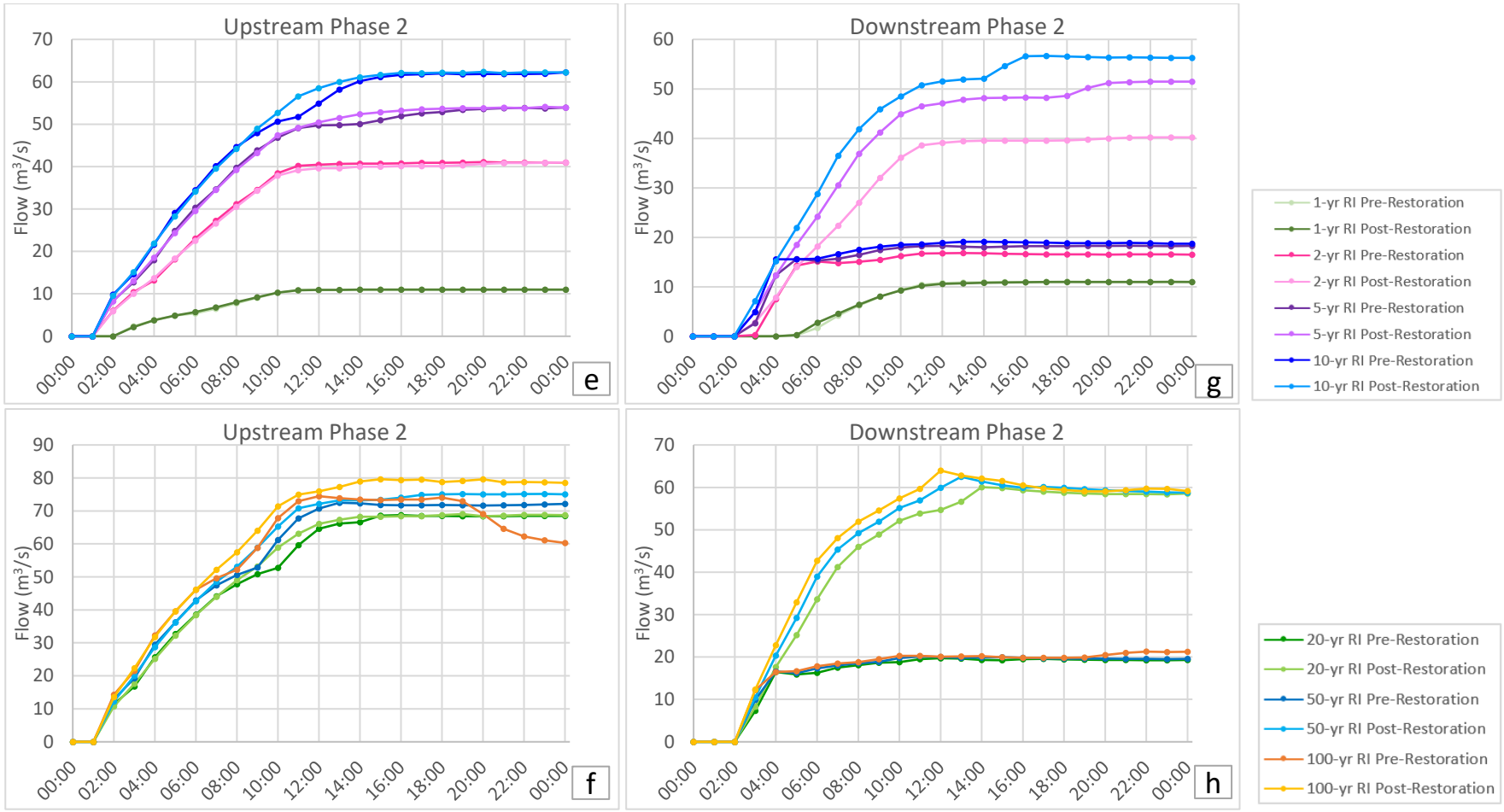

Figure 20. Quasi-steady-state hydrographs through the profile lines. Results for profile lines at Upstream Phase 1 (Figure 20a and Figure 20b), downstream Phase 1 (Figure 20c and Figure 20d), upstream Phase 2 (Figure 20e and Figure 20f), and downstream Phase 2 (Figure 20g and Figure 20h).

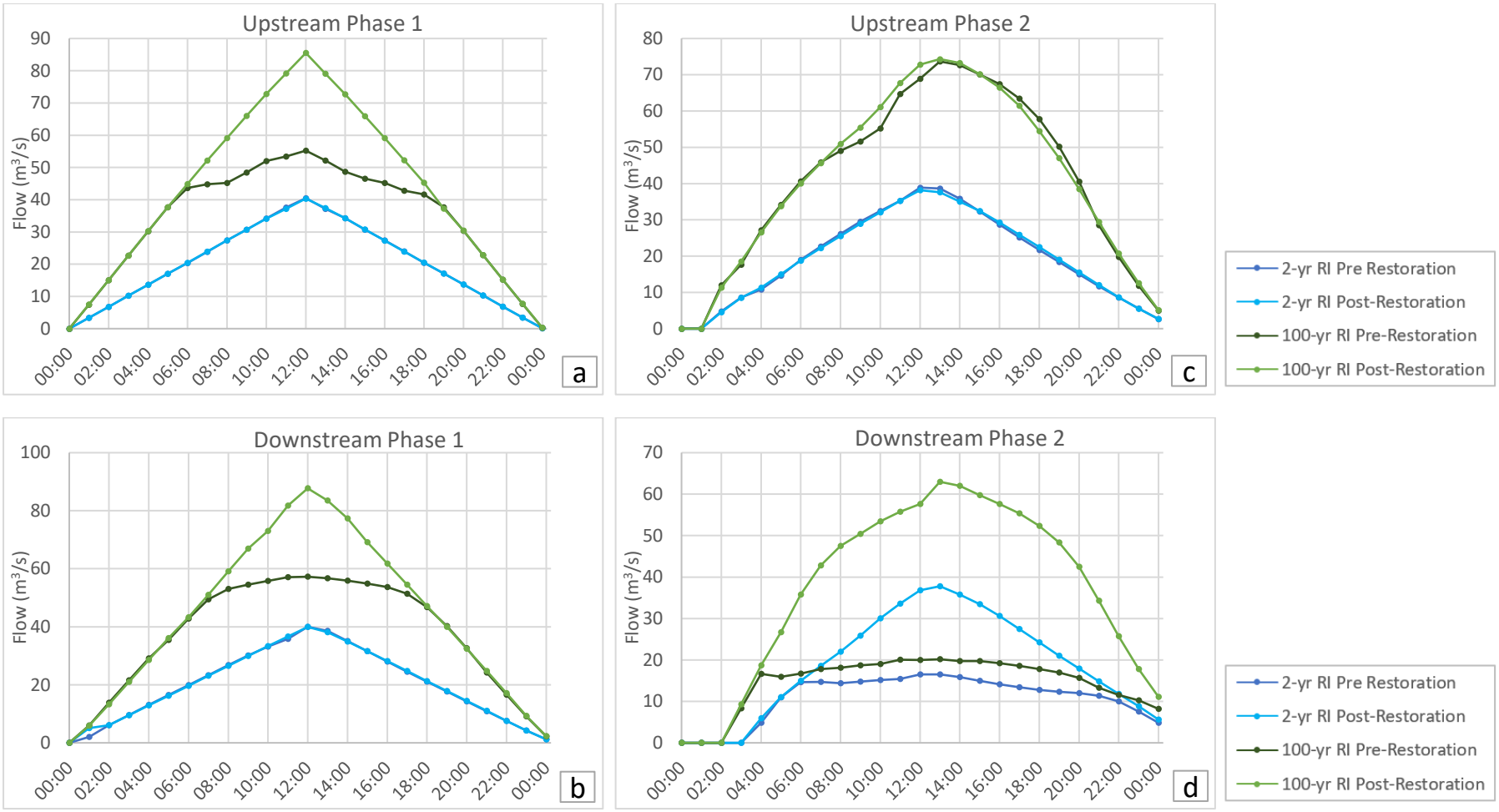

Figure 21. Unsteady state flow hydrographs through the profile lines for the 2-yr and 100-yr recurrence intervals. Results for profile lines at upstream Phase 1 (Figure 21a), downstream Phase 1 (Figure 21b), upstream Phase 2 (Figure 21c), and downstream Phase 2 (Figure 21d).

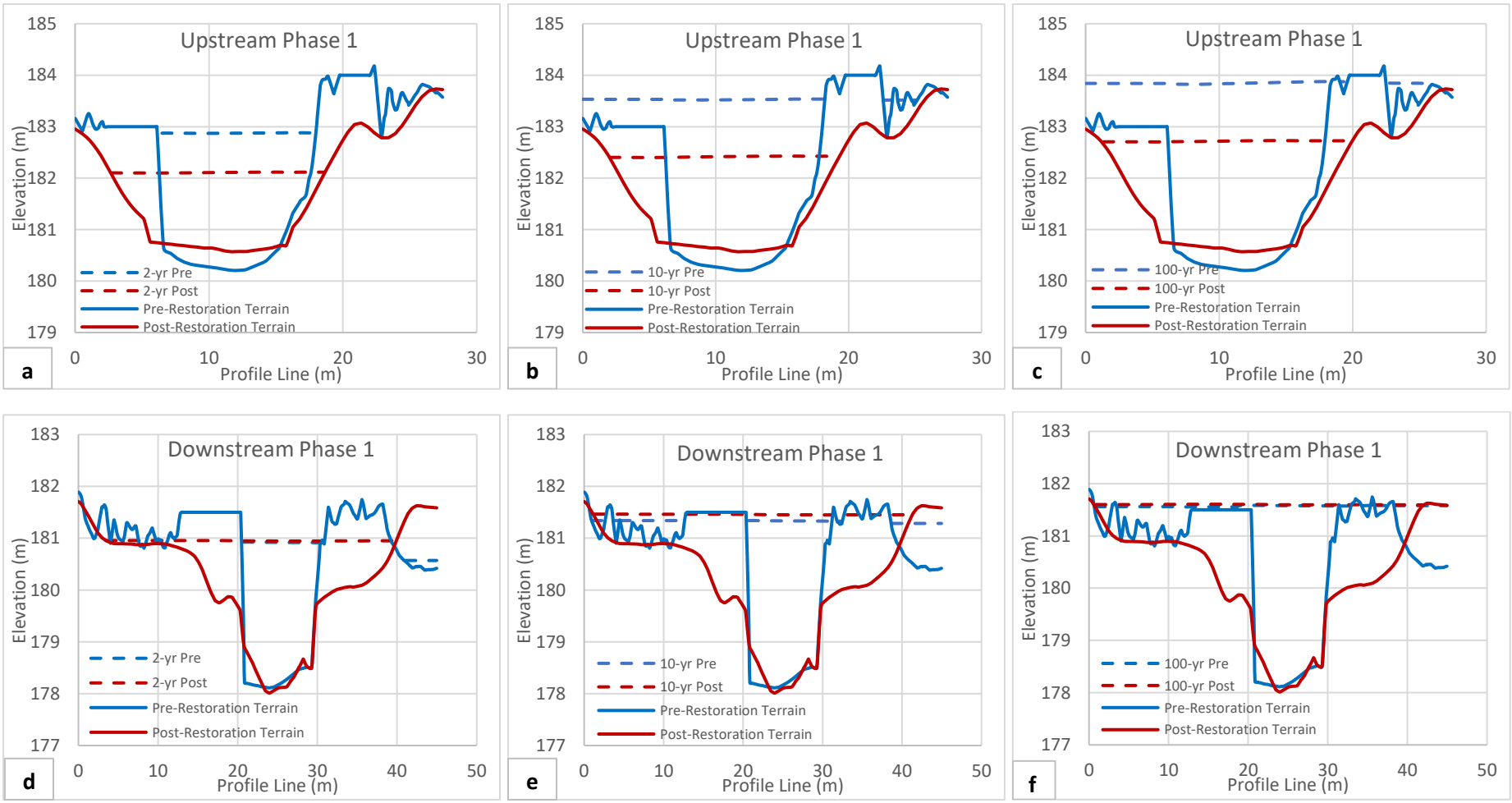

Figure 22. Flow levels through the profile lines for 2-yr, 10-yr, and 100-yr RIs. Results for profile lines at upstream Phase 1 (Figure 22a - Figure 22c), downstream Phase 1 (Figure 22d - Figure 22f), upstream Phase 2 (Figure 22g -Figure 22i), and downstream Phase 2 (Figure 22j -Figure 22l).

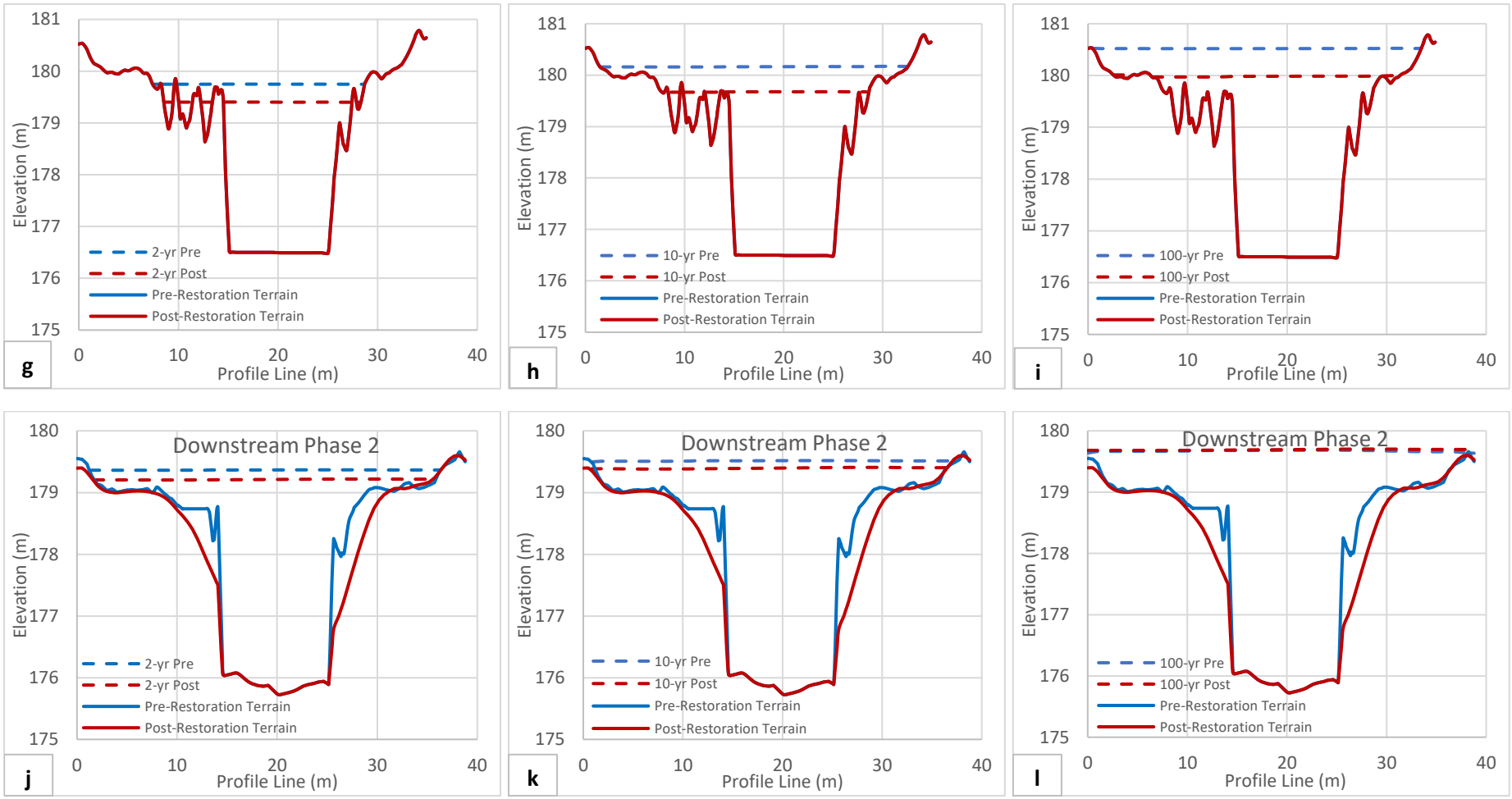

Figure 22. Flow levels through the profile lines for 2-yr, 10-yr, and 100-yr RIs. Results for profile lines at upstream Phase 1 (Figure 22a - Figure 22c), downstream Phase 1 (Figure 22d - Figure 22f), upstream Phase 2 (Figure 22g -Figure 22i), and downstream Phase 2 (Figure 22j -Figure 22l).

5.2.3 Water Depth

Water depth results for the different model runs are shown in Table 5, Figure 23, and Figure 24. The maximum depths vary from 4.83 to 6.67 m and are lower for the post-restoration than pre-restoration model runs for all recurrence intervals. However, as the maximum value represents just one value out of an entire range, it is not necessarily indicative of depth trends. The minimum depths are all 0.10 m as this was the lower limit that was set to assist in model accuracy. The mean depths are generally lower for the post-restoration flooding than pre-restoration, with the largest difference observed during the 1-yr and 2-yr RI runs and the pre-restoration mean depth being 39% and 40% larger, respectively. However, there is an exception to this in two scenarios; for the 5-year RI flood the post-restoration mean depth is very slightly larger (3%) and for the 20-year RI flood the two model runs have the same mean depth of 0.78 m.

Areas where the depth differences are especially clear are upper Phase 1, lower Phase 1, and the meander in Phase 2 (Figure 25, Figure 26, and Figure 27).

Table 5. Statistics associated with the water depth results. Results shown for each recurrence interval for both the pre-restoration and post-restoration model runs for entire modelled area. The mean values are emphasized in green as these are most representative of overall trends.

Depth (m)												
	Min			**Max**			**Mean**			**Std. Dev.**		
RI (yr)	2019	2022	% Diff.	2019	2022	% Diff.	2019	2022	% Diff.	2019	2022	% Diff.
1	0.10	0.10	NA	5.21	4.83	7%	1.95	1.40	28%	1.16	1.06	9%
2	0.10	0.10	NA	5.96	5.64	5%	1.25	0.89	28%	1.34	0.95	29%
5	0.10	0.10	NA	6.19	5.79	6%	0.87	0.90	-3%	0.99	0.84	14%
10	0.10	0.10	NA	6.35	5.88	7%	0.89	0.84	6%	0.91	0.80	12%
20	0.10	0.10	NA	6.45	5.96	8%	0.78	0.78	-1%	0.79	0.72	9%
50	0.10	0.10	NA	6.50	6.04	7%	0.98	0.91	6%	0.73	0.68	8%
100	0.10	0.10	NA	6.67	6.17	8%	1.13	1.06	6%	0.73	0.69	5%

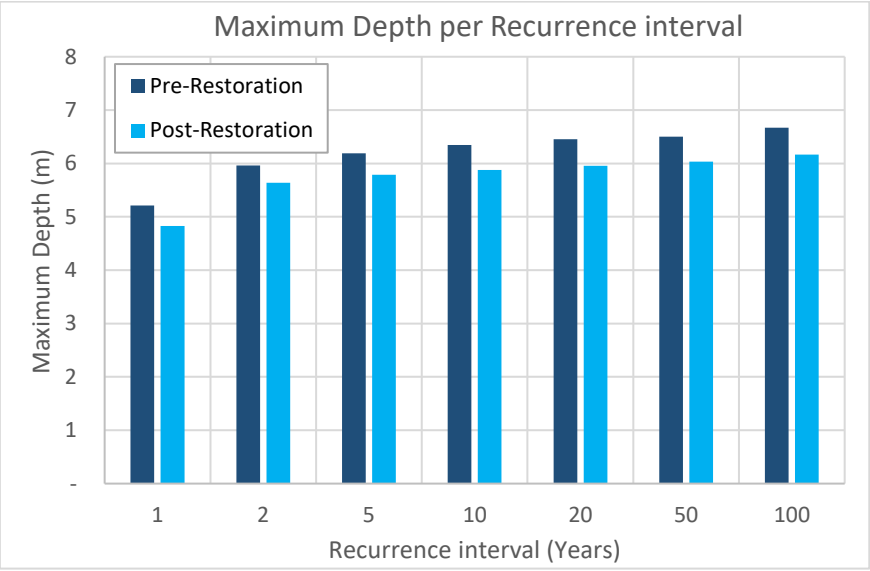

Figure 23. Maximum water depth results. Results shown for each recurrence interval flood scenario for both the pre-restoration and post-restoration topographies.

.

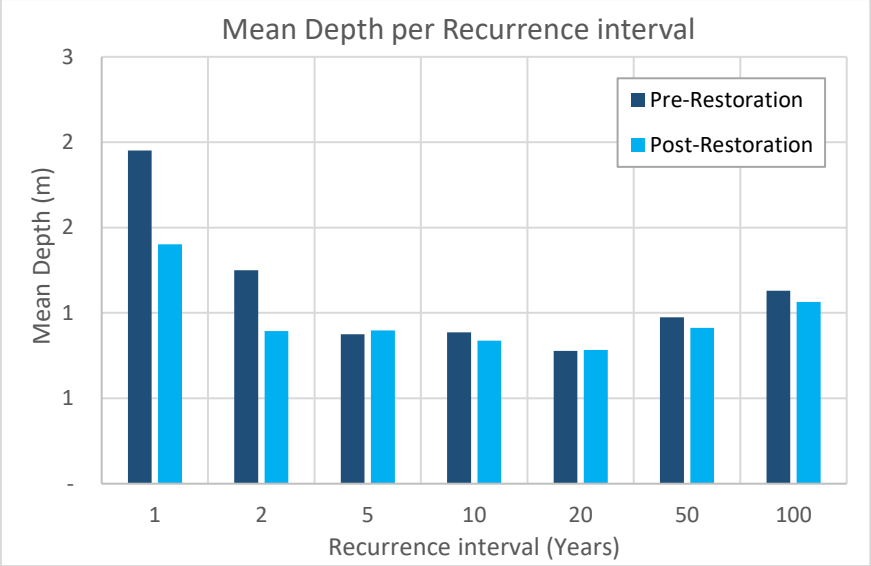

Figure 24. Mean water depth results. Results shown for each recurrence interval flood scenario for both the pre-restoration and post-restoration topographies.

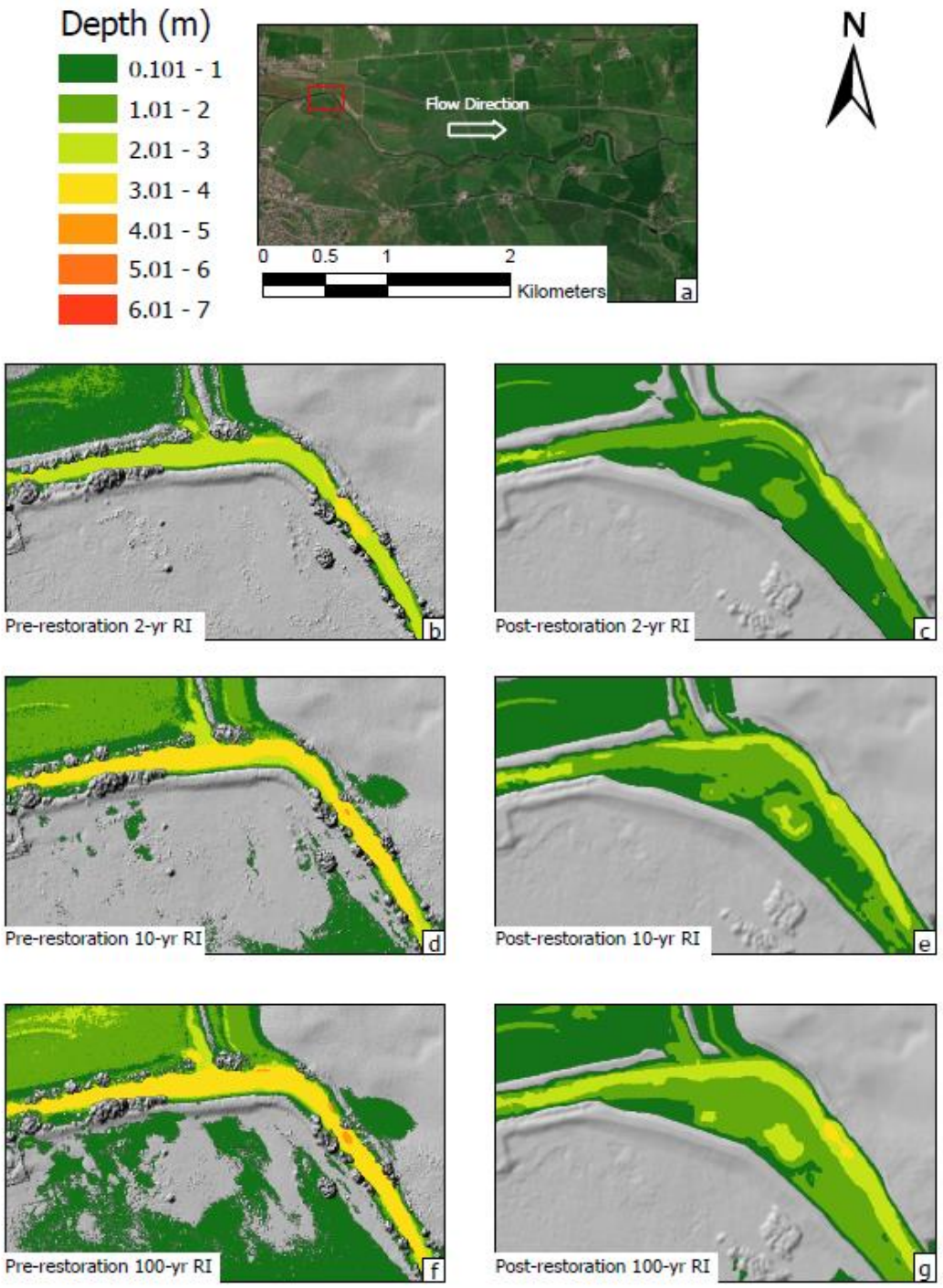

Figure 25. HEC-RAS depth raster results for upper Phase 1. Extent of the upper Phase 1 area (Figure 25a) and pre-restoration and post-restoration results for the 2-, 10-, and 100-yr recurrence intervals (Figure 25b through Figure 25g).

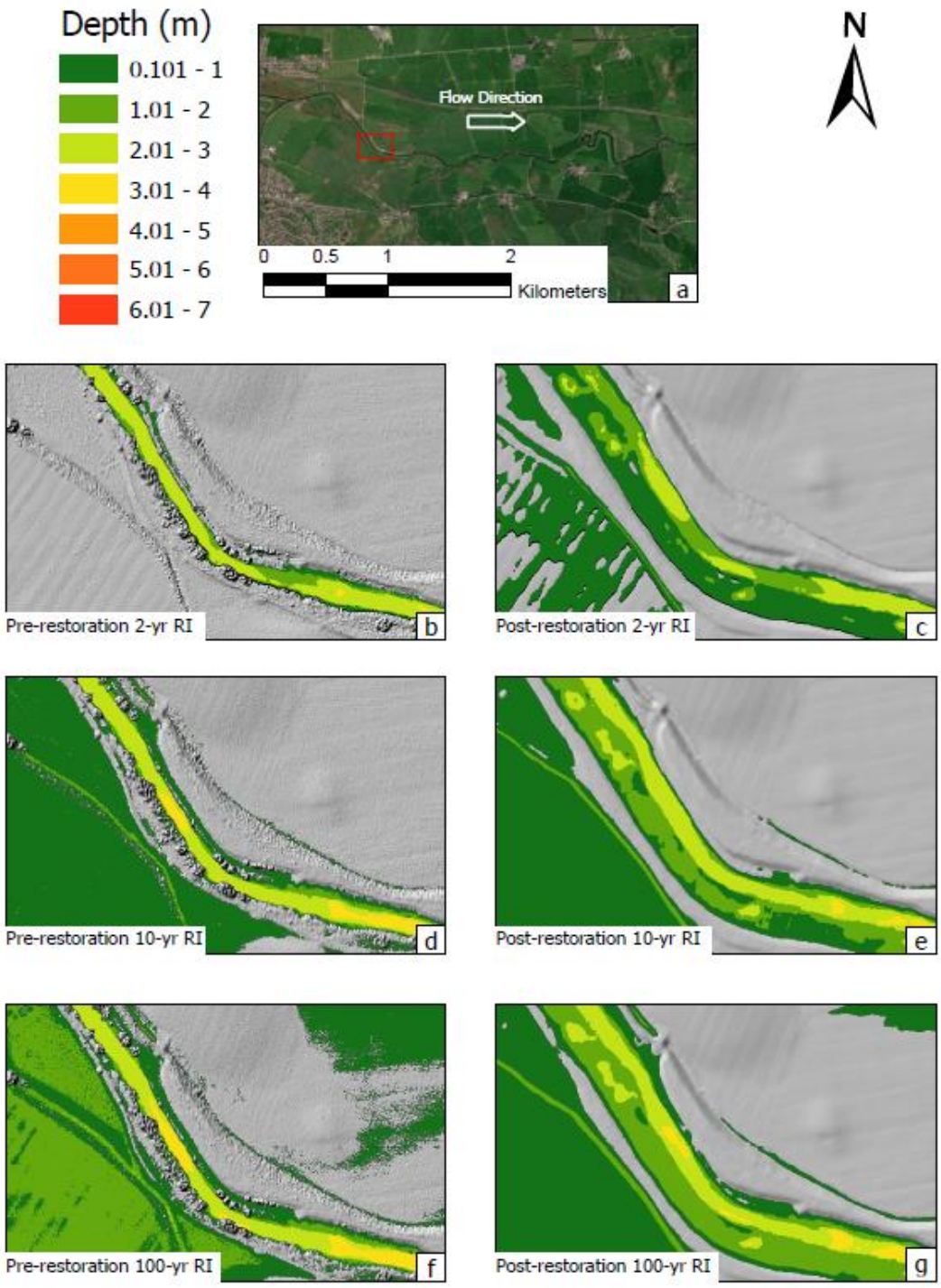

Figure 26. HEC-RAS depth raster results for lower Phase 1. Extent of the lower Phase 1 area (Figure 26a) and pre-restoration and post-restoration results for the 2-, 10-, and 100-yr recurrence intervals (Figure 26b through Figure 26g).

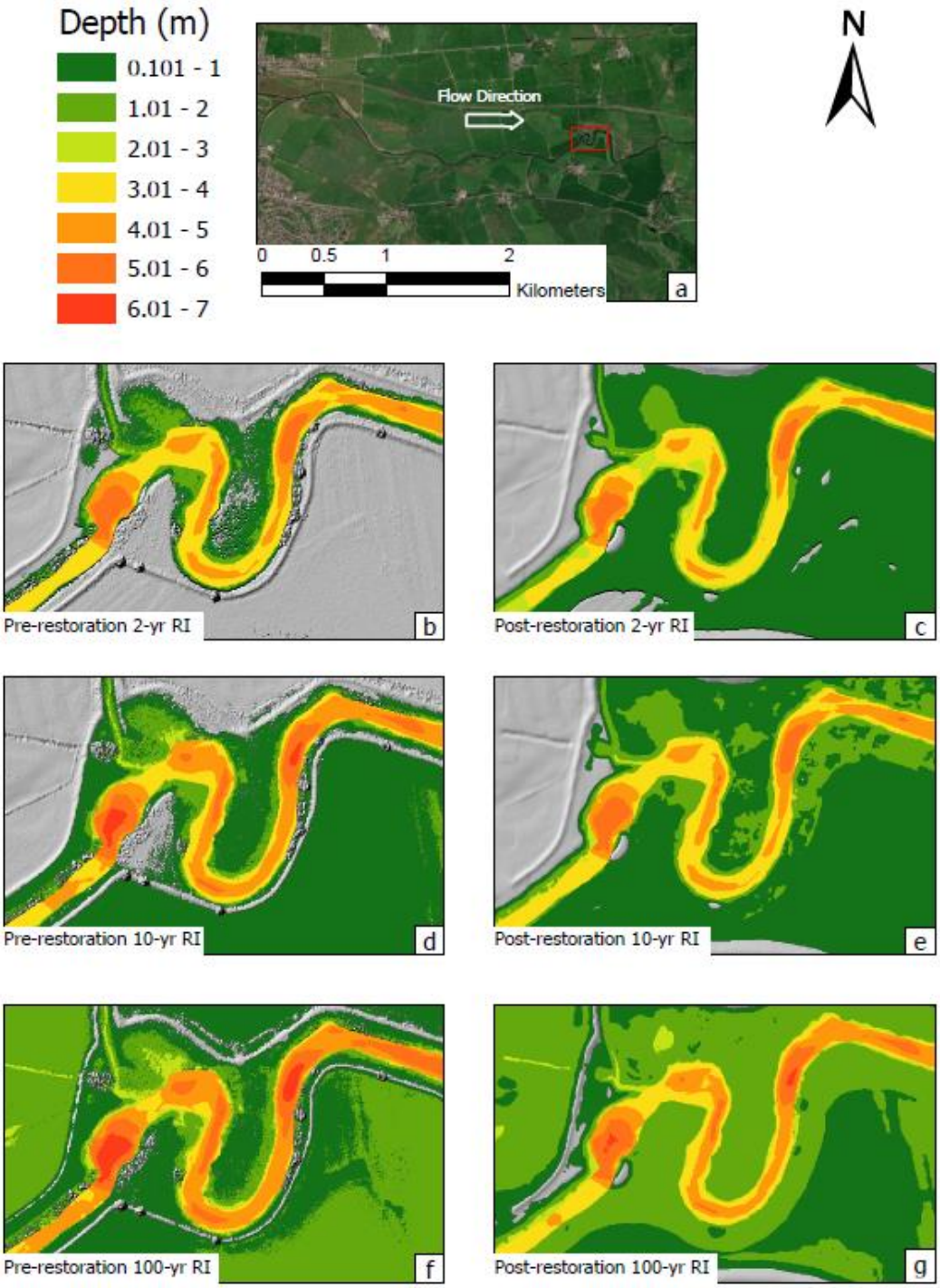

Figure 27. HEC-RAS depth raster results for the Phase 2 meander. Extent of the lower Phase 1 area (Figure 27a) and pre-restoration and post-restoration results for the 2-, 10-, and 100-yr recurrence intervals (Figure 27b through Figure 27g).

5.2.4 Shear Stress

Shear stress values vary over the different model runs with the minimum being 0 Nm^{-2} throughout all model runs and the maximum values ranging from 50.35 to 199.94 Nm^{-2} (Table 6 and Figure 28). The mean shear stress values generally decrease as the recurrence interval gets larger and have an overall range of 1.05 to 2.79 Nm^{-2} (Table 6 and Figure 29). The pre-restoration mean shear stress values are larger than the post-restoration values for 1-, 2-, 5- and 10-year RI runs but for the 20-, 50- and 100-yr RI the post-restoration values are larger.

In general, the pre-restoration shear stress values within the channel are higher than the post-restoration values, with the exception of the 1-year and 2-year RI results, which are generally quite similar between the two time-periods. The difference between the shear stress associated with the 2-, 10-, and 100-year RI pre-restoration and post-restoration model runs for three locations: upper Phase 1, lower Phase 1, and the meander in Phase 2 are shown in Figure 30, Figure 31, and Figure 32, respectively. As shown in Figure 30, the beginning of Phase 1 is the only location within the model where the shear stress values from the post-restoration runs are consistently larger than those from the pre-restoration. Lower Phase 1 shows a distinct difference between the two model runs (Figure 31a through Figure 31g). For example, the 10-yr RI flood peak shear stress, which occurs in the channel bend, is approximately 85 Nm^{-2} for pre-restoration and 25 Nm^{-2} for post-restoration (Figure 31d and Figure 31e). The typical values for the pre-restoration run range from 30 to 50 Nm^{-2}, while the post-restoration run is generally below 20 Nm^{-2}. Downstream at the Phase 2 meander, the 10-yr pre-restoration run shows a maximum of approximately 40 Nm^{-2} with a general range of 10-30 Nm^{-2} while the post-restoration maximum is approximately 15 Nm^{-2} with most of the area having a shear stress of less than 10 Nm^{-2} (Figure 32d and Figure 32e).

In addition to increased shear stress within the channel, the pre-restoration results show pockets of high shear stress located on the outside edge of the original embankment in both Phase 1 and Phase 2. For example, the 50-yr RI results show shear stress of up to approximately 200 Nm^{-2} (Figure 33a through Figure 33c).

Table 6. Statistics associated with the shear stress results. Results shown for each recurrence interval for both the pre-restoration and post-restoration model runs. The mean values are emphasized in green as these are most representative of overall trends.

Shear Stress (Nm^{-2})												
	Min			**Max**			**Mean**			**Std. Dev.**		
RI (yr)	2019	2022	% Diff.	2019	2022	% Diff.	2019	2022	% Diff.	2019	2022	% Diff.
1	0	0	NA	54.6	50.3	8%	2.8	2.4	14%	5.4	5.0	6%
2	0	0	NA	118.1	82.9	30%	2.7	1.8	33%	7.1	5.2	26%
5	0	0	NA	196.4	94.1	52%	1.6	1.6	1%	5.7	5.1	10%
10	0	0	NA	199.9	112.0	44%	1.4	1.4	3%	5.5	4.9	10%
20	0	0	NA	198.4	191.6	3%	1.1	1.1	-7%	4.5	4.6	-1%
50	0	0	NA	199.5	199.7	0%	1.1	1.1	-9%	4.9	4.8	3%
100	0	0	NA	199.9	199.4	0%	1.1	1.2	-16%	4.9	5.1	-3%

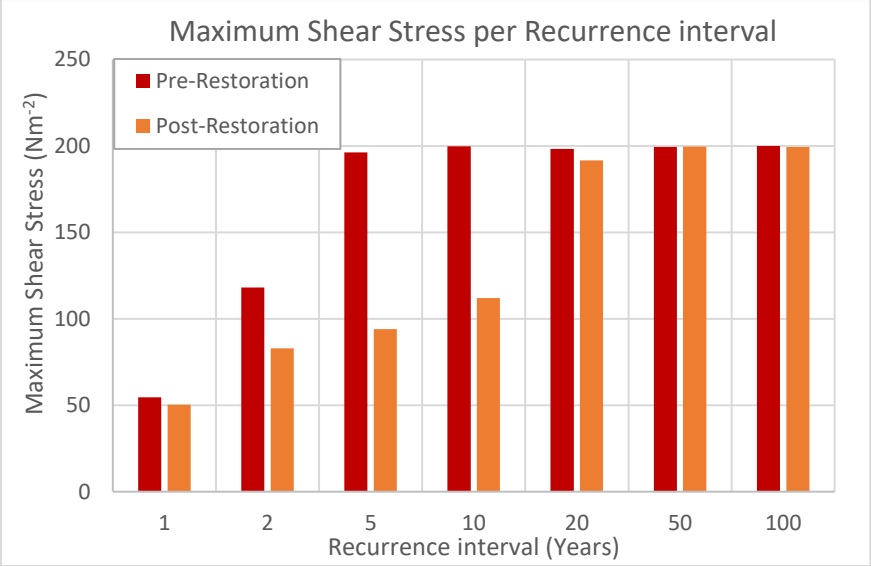

Figure 28. Maximum shear stress results. Results shown for each recurrence interval flood scenario for both the pre-restoration and post-restoration topographies.

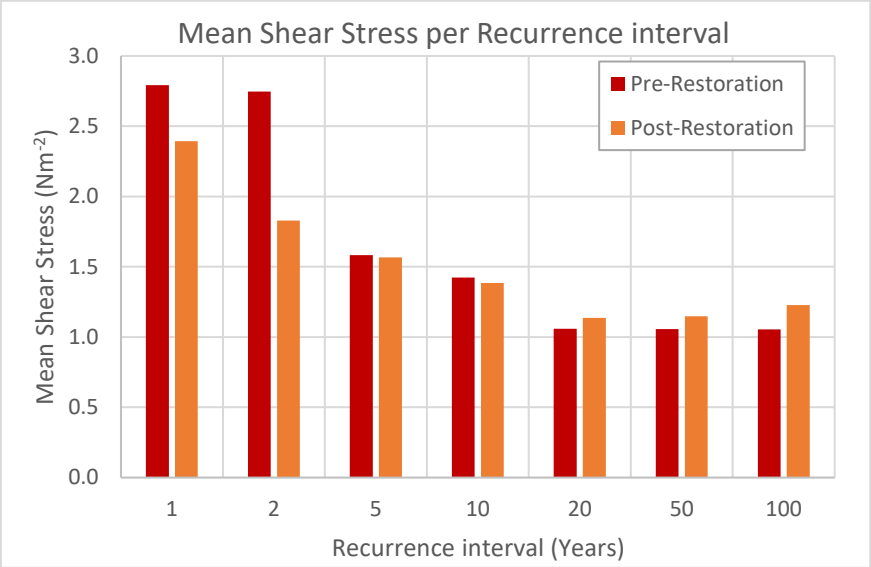

Figure 29. Mean shear stress results. Results shown for each recurrence interval flood scenario for both the pre-restoration and post-restoration topographies.

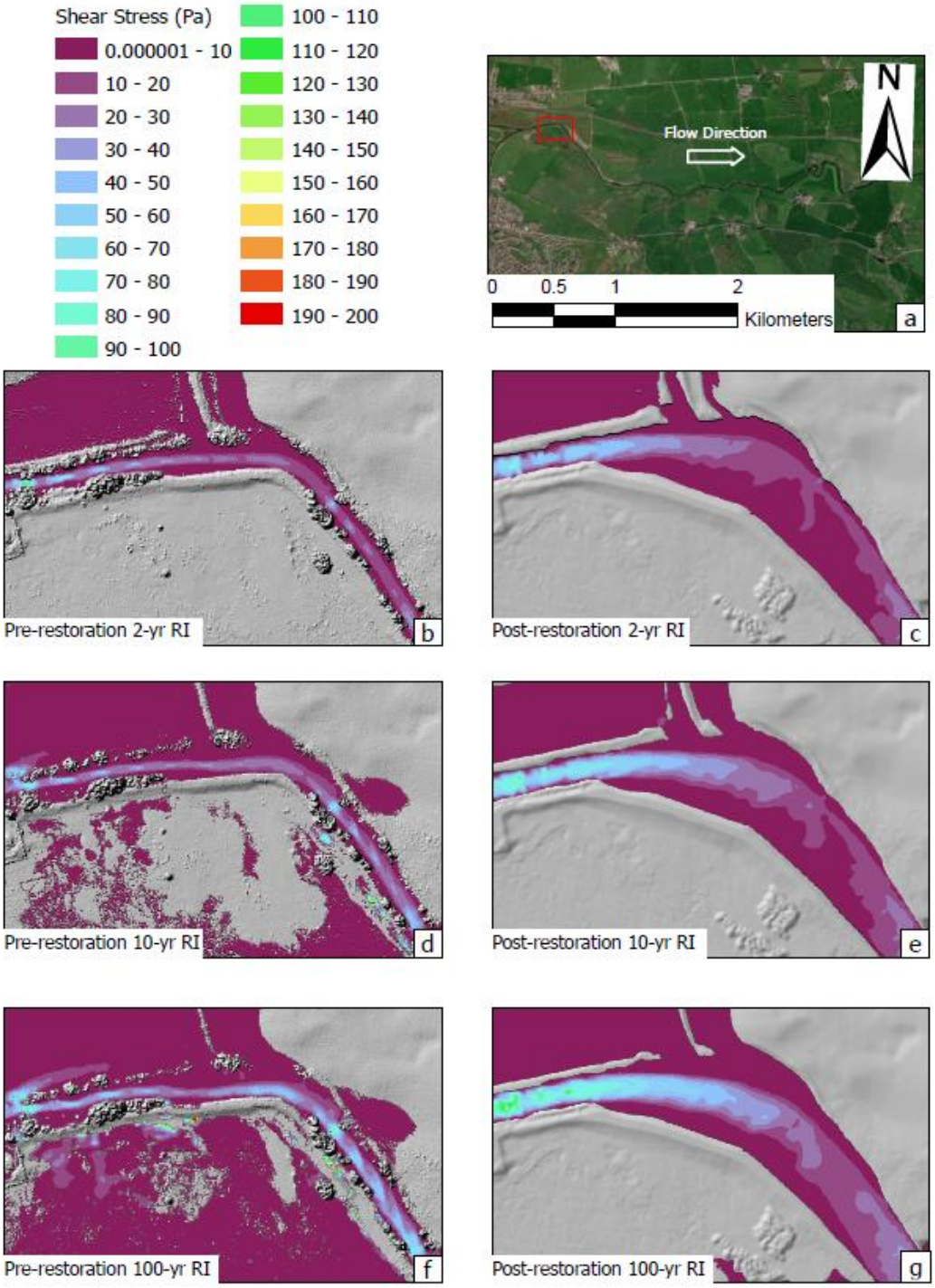

Figure 30. HEC-RAS shear stress raster results for upper Phase 1. Extent of the upper Phase 1 area (Figure 30a) and pre-restoration and post-restoration results for the 2-, 10-, and 100-yr recurrence intervals (Figure 30b through Figure 30g).

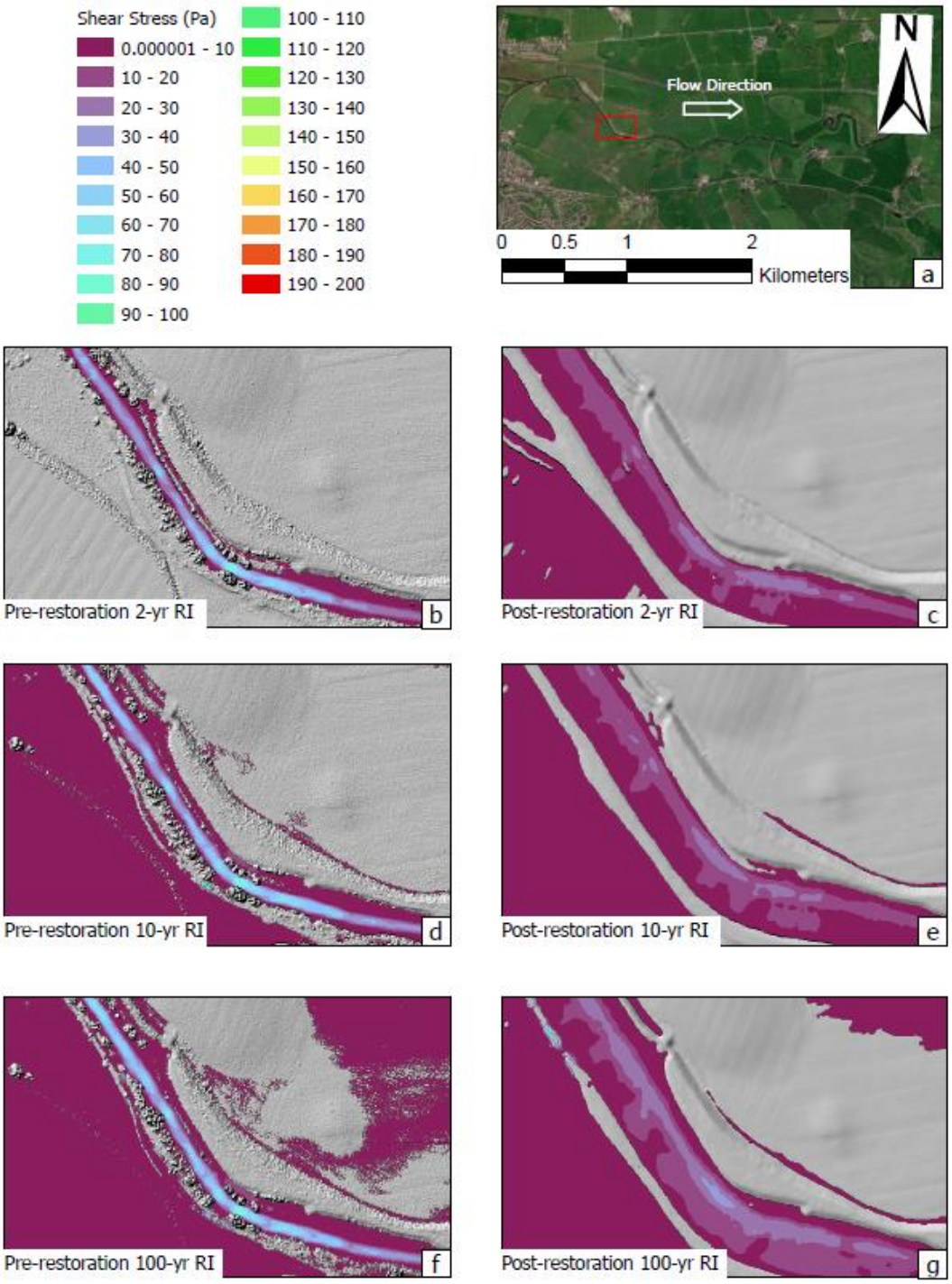

Figure 31. HEC-RAS shear stress raster results for lower Phase 1. Extent of the lower Phase 1 area (Figure 31a) and pre-restoration and post-restoration results for the 2-, 10-, and 100-yr recurrence intervals (Figure 31b through Figure 31g).

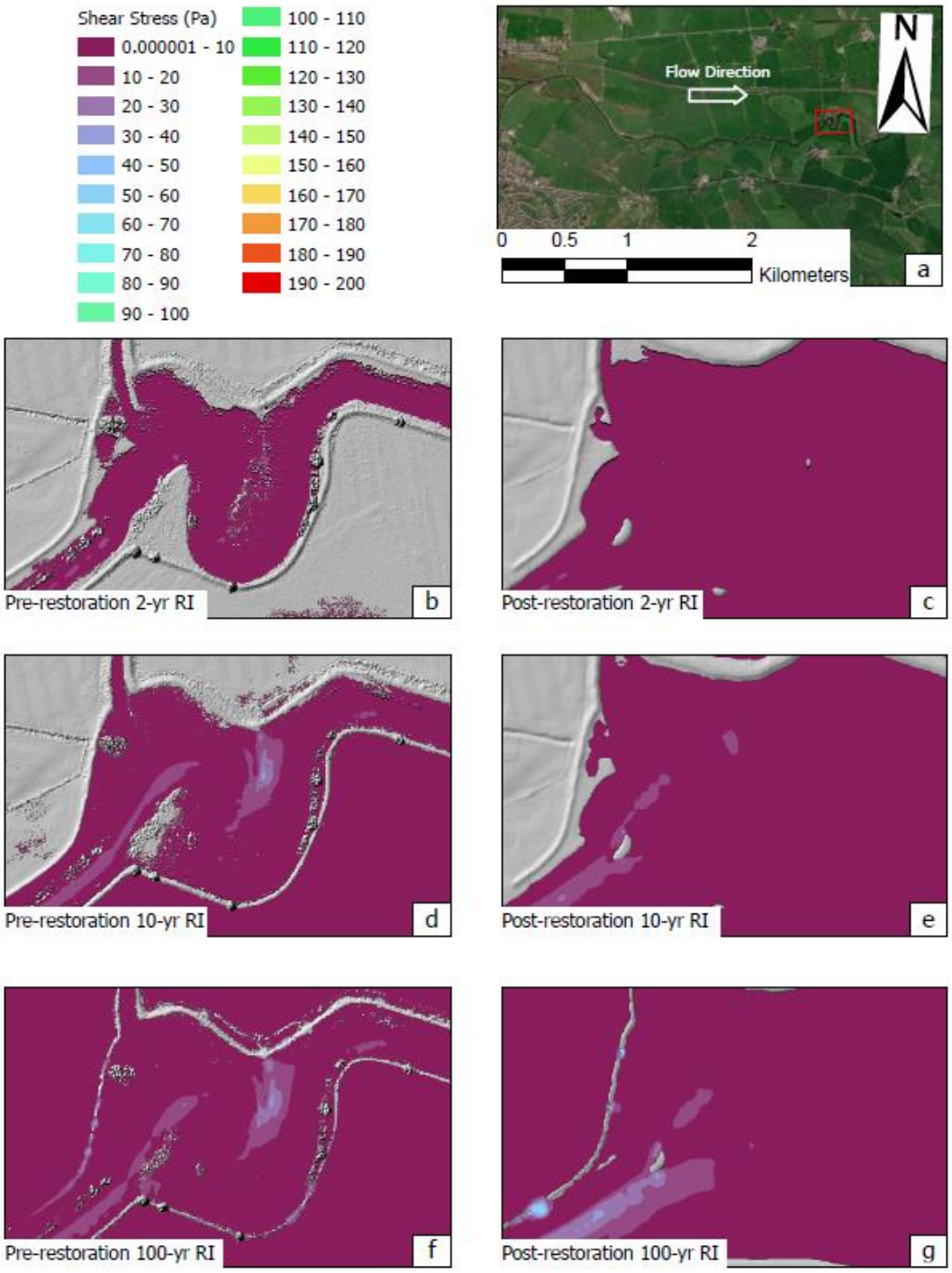

Figure 32. HEC-RAS shear stress raster results for the Phase 2 meander. Extent of the lower Phase 1 area (Figure 32a) and pre-restoration and post-restoration results for the 2-, 10-, and 100-yr recurrence intervals (Figure 32b through Figure 32g).

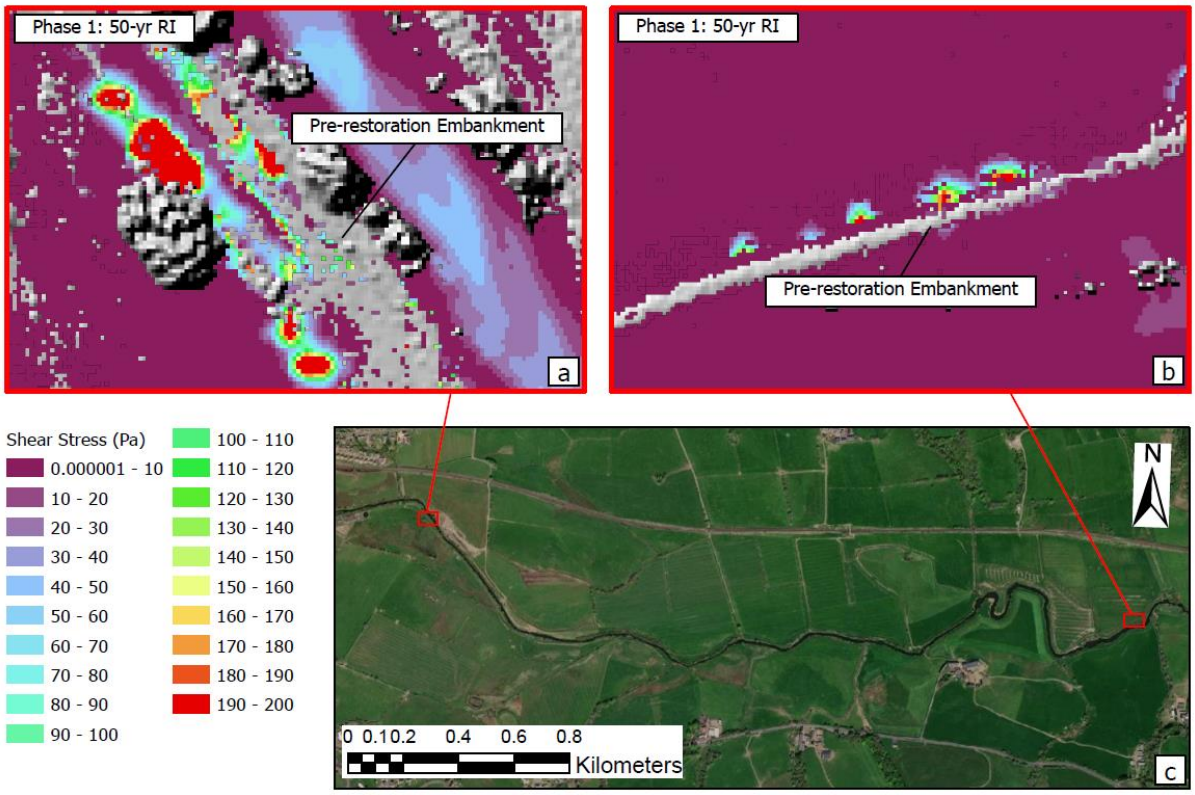

Figure 33. Pockets of apparent high shear stress. Located on the outer edge of the embankment for both Phase 1 (Figure 33a) and Phase 2 (Figure 33b) for the pre-restoration 50-yr RI model run. The locations of these two extents within the study area (Figure 33c).

6 Discussion

The section of the River Nith analysed for this thesis, while only part of a larger river system, displays characteristics common to a heavily engineered river that has recently had restoration works, such as two-stage channel design and embankment setbacks, completed. Therefore, it provides an appropriate case study to assess the impacts that river restoration can have on flood inundation and geomorphic change, which helps draw conclusions regarding floodplain-connectivity and habitat diversity. This section describes the implications of the above-mentioned results and what they indicate regarding changes from pre-restoration to post-restoration.

It is important to note that, while there are some distinct, overlying trends that indicate site-wide fluvial processes and results of the restoration work, there are several exceptions that make the results more nuanced. The variations in shear stress trends between different RI events as well as the flood dissipation variations over different locations suggest geomorphic change and influence from the restoration works has occurred but the specific outcomes are largely reliant on flood intensity and location rather than widespread, general trends.

6.1.1 Observed Geomorphic Change

The results from the DoDs created in GCD show that geomorphic change has occurred at the River Nith between 2019 and 2022. In Phase 1, erosion of the new point bar (Figure 16a) can be attributed to the increased connectivity between the river channel and floodplain. The constricting nature of the pre-restoration embankment, which was immediately adjacent to the channel, prevented flow from reaching this portion of the floodplain. However, the set-back post-restoration embankment enables connectivity during high-discharge flows and, because the discharge required for flow to reach this portion of the topography is high (between 11 m^3/s and 41 m^3/s), erosion rather than deposition is expected. This idea is supported by the findings of Brocchini et al. (2017) that net deposition is prevalent during low discharge while net erosion is a result of high discharge. Additionally, erosion capabilities increase with increased sediment transport capacity, which is a result of higher discharge rates (Dukic & Radic, 2014) and increased shear stress.

As shown in Figure 30, shear stress values in this area have increased from pre-restoration to post-restoration, for example the 10-yr RI has increases of approximately 20-30 Nm^{-2}, which aligns with the observed erosion on the point bar. It is also possible that some of the observed erosion is a result of the lack of vegetation filtering that was applied to the 2019 Airborne LiDAR. There is very little geomorphic change in the Phase 1 river channel. However, as noted in the results, deposition has occurred at both the upper and lower portion of Phase 1 (Figure 16b and Figure 16c). The widened channel area from the embankment setbacks has allowed for flow dispersion, resulting in slower flow in some areas. This reduced discharge rate subsequently results in the observed deposition. The deposition in the lower portion of Phase 1 (Figure 16d) can also be attributed to the shift in shear stress that occurs here.

Just upstream, as shown in Figure 31, the shear stress increases around the channel bend before dropping and allowing the deposition of sediment in both the pre- and post-restoration models. For example, during the 10-yr RI runs, the shear stress differences in this area are approximately 30 Nm^{-2} in the pre-restoration run and 10 Nm^{-2} in the post-restoration run. Therefore, the sediment deposition here results from a combination of channel morphology changes from the restored embankment as well as shear stress trends. Additionally, small lenses of deposition are present along the sides of the

channel (Figure 16d) indicating that the setback embankments are allowing for a variation in velocities compared to high, homogenous flow rates associated with channelisation. As a result, areas with increased friction and subsequent lower velocities (such as the shallower bank edges) enable deposition.

In Phase 2, while most of the geomorphic change is located on the point bars of the meander and primarily show erosion (Figure 17a), the shape of the channel is quite uniform between the two time periods. This stability of the meander shape as well as the knowledge that the 2019 Digimap Airborne LiDAR did not filter out vegetation indicates that this observed erosion is a result of the removal of vegetation in the 2022 UAV LiDAR. In the case that some of the shown erosion is representative of sediment changes, both the pre-restoration and post-restoration embankments allow access to the meander from the channel, therefore the erosion in this area is likely not directly related to the restoration work. Rather, the discharge necessary to deviate from the channel path and cut across the meander is higher than average and, as described above, higher discharge generally results in greater erosion rates (Brocchini et al., 2017). This relationship between discharge rates and sediment can also explain the deposition observed along the edges of the meander (Figure 17a) as an accumulation of suspended sediment deposition during lower flows. It is unlikely that this change is due to vegetation as the 2022 UAV LiDAR removed vegetation therefore new vegetation growth would not be shown. Downstream of the meanders, the mixture of erosion and deposition occurring on the channel bar can potentially be attributed to the increase in channel area which allows for more heterogeneous flows, enabling both deposition and erosion to occur as well as the removal of vegetation from the 2019 to the 2022 UAV LiDAR (Figure 17b). There is very little geomorphic change in the Phase 2 river channel, indicating that the bathymetry remained largely unchanged from 2019 to 2022.

During the time periods of observed geomorphic change (between 2019 and 2022) the maximum flow of the River Nith, through Hall Bridge Station, was 72.8 m^3/s (similar to the 20-yr RI event of 72 m^3/s) and the average flow rate was 6.5 m^3/s (NRFA, 2022b). Over this period, approximately 0.2% of flows exceeded the 5-yr RI value, 0.09% of flows were greater than the 10-yr RI and 0.004% of flows were greater than the 20-yr RI. No flows during this period exceeded the 50-yr or 100-yr RI events. While these higher flows likely contributed to some of the observed geomorphic change, the low frequency suggests that the majority of changes can be attributed to the shift in channel geometry from the restoration works.

6.1.2 Influence of Two-Stage Channel Design and Embankment Setbacks

The difference in inundation extents between pre-restoration and post-restoration suggests that the two-stage channel design and embankment setbacks have influenced the amount of area affected by flooding (Figure 18). The larger inundation extent associated with the post-restoration model, for the 1-yr through 50-yr RI model runs, is expected as the setback embankments allow for a less confined channel and subsequently increased floodplain connectivity which results in a larger flooded area (Clilverd et al., 2012; Maaß and Schüttrumpf, 2019). The 100-yr RI is the one exception to this, with the pre-restoration model run having a larger inundation area than the post-restoration model run. However, the difference in size is less than 3% and therefore not considered significant or indicative of any impact by the embankments. The large size difference between the 2-yr RI inundation extents, with the post-restoration extent being 56% larger than the post-restoration, can be attributed to embankment overtopping that occurred on the restored embankment. The 2022 escaped flow includes backflowing in the southeast portion of Phase 1 and embankment overtopping of the east portion of Phase 2 (Figure 34). The difference between extents is still significant for the 5-yr RI,

however, beginning with the 10-yr RI, the embankment overtopping occurs in similar places between the two topographies and therefore the inundation extents are more similar.

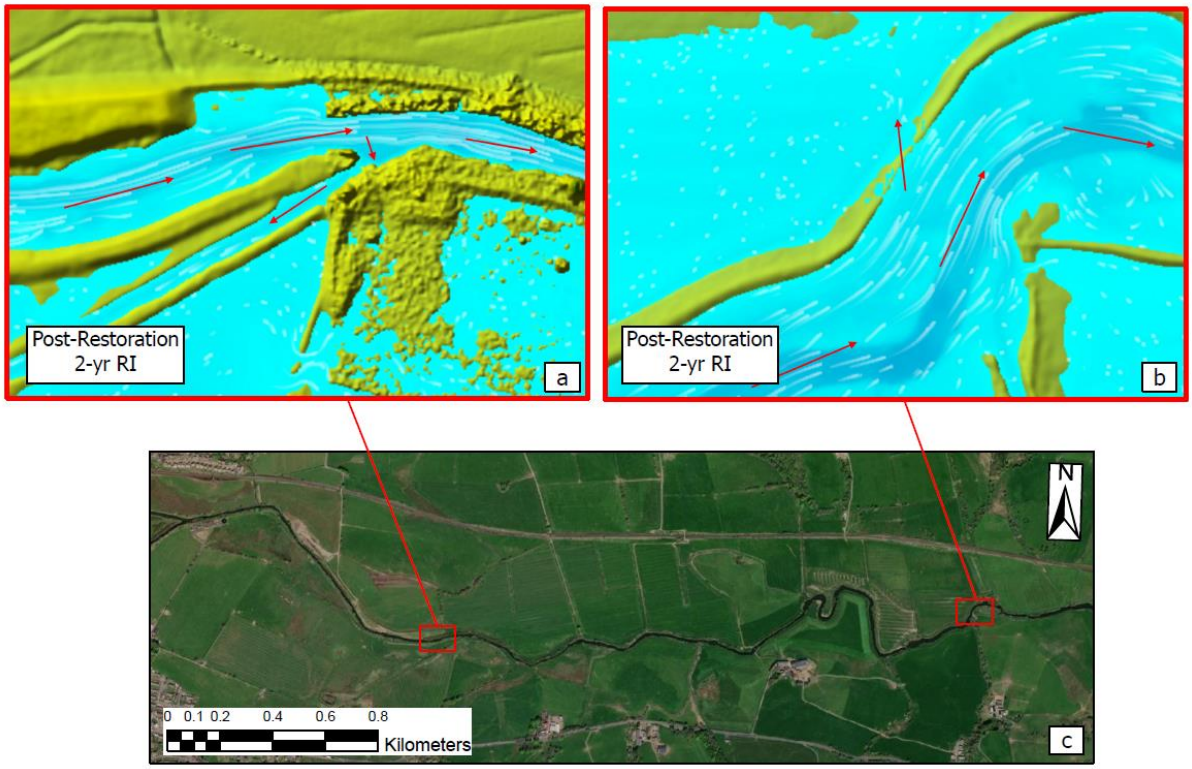

Figure 34. Two main areas of embankment overtopping in the 2-yr RI post-restoration flood model run. Southeast Phase 1 embankment overtopping location (Figure 34a) and eastern Phase 2 embankment overtopping location (Figure 34b). Red arrows indicate flow direction. Location of embankment overtopping within the site area (Figure 34c).

The effect that embankment setbacks and two-stage channel design have on flood characteristics is highlighted by the difference in flood discharge rates between pre- and post-restoration model runs (Figure 20a through Figure 20h). While the hydrographs are useful for generalizing flow trends, the location of the profile lines does need to be taken into consideration as this impacts the results. Therefore, these results are just specific examples, but a range of other possible outcomes could be produced from profile lines in different locations. Since the input discharge is the same for each RI between pre-restoration and post-restoration, it would be expected that the hydrographs would be the same as well if the same amount of water was being kept in the channel. An example of this is shown with the similar 1-yr RI floods which indicate that no water is escaping the channel in either scenario, therefore the same volume of water is passing through.

However, as discussed in the results, the discharge through the profile lines is substantially higher for the post-restoration events than the pre-restoration events beginning with the 5-yr RI. The higher discharge associated with the post-restoration floods suggests that a larger percentage of water remains within the channel and that overtopping is prevalent during the majority of pre-restoration floods. This theory is supported by the differences in discharge for the same RI event between profile lines as well as particle tracing and flow velocity. Flow escapes over the embankment at a much higher rate during the pre-restoration runs than during post-restoration due to water accumulating in the narrower channel with the incapability to spread out, thus forcing flow over the embankments. In the post-restoration runs, the setback embankments provide more room for the movement of water and therefore the flow is able to stay more contained between the realigned embankments. As a result,

the fraction of flow left in the channel is less during the pre-restoration model runs and therefore the discharge passing through the profile lines is lower.

At upper Phase 1, flow is overtopping the left embankment during both time periods, but significantly more so during the pre-restoration runs (Figure 35). Additionally, at this location, the pre-restoration run is bumpy while the post-restoration run is more constant due to the flow repeatedly entering and exiting the channel via the left-side of the original embankment. This may be partially due to how the embankments are represented in the DEMs, with the pre-restoration DEM still including vegetation which would impact the flow routes while the post-restoration embankment is a more uniform obstacle. At the downstream Phase 1 location, the pre-restoration flow is also lower than the post-restoration due to embankment overtopping, however the location of the overtopping occurs farther upstream on the right side of the channel (Figure 36). The slight increase in discharge rates for equivalent RI events between the upper and lower Phase 1 locations suggests that containment improves downstream from the upper location which allows the flow to accumulate and subsequently increase.

At the upper Phase 2 location, the similarities between flows of the pre-restoration and post-restoration (Figure 20e and Figure 20f) can be attributed to the lack of escaped flow immediately upstream of this section for all model runs except for the 50-yr and 100-yr RI floods. The drop observed in the 100-yr pre-restoration run is indicative of a response to the build-up of water which forces embankment overtopping upstream around this time (Figure 37). The observed increase in discharge rates between equivalent pre-restoration RI events suggests that containment improves from lower Phase 1 to upper Phase 2 for the pre-restoration channel while the slight decrease that occurs for the post-restoration events indicate containment decreases in the post-restoration topography. The large discrepancy between the majority of flows at the lower Phase 2 location is a result of increased channel area by setback flood embankments which has allowed the flow to remain more contained in the post-restoration floods while it extensively overtops the embankment in the pre-restoration floods (Figure 38). As described in the results, the drop in discharge rate from upper to lower Phase 2 is much larger for the pre-restoration runs than the post-restoration runs which indicates more flow is escaping the channel prior to the restoration works.

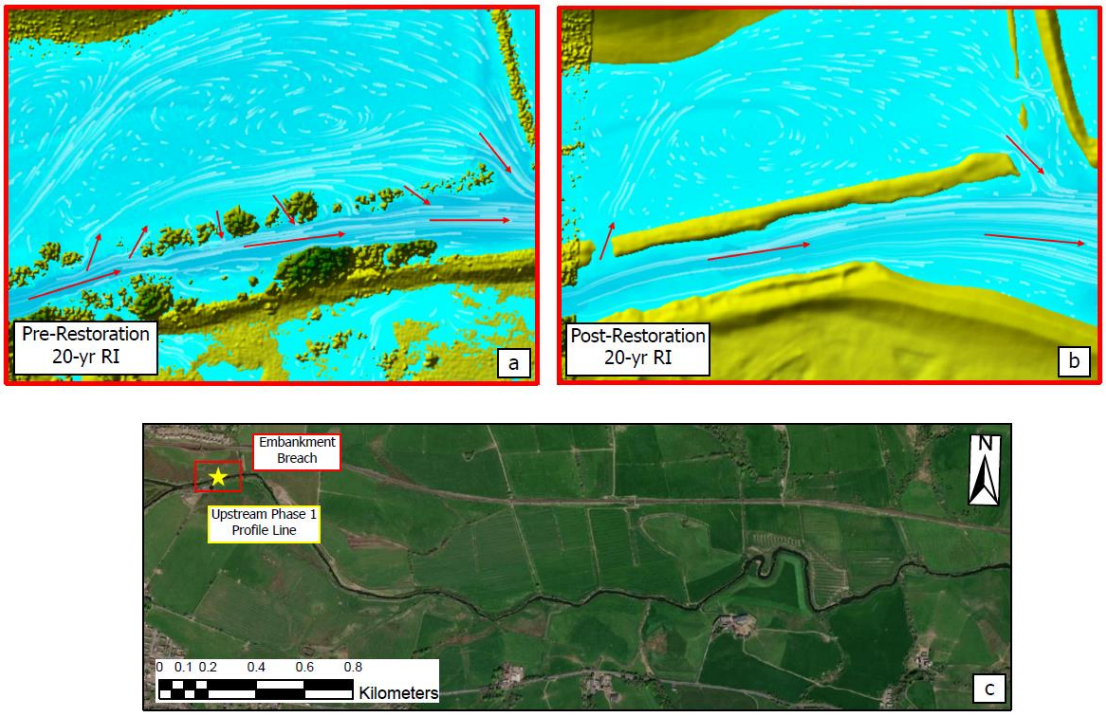

Figure 35. Embankment overtopping differences associated with the upstream Phase 1. Pre-restoration (Figure 35a) and post-restoration (Figure 35b). The effect that the vegetation in the unfiltered pre-restoration DEM has on the flow can be clearly seen in Figure 35a. Location of embankment overtopping within the site (red box) as it relates to the profile line (yellow star) (Figure 35c).

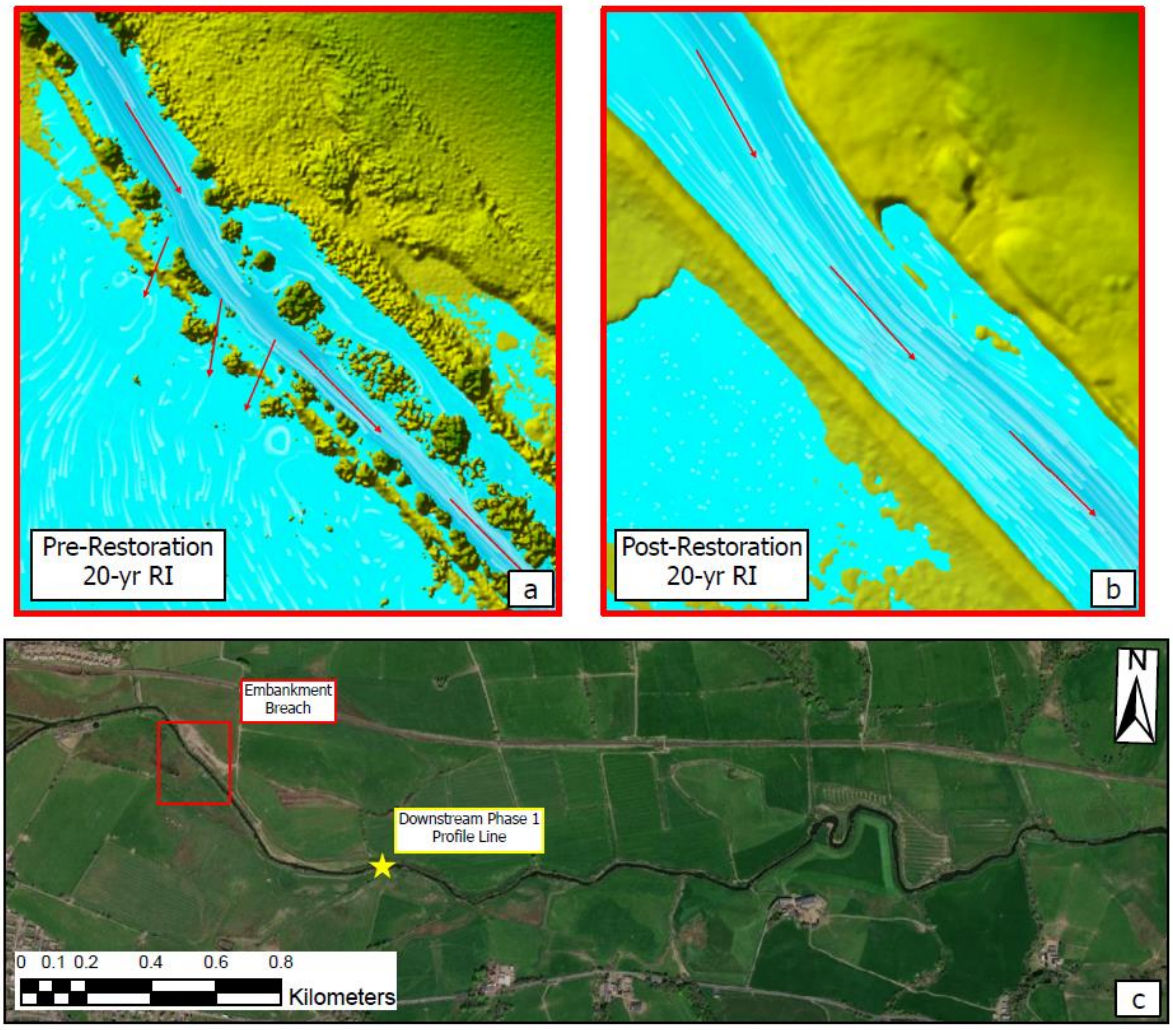

Figure 36. Embankment overtopping differences associated with the downstream Phase 1. Pre-restoration (Figure 36a) and post-restoration (Figure 36b). Location of embankment overtopping within the site (red box) as it relates to the profile line (yellow star) (Figure 36c).

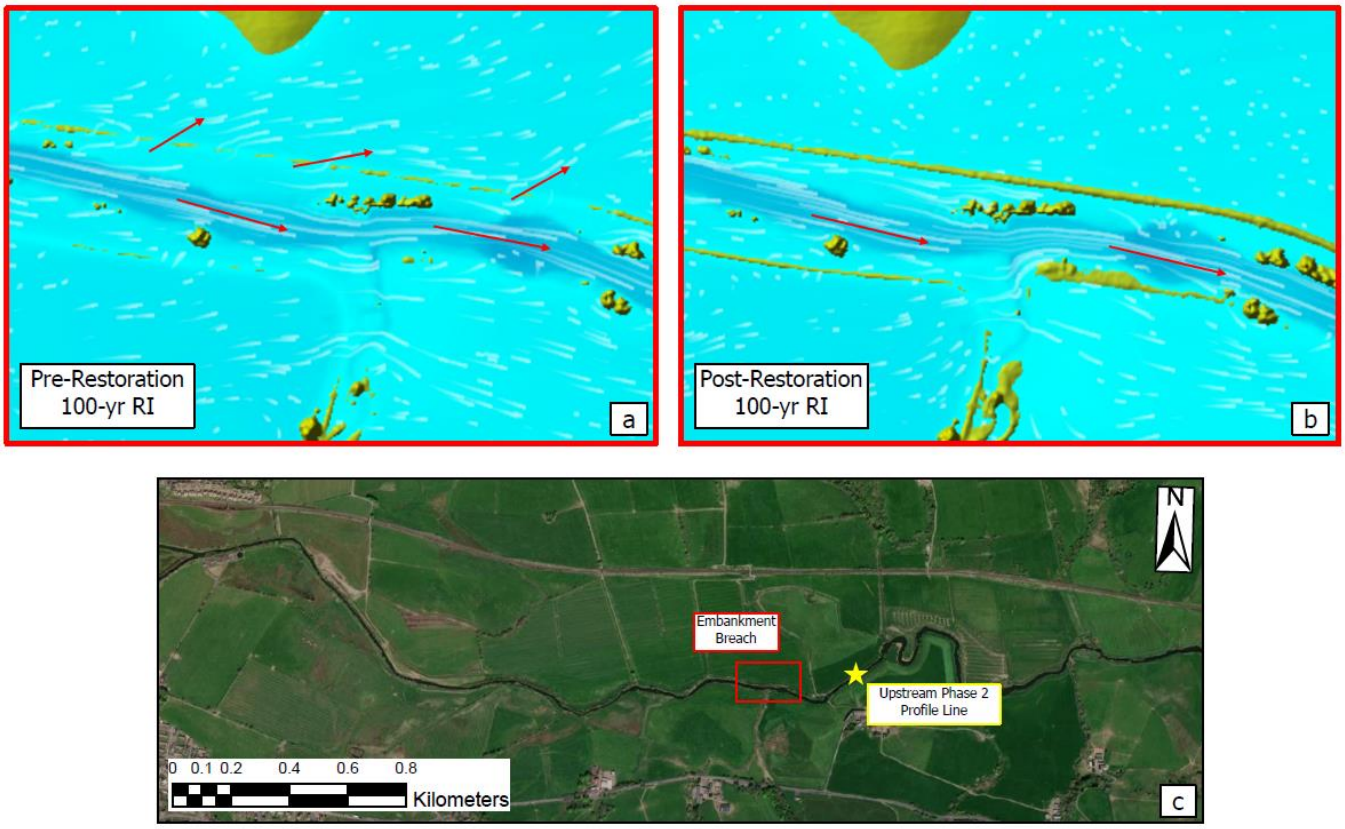

Figure 37. Embankment overtopping differences associated with the upstream Phase 2. Pre-restoration (Figure 37a) and post-restoration (Figure 37b). Location of embankment overtopping within the site (red box) as it relates to the profile line (yellow star) (Figure 37c).

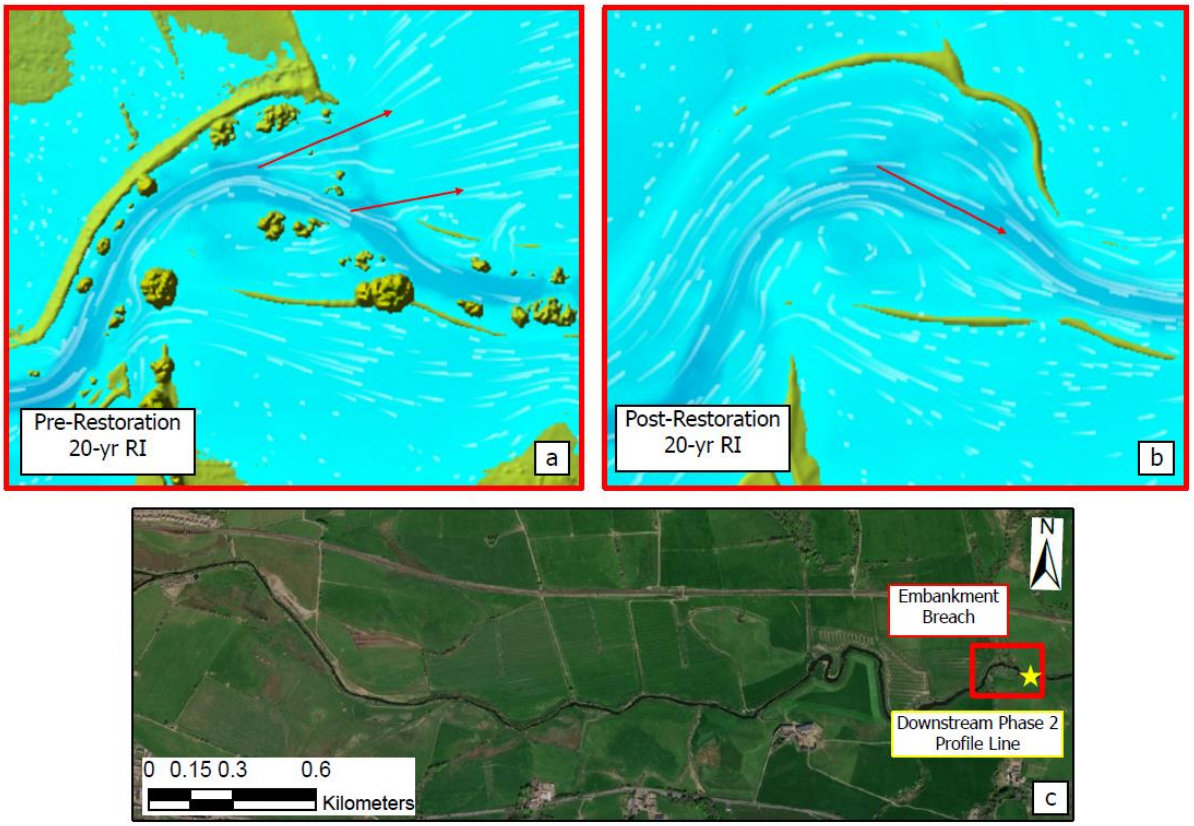

Figure 38. Embankment overtopping differences associated with the downstream Phase 2. Pre-restoration (Figure 38a) and post-restoration (Figure 38b). Location of embankment overtopping within the site (red box) as it relates to the profile line (yellow star) (Figure 38c).

Unsteady flow plots in Figure 21a through Figure 21d show similar results as those shown in the Figure 20 hydrographs. The difference in hydrograph shape, with the Phase 1 locations having a sharp peak and the Phase 2 locations being more rounded, indicates that as flow goes through the model it becomes less flashy and more constant. This difference between upstream and downstream locations can be attributed to the way water is introduced and removed suddenly at the model inlet. There is no distinct lag-time between the two topographies as was considered a possibility with the setback embankments which could have potentially delayed the post-restoration flow. While the embankment restoration did not affect the flow in this way, the difference in flow through the profile lines, as described above, indicate that the floods are influenced by the set-back embankments.

Depth results indicate an influence from embankment setbacks, with the mean depth being consistently larger for pre-restoration for the majority of the results (Figure 25, Figure 26, Figure 27). The deeper water associated with the original embankments corresponds with constrained channel characteristics that prohibits lateral dispersion of flow, forcing the water to become more concentrated and thus deeper. With the widened channel area allowed for by the setback embankments, the flow is able to spread out and subsequently becomes shallower. This is supported by the depth cross sections shown in Figure 22a through Figure 22l, which generally show the pre-restoration events being deeper than the post-restoration runs. Exceptions to this are shown at the lower Phase 1 profile line where the levels are equal for the 2-yr and 100-yr RIs and the post-restoration levels are greater than the pre-restoration. However, as this is just one location, and represents only a slice of the overall depths, these results are considered the exception to the larger trend which indicates that the pre-restoration events have larger depths than the post-restoration events. Additional exceptions to this trend are present in the 5-yr RI where the post-restoration mean

depth is just slightly greater than the pre-restoration (0.90 m vs 0.87 m) and the 20-yr RI where the mean depths are equal for both time periods. While the means for the total inundated area are alike, there is still a distinct difference in depths within the channel area between the two topographies, with the post-restoration depths being significantly smaller than those of the pre-restoration.

Shear stress results suggest an impact from embankment setbacks as Figure 31 and Figure 32 show that in lower Phase 1 and the meander in Phase 2 the narrower pre-restoration channel areas there is higher shear stress than in the post-restoration channel where the water has been able to disperse. These observations represent site-wide trends and highlight the effect of similar magnitude flow moving through contained areas of different sizes. Shear stress is a measure of force applied over area (F/a) and therefore when there is an increase in area that allows the flood to spread out, the shear stress will decrease, assuming a constant or similar discharge occurs.

However, one exception to these findings can be seen in Figure 30 at upper Phase 1 where the shear stress in the post-restoration channel is higher than in the channel with the original embankment. As indicated by the profile line at this location and the accompanying HEC-RAS image (Figure 20a, Figure 20b, and Figure 35), the water in the pre-restoration model runs continuously exits and enters the channel in different locations via the left embankment while with the restored embankment the flow largely remains within the channel. Therefore, the more contained and concentrated post-restoration flow increases the amount of force applied to the channel which results in the higher shear stress observed at this location.

The mean shear stress values steadily decrease from the 1-yr to 20-yr RI before generally stabilizing through the 100-yr RI (Table 6, Figure 29). However, from the 20-yr to the 100-yr RI, the mean shear stress results are slightly higher for post-restoration than pre-restoration, which contradicts the observed trends within the channel areas. A likely explanation for this discrepancy is that because of the lower overall shear stress values during the higher RI model runs, areas with higher shear stress more greatly impact the mean. In these model runs the area with highest shear stress is the model inlet and, as described above, this area is the one place where the shear stress is consistently higher for post-restoration than pre-restoration and is therefore the likely reason for the higher mean values.

The pockets of high shear stress located on the outside edge of the pre-restoration embankment (Figure 33) may indicate that water is being forced out of the channel due to the limited space and the force required to do this is reflected in the larger shear stress values. However, these pockets could also be representative of model instabilities as they occur in areas of very low depth and projected high velocity. This combination, which may incorrectly present as pockets of high shear stress, is improbable and in reality there would likely be insufficient water to produce such a high shear stress value.

6.1.3 Project Development Options

While this investigation encompassed a variety of survey methods and data processing techniques, as with any project there are further steps that could be taken to increase the overall rigour. The following methods could potentially increase the hydraulic model's reliability.

Methods of further ensuring the accuracy of a model include calibration and sensitivity analysis which quantify uncertainties associated with boundary conditions. While the scope of this project did not allow time for executing these processes, a description of the steps and benefits are provided. Model calibration would be conducted by obtaining a satellite image of the project area with clear flood

inundation and comparing this with model output inundation extents. The model would be run at the known actual discharge values, calculated from spatial scaling of downstream gauge station data (i.e., Hall Bridge), with varying Manning's roughness coefficients and mesh resolutions. The output inundation extents would then be compared to the actual inundation extent and the parameters would be adjusted to obtain a model output as close to the actual extent as possible. The parameters most closely representing actual conditions would then be applied throughout the different recurrence interval runs to obtain realistic results. While simple in theory, it must be noted that there are multiple possible parameter combinations that give similar results, and this is thus a limitation of calibrating hydraulic models (Hall et al., 2005). A sensitivity analysis would be conducted by running one flow hydrograph through a variety of Manning's roughness and mesh resolution values. The output inundation extents would then be compared to quantify how each parameter effects the results. Unlike the calibration analysis, which is a measure of accuracy, the purpose of the sensitivity analysis is to recognize which model inputs impact the results. However, the existing methods used to define parameters and model characteristics are adequately justifiable for the pre- and post-restoration comparisons undertaken here, as described in previous sections.

Another step that would be useful for increasing the dependability of the presented results would be to filter the LiDAR data used for the pre-restoration topography and remove any topographic blocks such as buildings and trees. However, as this data was sourced from an online data delivery site (Digimap, 2022a & Digimap, 2022b) and was the only 50 cm LiDAR survey conducted over the study site immediately prior to the investigation, it was deemed allowable to work around these features. Additionally, because building and trees are of significant height (scale of m) and a DoD comparison using both a filtered (buildings and trees removed) and non-filtered DEM (buildings and trees included) will produce substantial change on the scale of meters, these anomalies can be confidently identified and worked around as the actual geomorphic changes occurring in the study area are significantly smaller, generally on a scale of cm.

As described in the methods section, it was determined that one Manning's coefficients would be applied to both the channel and floodplain areas to represent the topography roughness. Using two separate Manning's coefficients would be more representative of actual conditions as the wet and dry areas rarely have the same roughness values. However, the similarity in the ranges of possible roughness coefficients between the channel and floodplains allowed for one coefficient to be reasonably applied to the whole of the modelled area.

To account for potential backwater effect, which may influence the results through the most downstream profile line, the model could be extended further downstream of the outlet. This would ensure that all flows through the profile line represent the discharge moving downstream as opposed to any effects from uncertainty in the downstream boundary level. As the river is largely confined between embankments immediately downstream of the upstream boundary, the distance from the model inlet is acceptable and unlikely to cause uncertainties in water depth and velocity predictions beyond the first few rows of model cells.

In the case that more specific analyses were requested, such as investigating the effects of embankment setbacks and two-stage channel design separately, the model could be adjusted. Two-stage channel design carves out benches (e.g., lowering elevation surrounding the channel) to create a floodplain while embankment setbacks push existing embankments back but leave the floodplain at its original elevation. These restoration methods could be distinguished in the model by altering the input DEMs so that there are two scenarios: one where the elevation surrounding the channel is

lowered (as presented in this study), and one where it is not. This would represent a situation where only the embankment setbacks are influencing channel flow and the impacts from both restoration techniques could then be separated out.

6.1.4 Investigation Implications

Globally, rivers have been subjected to intense hard engineering practises such as channelisation via channel straightening and embankment implementation (Heritage & Entwistle, 2020). Such practises have led to substantial degradation of river systems in terms of ecological diversity and channel-floodplain connectivity (Mondal & Patel, 2018). This investigation of river restoration along the River Nith demonstrates how a previously channelised single-thread river responds in terms of hydrology and morphology to embankment setback and two-stage channel design implementation.

The results suggest that floodplain connectivity is improved with the application of embankment setbacks and two-stage channel design. This is supported by the larger inundation extent generally associated with the post-restoration topography which indicates that, when given the opportunity and space, the river will spread out and reconnect to its floodplain. Results also indicate that discharges associated with post-restoration, where the channel is less constrained by hard engineering, generally record lower shear stress values and shallower mean depths within the channel area. If the River Nith continues to respond in this manner (e.g., decreased flow depths and bed shear stress), positive impacts such as increased habitat diversity and bank stability should prevail in the future. Additionally, the general decrease in shear stress may result in long-term aggradation of sediment which could be confirmed with future LiDAR and bathymetry surveys. However, in some places such as upper Phase 1, an increase in shear stress is observed as an exception to the overall decreasing trend. As explained above, this is due to the flow continuously exiting and entering the pre-restoration model while remaining more contained during the post-restoration model, with the increased shear stress subsequently resulting in the erosion observed at the newly accessible point bar.

Long-term monitoring (e.g., 10 years) would be beneficial to assess and quantify all of these potential outcomes. Further monitoring, such as fish and macro-invertebrate surveys, could be conducted in the years following this restoration to assess whether the predicted habitat increase has influenced fauna populations within the river. Particularly in Phase 1, where floodplain connectivity was substantially increased, it would be expected that over time flow velocities would drop as water is dispersed onto the floodplain (Opperman et al., 2010). This could be analysed with long-term field measurements as well as further numerical modelling that analyses velocity along with shear stress. Additionally, satellite imagery over the following years could be used to determine the real-world influence that this restoration has had on flooding within the study area and use these as a comparison against the predicted outcomes.

Climate change is predicted to increase the magnitude and frequency of flood events around the world (Hirabayashi et al., 2021). As a result of this increase in scale of discharges, rivers will require more space to accommodate the larger volume of water which they will receive (Arnell & Gosling, 2014; Heritage & Entwistle, 2020). Setting back channels and removing embankments will allow rivers to adjust their morphology (e.g., widening) and take advantage of the increased floodplain to dissipate the impacts of intensified discharges. Without additional space, rivers will continue to degrade via incision and bed armouring and will become further depleted in wildlife habitats and ecological functionality. This study suggests that embankment setbacks and restored floodplain connectivity generally impact shear stress and flood inundation in a way that is potentially beneficial to habitat

creation and flood mitigation. It is recommended that both two-stage channel design and embankment setbacks be considered as a restoration option for other similarly incised rivers, the method depending on whether embankments are already present. While in an ideal scenario embankments and channel armouring would be completely removed, this is unlikely to be feasible at all locations, as both agricultural and industrial land uses need to be taken into consideration. Therefore, the restoration methods observed in this thesis are essential to provide a balance between restoring healthy river systems and upholding surrounding land use practices.

7 Conclusion

This investigation indicates that embankment setbacks and two-stage channel design have had an influence on flood impacts along the upper River Nith. Although limited in spatial extent, there is evidence of post-restoration geomorphic change that is likely to be associated with embankment setbacks. These include increasing geomorphic change and inundation extent while decreasing flow depth and shear stress. With respect to the initial research questions outlined in the Introduction, the following conclusions have been made:

Geomorphic change in response to the embankment setbacks has occurred between 2019 and 2022. While some elevation change can be attributed to anthropogenic cut and fill, there are locations where the difference can be associated with geomorphic processes. Specifically, DoD results showing erosion on the newly created point bar in the upstream Phase 1 reach indicate that floodplain connectivity has increased, as the flow can now access this area that was previously covered by an embankment. Additionally, DoD results show deposition within the lower Phase 1 channel area where shear stress has decreased. This response is twofold, with the source of deposited sediment likely being erosion at the upstream point bar and the lower shear stress resulting from high flow discharge now spreading out across a wider lateral extent due to embankment setbacks.

Inundation extents are generally larger for the post-restoration hydraulic model simulations compared to the pre-restoration hydraulic model simulations. While an exception to this is the 100-yr RI event where the pre-restoration inundation extent is just slightly larger, the 3% difference in size is not considered significant. The overall trends of larger inundation extents generally being associated with the post-restoration models suggest that floodplain connectivity has increased because of the embankment setbacks and two-stage channel design providing the river with more room to spread out high flows.

Despite the input flood discharges being the same, the predicted post-restoration hydrographs generally show higher discharges than the pre-restoration floods. Additionally, while the discharge associated with each RI decreases as the flood moves downstream, the decreases are greater for the pre-restoration model runs than for the post-restoration model runs. For example, the 20-yr RI pre-restoration flood drops from approximately 50 m^3/s to 20 m^3/s from the upstream Phase 1 profile line to the downstream Phase 2 profile line while the 20-yr RI post-restoration flood drops only 10 m^3/s, going from 70 m^3/s to 60 m^3/s, respectively. This suggests that, while embankment overtopping occurs in both pre-restoration and post-restoration model runs, overtopping is more prevalent in the pre-restoration topography and a larger percentage of water remains within the channel during in the post-restoration topography. Therefore, embankment setbacks and two-stage channel design appear to enable higher flow containment, especially when input flood discharge rates increase.

In addition to changes in inundation extent, hydraulic model predictions show that both the depth and shear stress within the channel generally decrease from pre- to post-restoration. While there are a few exceptions to this, such as increased shear stress at upper Phase 1 and post-restoration having a larger mean depth than pre-restoration for the 5-yr RI, overall trends indicate that a widened channel area, from embankment setbacks and two-stage channel design, results in shallower flows and reduced shear stresses.

The restoration work conducted by SEPA on the upper River Nith indicate that the implementation of embankment setbacks and two-stage channel design increases floodplain connectivity and inundation extents while decreasing the amount of water overtopping the embankments and reducing depth and

shear stress within the channel. This, coupled with the finding of some geomorphic change from the initiation of geomorphic processes in some locations, suggest that natural river processes are becoming re-established and are likely to promote ecological diversity. Overall, this project provides an important assessment of the value of embankment setbacks and two-stage channel design on channelised rivers in a real-world setting. Although just one example, the results from this thesis will help to expand the knowledge of the effects that these river restoration techniques have on flood characteristics and provide a guide for further expansion of these techniques to additional river locations both in Scotland and farther afield.

8 References

Acreman, M., Riddington, R., Booker, D. (2003). Hydrological impacts of floodplain restoration: a case study of the River Cherwell, UK. *Hydrology and Earth System Sciences Discussions 7*, 75–85. doi: 10.5194/hess-7-75-2003

Arcement Jr., G. J. & Schneider, V. R. (1989). *Guide for selecting Manning's roughness coefficients for natural channels and flood plains (water-supply paper 2239).* Washington, DC: United States Geological Survey. doi:10.3133/wsp2339

Arnell, N. W. & Gosling, S. N. (2014). The impacts of climate change on river flood risk at the global scale. *Climatic Change, 134*(3), 387-401. doi:10.1007/s10584-014-1084-5

Bangen, S. G., Wheaton, J. M., Bouwes, N., Bouwes, B., & Jordan, C. (2014). A methodological intercomparison of topographic survey techniques for characterizing wadeable streams and rivers. *Geomorphology, 206*, 343-361. doi:10.1016/j.geomorph.2013.10.010

Bates, P. D. & De Roo, A. P. J. (2000). A simple raster-based model for flood inundation simulation. *Journal of Hydrology, 236*, 54-77. doi:10.1016/S0022-1694(00)00278-X

Benda, L., Poff, N. L., Miller, D., Dunne, T., Reeves, G., Pess, G., & Pollock, M. (2004). The network dynamics hypothesis: how channel networks structure riverine habitats. *BioScience 54*(5). doi:0.1641/0006-3568(2004)054[0413:TNDHHC]2.0.CO;2)

Black, A. R. & Werrity, A. (1997) Seasonality of flooding: a case study of North Britain. *Journal of Hydrology*, *195*(1-4), 1-25. doi:10.1016/S0022-1694(96)03264-7

Blanckaert, K. (2010). Topographic steering, flow recirculation, velocity redistribution, and bed topography in sharp meander bends. *Water Resources Research, 46*(9). doi:10.1029/2009wr008303

Bradford, M. J., Korman, J., & Higgins, P. S. (2005). Using confidence intervals to estimate the response of salmon populations (Oncorhynchus spp.) to experimental habitat alterations. *Canadian Journal of Fisheries and Aquatic Sciences, 62*(12), 2716-2726. doi:10.1139/f05-179

Brasington, J., Langham, J., & Rumsby, B. (2003). Methodological sensitivity of morphometric estimates of coarse fluvial sediment transport. *Geomorphology, 53*(3-4), 299-316. doi:10.1016/s0169-555x(02)00320-3

Brede, B., Lau, A., Bartholomeus, H. M., & Kooistra, L. (2017). Comparing RIEGL RiCOPTER UAV LiDAR Derived Canopy Height and DBH with Terrestrial LiDAR. *Sensors (Basel), 17*(10). doi:10.3390/s17102371

Brierley, G. & Fryirs, K. (2009). Don't fight the site: three geomorphic considerations in catchment-scale river rehabilitation planning. *Environ Manage, 43*(6), 1201-1218. doi:10.1007/s00267-008-9266-4

Brocchini, M., Calantoni, J., Postacchini, M., Sheremet, A., Staples, T., Smith, J., Reed, A. H., Braithwaite III, E. F., Lorenzoni, C., Russo, A., Corvaro, S., Mancinelli, A., & Soldini, L. (2017). Comparison between the wintertime and summertime dynamics of the Misa Estuary. *Marine Geology, 385,* 27-40. doi:10.1016/j.margeo.2016.12.005

Burrel, B. C., Davar, K., & Hughes, R. (2007). A Review of Flood Management Considering the Impacts of Climate Change. *Water International, 32*(3), 342-359. doi:10.1080/02508060708692215

CBEC. (2013). *Physical restoration options to address morphology and flood pressures on the River Nith – a pilot study* (U13-1007).

CBEC. (2015). *Pilot Catchment Project Options Appraisal - River Nith, Sanquhar to New Cumnock* (U14-1020).

Chappell, A., Heritage, G. L., Fuller, I. C., Large, A., & Milan, D. J. (2003). Geostatistical analysis of ground-survey elevation data to elucidate spatial and temporal river channel change. *Earth Surface Processes and Landforms, 28,* 349-370. doi:10.1002/esp.444

Church, M. (2006). Bed Material Transport and the Morphology of Alluvial River Channels. *Annual Review of Earth and Planetary Sciences, 34*(1), 325-354. doi:10.1146/annurev.earth.33.092203.122721

Clilverd, H. M., Thompson, J. R., Heppell, C. M., Sayer, C. D., Axmacher, J. C. (2013). River– floodplain hydrology of an embanked lowland Chalk river and initial response to embankment removal. *Hydrological Sciences Journal 58*(3), 627–650. doi:10.1080/02626667.2013.774089

Cluer, B. & Thorne, C. (2014). A stream evolution model integrating habitat and ecosystem benefits. *River Research and Applications, 30*(2), 135-154. doi:DOI 10.1002/rra.2631

Curran, P. J. & Atkinson, P. M. (1998). Geostatistics and remote sensing. *Progress in Physical Geography, 22,* 61-78. doi:10.1177/030913339802200103

Digimap. (2020a). Lidar Composite Digital Terrain Model Scotland (Phase4) 50cm resolution [ASC geospatial data], Scale 1:2000, Tiles: ns61sw, Updated: 20 November 2020, Open Government Licence, Using: EDINA LIDAR Digimap Service, <https://digimap.edina.ac.uk>, Downloaded: 2022-03-02 12:46:43.588

Digimap. (2020b). Lidar Composite Digital Terrain Model Scotland (Phase4) 50cm resolution [ASC geospatial data], Scale 1:2000, Tiles: ns61se, Updated: 20 November 2020, Open Government Licence, Using: EDINA LIDAR Digimap Service, <https://digimap.edina.ac.uk>, Downloaded: 2022-03-02 12:46:43.588

Duck, R. W. (2011). Pioneering, Scottish nineteenth century studies of sedimentary processes in fluvial, estuarine, and coastal environments. *Scottish Journal of Geology, 47,* 81-87. doi:10.1144/0036-9276/01-42

Dukic, V. & Radic, Z. (2014). GIS Based Estimation of Sediment Discharge and Areas of Soil Erosion and Deposition for the Torrential Lukovska River Catchment in Serbia. *Water Resources Management, 28,* 4567-4581. doi:10.1007/s11269-014-0751-7

Evans, J. S. & Hudak, A. T. (2007). A Multiscale Curvature Algorithm for Classifying Discrete Return LiDAR in Forested Environments. *IEEE Transactions on Geoscience and Remote Sensing*, *45*(4), 1029-1038. doi: 10.1109/TGRS.2006.890412

Falter, D., Schröter, K., Nguyen, D., Vorogushyn, S., Kreibich, H., Hundecha, Y., Apel, H., & Merz, B. (2015). Spatially coherent flood risk assessment based on long-term continuous simulation with a coupled model chain. *Journal of Hydrology*, *524*. doi:10.1016/j.jhydrol.2015.02.021.

Flatley, A., Rutherfurd, I. D., & Hardie, R. (2018). River Channel Relocation: Problems and Prospects. *Water, 10*(10), 1360. doi:10.3390/w10101360

Fuller, I. C. & Hutchinson, E. L. (2007). Sediment flux in a small gravel-bed stream: Response to channel remediation works. *New Zealand Geographer, 63*(3), 169-180. doi:10.1111/j.1745-7939.2007.00106.x

Gallay, M. & Jozef, P. (2013). Section 2.1.4: Direct Acquisition of Data: Airborne laser scanning. In: Clarke, L.E & Nield, J.M. (Eds.) *Geomorphological Techniques* (Online Edition). British Society for Geomorphology; London, UK, pp. 1-17. Retrieved from: https://www.semanticscholar.org/paper/Direct-Acquisition-of-Data%3A-Airborne-laser-scanning-Gallay-Jozef/539e9766885cb31c705565c89b17ba44edaa6bf9

Geikie, A. (1868). On Denudation - Now in Progress. *Geological Magazine, 5*(48), 249-254. doi:10.1017/s0016756800207930

Gilvear, D. J., Heal, K. V., & Stephen, A. (2002). Hydrology and the ecological quality of Scottish river ecosystems. *The Science of the Total Environment, 294*(1-3), 131-159. doi:10.1016/s0048-9697(02)00060-8

Griffin, I., Perfect, C., & Wallace, M. (2015). River restoration and biodiversity. *Scottish Natural Heritage Commissioned Report No. 817.* Retrieved from: https://www.crew.ac.uk/sites/www.crew.ac.uk/files/sites/default/files/publication/River%20Restoration%20and%20Biodiversity_for%20web_high.pdf

Grimaldi, S., Schumann, G. J. P., Shokri, A., Walker, J. P., & Pauwels, V. R. N. (2019). Challenges, Opportunities, and Pitfalls for Global Coupled Hydrologic-Hydraulic Modeling of Floods. *Water Resources Research, 55*(7), 5277-5300. doi:10.1029/2018wr024289

Hall, J. W., Tarantola, S., Bates, P. D., & Horritt, M. S. (2005). Distributed Sensitivity Analysis of Flood Inundation Model Calibration. *Journal of Hydraulic Engineering, 131*(2), 117-126. doi:10.1061/(asce)0733-9429(2005)131:2(117)

Heritage, G. & Entwistle, N. (2020). Impacts of River Engineering on River Channel Behaviour: Implications for Managing Downstream Flood Risk. *Water, 12*(5). doi:10.3390/w12051355

Hirabayashi, Y., Tanoue, M., Sasaki, O., Zhou, X., & Yamazaki, D. (2021). Global exposure to flooding from the new CMIP6 climate model projections. *Scientific Reports, 11*(1), 3740. doi:10.1038/s41598-021-83279-w

Huang, S. & Hattermann, F. F. (2018) Coupling a global hydrodynamic algorithm and a regional hydrological model for large-scale flood inundation simulations. *Hydrology Research*, *49*(2), 438–449. doi:10.2166/nh.2017.061

Huţanu, E., Mihu-Pintilie, A., Urzica, A., Paveluc, L. E., Stoleriu, C. C., & Grozavu, A. (2020). Using 1D HEC-RAS Modeling and LiDAR Data to Improve Flood Hazard Maps Accuracy: A Case Study from Jijia Floodplain (NE Romania). *Water, 12*(6). doi:10.3390/w12061624

Hutchinson, M.F. & Gallant, J.C. (2000). Digital elevation models and representation of terrain shape. In: J.P. Wilson and J.C. Gallant (Eds.) *Terrain Analysis*. Wiley, New York, pp. 29–50.

James, L. A., Hodgson, M. E., Ghoshal, S., & Latiolais, M. M. (2012). Geomorphic change detection using historic maps and DEM differencing: The temporal dimension of geospatial analysis. *Geomorphology, 137*(1), 181-198. doi:10.1016/j.geomorph.2010.10.039

Jowett, I. & Duncan, M.. (2011). Effectiveness of 1D and 2D hydraulic models for instream habitat analysis in a braided river. *Ecological Engineering, 48*. doi:10.1016/j.ecoleng.2011.06.036.

Konrad, C. P., Black, R. W., Voss, F., & Neale, C. M. U. (2008). Integrating remotely acquired and field data to assess effects of setback levees on riparian and aquatic habitats in glacial-melt water rivers. *River Research and Applications, 24*(4), 355-372. doi:10.1002/rra.1070

Krider, L., Magner, J., Hansen, B., Wilson, B., Kramer, G., Peterson, J., & Nieber, J. (2017). Improvements in Fluvial Stability Associated with Two-Stage Ditch Construction in Mower County, Minnesota. *Journal of the American Water Resources Association, 53*(4), 886-902. doi:10.1111/1752-1688.12541

Kundzewicz, Z. W. (2002). Non-structural Flood Protection and Sustainability. *Water International, 27*(1), 3-13. doi:10.1080/02508060208686972

Larsen, E., Girvetz, E., & Fremier, A. (2006). Assessing the Effects of Alternative Setback Levee Scenarios Employing a River Meander Migration Model. *Environmental Management, 37*, 880-897. doi:10.1007/s00267-004-0220-9

Leitão, J. P., Moy de Vitry, M., Scheidegger, A., & Rieckermann, J. (2016). Assessing the quality of digital elevation models obtained from mini unmanned aerial vehicles for overland flow modelling in urban areas. *Hydrology and Earth System Sciences, 20,* 1637–1653, doi:10.5194/hess-20-1637-2016, 2016.

Li, B. Y., Hou, J. M., Li, D. L., Yang, D., Han, H., Bi, X., Wang, X., Hinkelmann, R., & Xia, J. Q. (2021). Application of LiDAR UAV for High-Resolution Flood Modelling. *Water Resources Management, 35*(5), 1433-1447. doi:10.1007/s11269-021-02783-w

Maaß, A. L., Schüttrumpf, H. (2019). Reactivation of floodplains in river restorations: long-term implications on the mobility of floodplain sediment deposits. *Water Resources Research 55* (10), 8178–8196. doi:10.1029/2019WR024983

Mackay, E. C., Shewry, M. C., & Tudor, G. J. (1998). *Land Cover Change: Scotland from the 1940s to the 1980s – The Natural Heritage of Scotland Series Vol. 6*. The Stationary Office.

Maniatis, G., Williams, R. D., Hoey, T. B., Hicks, J., & Carroll, W. (2020). A decision support tool for assessing risks to above-ground river pipeline crossings. *Proceedings of the Institution of Civil Engineers - Water Management, 173*(2), 87-100. doi:10.1680/jwama.18.00054

Mapstone, B. D. (1995). Scalable Decision Rules for Environmental Impact Studies: Effect Size, Type I, and Type II. *Ecological Society of America 5*(2), 401–410. doi:10.2307/1942031.

Marteau, B., Vericat, D., Gibbins, C., Batalla, R. J., & Green, D. R. (2017). Application of Structure-from-Motion photogrammetry to river restoration. *Earth Surface Processes and Landforms, 42*(3), 503-515. doi:10.1002/esp.4086

Mayne, J. (1806). *Apostrophe, to the River Nith*. The Literary Panorama.

McDonald, A. & Ledger, D. (1981). Flood area modelling from an elementary data base. *Journal of Hydrology, 53*(1-2), 85-94. doi: 10.1016/0022-1694(81)90038-X.

Merz, B., Apel, H., Nguyen, D., Falter, D., Hundecha, Y., Kreibich, H., Schröter, K., & Vorogushyn, S. (2016). Large-scale flood risk assessment using a coupled model chain. *E3S Web of Conferences, 7,* 11005. doi:10.1051/e3sconf/20160711005.

Mondal, S. & Patel, P. P. (2018). Examining the utility of river restoration approaches for flood mitigation and channel stability enhancement: a recent review. *Environmental Earth Sciences, 77*(5). doi:10.1007/s12665-018-7381-y

Montgomery, D. R. (2008). Dreams of Natural Streams. *Science, 319*. doi:10.1126/science.1153480

Muste, M., Dongsu, K., & Merwade, V. (2012). Modern Digital Instruments and Techniques for Hydrodynamic and Morphologic Characterization of River Channels. In: Church, M., Biron, P. M., & Roy, A.G. (Eds.) *Gravel-bed rivers: processes, tools, environments*. Chichester: John Wiley & Sons, Ltd, pp. 315–341.

Newall, W. (1847). *Nith - Section from Southerness to Dumfries* [Map]. National Library of Scotland. Retrieved from: https://maps.nls.uk/transport/rivers/rec/9694

NRFA. (2022a). *UK River and Flow Regimes*. Retrieved from: https://nrfa.ceh.ac.uk/uk-river-flow-regimes

NRFA. (2022b). 79003 - Nith at Hall Bridge. Retrieved 7 July 2022 from https://nrfa.ceh.ac.uk/data/station/info/79003

Opperman, J. J., Luster, R., McKenney, B. A., Roberts, M., & Meadows, A. W. (2010). Ecologically Functional Floodplains: Connectivity, Flow Regime, and Scale. *Journal of the American Water Resources Association, 46*(2), 211-226. doi:10.1111/j.1752-1688.2010.00426.x

Passalacqua, P., Belmont, P., Staley, D., Simley, J., Arrowsmith, R., Bode, C., Crosby, C., DeLong, S., Glenn, N., Kelly, S., Lague, D., Sangireddy, H., Schaffrath, K., Tarboton, D., Wasklewicz, T., & Wheaton, J. (2015). Analyzing high resolution topography for advancing the understanding of mass and energy transfer through landscapes: A review. *Earth-Science Reviews, 148*. doi:10.1016/j.earscirev.2015.05.012

Perfect, C., Addy, S., & Gilvear, D. (2013). *The Scottish Rivers Handbook - A guide to the physical character of Scotland's rivers*. Retrieved from https://www.crew.ac.uk/publication/scottish-rivers-handbook

Pierce, S. C., Kroger, R., & Pezeshki, R. (2012). Managing artificially drained low-gradient agricultural headwaters for enhanced ecosystem functions. *Biology (Basel), 1*(3), 794-856. doi:10.3390/biology1030794

Power, M., Parker, G., Dietrich, W., & Sun, A. (1995). How does floodplain width affect floodplain river ecology? A preliminary exploration using simulations. *Geomorphology, 13*, 301-317. doi:10.1016/0169-555X(95)00039-8

Reid, H. E., Williams, R. D., Brierley, G. J., Coleman, S. E., Lamb, R., Rennie, C. D., & Tancock, M. J. (2018). Geomorphological effectiveness of floods to rework gravel bars: Insight from hyperscale topography and hydraulic modelling. *Earth Surface Processes and Landforms, 44*(2), 595-613. doi:10.1002/esp.4521

NDSFB. (2008). *River Nith Catchment Fishery Management Plan.* Retrieved from: https://www.river-nith.com/wp-content/uploads/2014/01/RNCFMP-emailable.pdf

Roussel, J. & Auty, D. (2022). *Airborne LiDAR Data Manipulation and Visualization for Forestry Applications*. R package version 4.0.1. Retrieved from: https://cran.r-project.org/package=lidR.

Roussel, J., Auty, D., Coops, NC., Tompalski, P., Goodbody, T. R., Meador, A. S., Bourdon, J., de Boissieu, F., & Achim, A. (2020). lidR: An R package for analysis of Airborne Laser Scanning (ALS) data. *Remote Sensing of Environment*, *251.* doi:10.1016/j.rse.2020.112061.

Sargent, R. J. & Ledger, D. C. (1995). Derivation of a 130 year runoff record from sluice records for the Loch Leven catchment, southeast Scotland. *Proceedings of the Institution of Civil Engineers – Water, Maritime and Energy, 112*(1), 79-80. doi:10.1680/iwtme.1992.09827

Scotlandinfo.eu. (2022). *Scotland Weather and Climate*. Scotland Info Guide. Retrieved 23 September 2022 from https://www.scotlandinfo.eu/scotland-weather-and-climate/

SEPA. (2007). *Scotland's Water Environment Review 2000-2006.* Retrieved from: https://www.sepa.org.uk/media/38462/scotlands-water-environment-review-2000-2006-main-report.pdf

SEPA. (2015). *Natural Flood Management Handbook*. Retrieved from: https://www.sepa.org.uk/media/163560/sepa-natural-flood-management-handbook1.pdf

Sinha, R., Bapula, G. V., Sing, L. K., & Rath, B. (2008). Flood Risk Analysis in the Kosi River Basin, North Bihar using Multi-Parametric Approach of Analytical Hierarchy Process (AHP). *Journal of the Indian Society of Remote Sensing, 36,* 335-349. doi:10.1007/s12524-008-0034-y

Smith, M. W., Carrivick, J. L., & Quincey, D. J. (2015). Structure from motion photogrammetry in physical geography. *Progress in Physical Geography: Earth and Environment, 40*(2), 247-275. doi:10.1177/0309133315615805

Smith, I. R. & Lyle, A. A. (1994). Running waters. In: Maitland PS, Boon P, McClusky DS (Eds.) *The Freshwaters of Scotland, a National Resource of International Significance.* Chichester: Wiley, pp. 17–34.

Soulsby, C., Black, A. R., & Werritty, A. (2002). Hydrology in Scotland: towards a scientific basis for the sustainable management of freshwater resources--foreword to thematic issue. *Science of the Total Environment, 294*(1-3), 3-11. doi:10.1016/s0048-9697(02)00048-7

Steele, M. E., Black, A. R., Werrity, A., & Littlewood, I. G. (1999). Reassessment of flood risk for Scottish rivers using synthetic runoff data. In: Gottschalk, L. (Ed.) *Hydrological Extremes: Understanding, Predicting, Mitigating.* IAHS Publishing No. 255, pp. 209-215.

Stevenson, D. & Stevenson, T. (1861). *Nith - working drawing of extension of wall to opposite Conheath* [Map]. National Library of Scotland. Retrieved from: https://maps.nls.uk/transport/rivers/rec/9695

Štroner, M., Urban, R., & Línková, L. (2021). A New Method for UAV Lidar Precision Testing Used for the Evaluation of an Affordable DJI ZENMUSE L1 Scanner. *Remote Sensing, 13*(23). doi:10.3390/rs13234811

Tomsett, C. & Leyland, J. (2019). Remote sensing of river corridors: A review of current trends and future directions. *River Research and Applications, 35*(7), 779-803. doi:10.1002/rra.3479

USACE. (2010). *HEC-RAS River Analysis System - Hydraulic Reference Manual*. USACE Hydrologic Engineering Center. Retrieved from: https://www.hec.usace.army.mil/software/hec-ras/documentation/HEC-RAS%205.0%20Reference%20Manual.pdf

USACE. (2022a). *HEC-RAS - Creating Land Cover, Manning's n values, and % Impervious Layers*. USACE Hydrologic Engineering Center. Retrieved from: https://www.hec.usace.army.mil/confluence/rasdocs/r2dum/latest/developing-a-terrain-model-and-geospatial-layers/creating-land-cover-mannings-n-values-and-impervious-layers

USACE. (2022b). *HEC-RAS - Shallow Water or Diffusion Wave Equations.* USACE Hydrologic Engineering Center Retrieved from https://www.hec.usace.army.mil/confluence/rasdocs/r2dum/latest/running-a-model-with-2d-flow-areas/shallow-water-or-diffusion-wave-equations

Vayssière, A., Castanet, C., Gautier, E., Virmoux, C., Dépret, T., Gandouin, E., Develle., A. L., Mokadem, F., Saulnier-Copard, S., Sabatier, P., & Carcaud, N. (2020). Readjustments of a sinuous river during the last 6000 years in northwestern Europe (Cher River, France): from an active

meandering river to a stable river course under human forcing. *Geomorphology, 370*. doi:10.1016/j.geomorph.2020.107395

Wahlstrom, M. & Debarati, G. S. (2015). *The Human Cost of Weather-Related Disasters 1995-2015*. CREC & UNDRR. Retrieved from https://reliefweb.int/report/world/human-cost-weather-related-disasters-1995-2015

Wang, H., Huang, B., Cheng, L., & Sun, X. (2021). Demarcation of River based on UAV LIDAR Point Cloud Data. *Journal of Physics: Conference Series*, *1775*(01). doi:10.1088/1742-6596/1775/1/012002

Ward, A.D., Mecklenburg, D., Powell, G. E., Brown, L.C., & Jayakaran, A. C. (2004). Designing Two-Stage Agricultural Drainage Ditches. *ASAE 8th International Drainage Symposium, Sacramento, California, March 21-24*, 386-397. doi:10.13031/2013.15745

Wehr, A. (2009). LiDAR Systems and Calibration. In Shan, J., Toth, C. K. (Eds.) *Topographic Laser Ranging and Scanning Principles and Processing*. pp. 129-172. Retrieved from: https://www.researchgate.net/publication/230642410_Topographic_Laser_Ranging_and_Scanning_Principles_and_Processing

Wheaton JM. (2008). *Uncertainty in Morphological Sediment Budgeting of Rivers*. Unpublished PhD Thesis, University of Southampton, Southampton, 412 pp. Retrieved from: http://etalweb.joewheaton.org.s3-us-west-2.amazonaws.com/Wheaton/Downloads/Thesis/JMWthesis_V7_LR.pdf

Wheaton, J. M., Brasington, J., Darby, S. E., & Sear, D. A. (2010). Accounting for uncertainty in DEMs from repeat topographic surveys: improved sediment budgets. *Earth Surface Processes and Landforms, 35,* 136-156. doi:10.1002/esp.1886

Williams, R. D. (2012). DEMs of Difference. *Birtish Society for Geomorphology, 2,* 1-17. Retrieved from: https://www.researchgate.net/publication/310596075_DEMs_of_Difference

Williams, R. D., Bangen, S., Gillies, E., Kramer, N., Moir, H., & Wheaton, J. (2020). Let the river erode! Enabling lateral migration increases geomorphic unit diversity. *Science of the Total Environment, 715*, 136817. doi:10.1016/j.scitotenv.2020.136817

Williams, R. D., Brasington, J., Hicks, M., Measures, R., Rennie, C. D., & Vericat, D. (2013). Hydraulic validation of two-dimensional simulations of braided river flow with spatially continuous aDcp data. *Water Resources Research, 49*(9), 5183-5205. doi:10.1002/wrcr.20391

Zachariah, M. B. K. (2019). *The spatial-temporal geomorphology of meandering river channels in distributive fluvial systems.* Unpublished Masters Thesis, University of Bergen, Bergen, 97 pp. Retrieved from: https://bora.uib.no/bora-xmlui/bitstream/handle/1956/20494/Master-Thesis-Zachariah.pdf?sequence=1&isAllowed=y